Robot Looseness Fault Diagnosis

by

M.G. Lipsett, P.Eng.

A thesis submitted to the Department of Mechanical Engineering
in conformity with the requirements
for the degree of Doctor of Philosophy

Queen's University
Kingston, Ontario, Canada
July, 1995

Abstract

With higher demand in industry for accurate, reliable manipulators comes an implicit need for robot users to know well the condition of their machines. Rising expectations of performance require improved methods of performance assessment to improve reliability.

The present work is a study of one aspect of robot reliability: the integrity of the mechanical structure of the manipulator. This work investigates how to include looseness faults in a manipulator model, and how to assess the integrity of the structure with a reasonable number of sensors. Alternative modeling strategies were assessed in the context of looseness diagnostics, leading to the choice of a model based on joint and end effector motion.

A method is developed for locating a single looseness fault in a serial-link manipulator from random joint inputs. The method looks for changes in manipulator end effector motions when looseness is suspected, by producing normal random motions in the manipulator joints. The direction of the non-normal component of end effector motion is the direction of looseness. Individual joints are then moved to new poses, starting from the proximal end, until the link of concern changes orientation with respect to the end effector, causing a change in the direction of the looseness motion.

Parametric and nonparametric methods were investigated for identifying the direction of looseness motion at the end effector. Results came both from simulation and from experiment using an industrial manipulator, a custom-designed looseness rig, and a planar manipulator with variable kinematics. Both structural looseness and joint backlash were successfully identified in the planar manipulator.

The conclusion discusses industrial implementation of the method, and recommends further work and strategies for robot diagnostics.

Acknowledgments

The last thing one settles in writing a book is what one should put in first. — *Pascal*

Without the help and guidance—and patience—of many people, this work would never have been completed. It developed over several years, growing from a Master's project into the hefty wad of papers you now hold.

The work described was done in three places: Kyoto, Japan; Chalk River, Ontario; and Kingston, Ontario.

The idea germinated while I was in Japan studying at Kyoto University in the Division of Applied Systems Science at Uji. Professor Tsuneo Yoshikawa was an invaluable source of personal inspiration and encouraged me greatly with this project. Yasuyoshi Yokokohji introduced me to the nuts and bolts of designing and controlling robots.

I finished this work while employed in Chalk River by AECL Research. Once I began to approach this investigation as a project to manage, my efforts focused, thanks to the assistance of Dick Faught and Ken Hagen, and to the encouragement of my manager, Dr. Peter Janzen, who allowed me the use of facilities and equipment.

The lion's share of the theoretical and experimental development happened in Kingston. I was fortunate to have excellent technical support at Queen's while I worked on the project; Andrew Bryson turned vague sketches into the shiny components that made up the experimental rig. Jim Tregenza was a valuable sounding board for my half-baked ideas at important stages of the design. Ossama Ismaeil, Darko Matovic, and Bryan Cornwall gave good advice, and engaged me in late-night conversations. Dr. Norman Beaulieu offered pithy insights into stochastic systems, and Dr. Jack Jeswiet never failed to offer a fresh perspective to any problem.

I wish to thank John Ballantyne of Spar Aerospace, Terry Jones of CRS Robotics, Karl Rody of Ontario Hydro, and Claudio Girolami of General Motors Canada, for giving me an industrial perspective of the diagnostic needs of robot manufacturers and users.

I am unable to express adequately the debt I owe to Dr. Tom Moore and Dr. Randy Ellis. Dr. Ellis patiently guided me through much of the theory of robot kinematics and dynamics, and steered me away from some numerical instabilities.

As my supervisor, Dr. Moore gave me the latitude I wanted with the guidance I needed. In a multidisciplinary project, it would have been easy to let the project become ill-defined. But Dr. Moore consistently kept me on track, no matter how often I tried to rush off madly "in all directions."

Finally, I must thank my parents. My mother has given consistent encouragement

throughout this work; and my father has shown me how technical skill can be coupled with humanity. Without their help, I would not have been able to achieve even this small effort.

To Ruth,
my wife and best friend

Contents

List of Figures

List of Tables

Nomenclature

Symbols used only once in text for illustrative examples are not listed.

$\vec{0}$	zero vector
${}_{n,m}\mathbf{A}$	matrix A with n rows and m columns
a_i	i-th parameter of model z
$\hat{\mathbf{b}}_i$	unit vector in plane of looseness motion
$\mathbf{C}(\mathbf{q}, \dot{\mathbf{q}}, \mathbf{k_d}, \mathbf{t})$	vector of centripetal and Coriolis terms in equation of motion
C_n	maximum magnitude of $\mathbf{r}$, no looseness
C_p	maximum magnitude of $\mathbf{r}$, low preload
C_f	maximum magnitude of $\mathbf{r}$, looseness fault
C_b	maximum magnitude of $\mathbf{r}$, backlash fault
C_f^*	maximum fault vector normalised against maximum nominal vector
$C_\theta,\ C_1,\ C_{12\beta}$	$\cos(\theta),\ \cos(\theta_1),\ \cos(\theta_1 + \theta_2 + \beta)$
${}^i c_j$	value of point ${}^i\vec{p}_j$ in histogram in plane (i)
$d,\ d_l$	prismatic looseness displacement
$\mathrm{mag}(\vec{\mathrm{D}})$	looseness index based on correlation vectors
$E[X]$	expected value of RV x
$\vec{E}$	cross product of maximum correlation vectors
$\mathbf{e}$	error of actual $\mathbf{p}$ from nominal $\mathbf{p}$
$\mathbf{F}$	vector of applied generalised forces
$\mathbf{f}$	six-element vector of end effector forces and moments
$f(x, y)$	function of x and y
$f_{xy}(x, y)$	two-dimensional probability density function (PDF) of RVs x and y
$f_x(x)$	marginal distribution (one-dimensional) function of RV x
$G(s)$	transfer function
g_i	value of datum at time $t + t_i$
${}^i h_j$	distance of point ${}^i\vec{p}_j$ from histogram centroid $({}^i\overline{x}, {}^i\overline{y})$ in plane (i)
$\mathbf{I}$	identity matrix
I	mass moment of inertia
${}_n\mathbf{J}$	Jacobi matrix (Jacobian) with n columns
$\mathbf{J}^T$	transpose of the Jacobian
$\mathbf{J}^{-1}$	inverse of the Jacobian
${}_n\mathbf{J}_i$	column (i) of Jacobian with n columns
$\mathbf{K}(\mathbf{q}, \mathbf{k_d}, \mathbf{t})$	vector of potential terms in dynamic equation of motion
$\mathbf{k}$	vector of kinematic parameters not including $\mathbf{q}$
$\mathbf{k_d}$	vector of dynamic parameters
$\Delta\mathbf{k}$	change in vector $\mathbf{k}$
$\tilde{\mathbf{k}}$	estimate of parameters in $\mathbf{k}$
L_i	length of link (i)
$\mathbf{M}(\mathbf{q}, \mathbf{k}, \mathbf{k_d}, \mathbf{t})$	mass matrix in dynamic equation of motion
$M_i,\ m_i$	mass of body (i)
m	number of degrees of freedom of end effector motion
n	number of joints
N_{para}	number of kinematic parameters
$N(x)$	normally distributed RV x

${}^{i}\mathbf{p}$	vector of end effector displacements with respect to frame (i)
${}^{i}\dot{\mathbf{p}}$	vector of end effector velocities with respect to frame (i)
${}^{i}\ddot{\mathbf{p}}$	vector of end effector accelerations with respect to frame (i)
$\mathbf{p}_l$	vector of end effector displacements with looseness
$\overline{\mathbf{p}}$	vector of end effector random displacements
$\tilde{\dot{\mathbf{p}}}$	vector of velocity estimates
$\breve{\dot{\mathbf{p}}}$	vector of random velocities
${}^{i}_{i+1}\mathbf{p}$	relative displacement of frame $(i+1)$ with respect to frame (i)
$\{{}^{i}\vec{p}_j\}$	set of j data points $({}^{i}p_x, {}^{i}p_y, {}^{i}p_z)$ in frame (i)
${}^{i}\vec{p}_j$	j-th data point $({}^{i}p_{jx}, {}^{i}p_{jy}, {}^{i}p_{jz})$ in frame (i)
P_{fd}	transitional probability between regions f and d
q_i	displacement of joint (i)
q_l	displacement of looseness joint
${}_{l}q_i$	displacement of looseness joint in link (i)
${}_{i}q_a$	displacement of actuator of joint (i)
$\mathbf{q}$	vector of joint displacements
$\dot{\mathbf{q}}$	vector of joint velocities
$\ddot{\mathbf{q}}$	vector of joint accelerations
$\mathbf{q}_l$	vector of joint displacements with looseness
$\overline{\mathbf{q}}$	vector of random joint displacements
${}^{i}_{i+1}\mathbf{R}$	rotation of frame $(i+1)$ with respect to frame (i)
$\vec{R}_i$	moment arm vector for revolute joint (i) motion contribution to $\mathbf{p}$
R_i	magnitude of $\vec{R}_i$
r	linear correlation coefficient
$\mathbf{r}$	correlation vector with magnitude r at direction ϕ
$S_\theta,\ S_1,\ S_{12\beta}$	$\sin(\theta),\ \sin(\theta_1),\ \sin(\theta_1+\theta_2+\beta)$
s	offset between common normals in Denavit-Hartenberg transformation
${}^{i}_{i+1}\mathbf{T}$	homogeneous transformation of frame $(i+1)$ with respect to frame (i)
t	time
Δt	time step
$\overline{x}$	mean of RV x
$\hat{\mathbf{x}}_i$	unit vector in x direction for frame (i) (along link axis in planar case)
$({}^{2}\mathbf{x}, {}^{2}\mathbf{y})$	plane of end effector motion in experiments
$\mathbf{y}$	vector of generalised coordinates for equations of motion
${}^{p}\vec{y}$	direction of random excitation
$\hat{\mathbf{z}}_i$	unit vector of joint (i) axis
$\hat{\mathbf{z}}_l$	unit vector in direction of looseness
z	model function of end effector motion RVs
α	angle of acceleration motions (Experiment Two)
α_3	skewness of sampled distribution of an RV
α_4	kurtosis of sampled distribution of an RV
β	angle of looseness (radians)
Δ_i	change in displacement of joint (i)
$\zeta,\ \rho$	azimuth and elevation of plane of interest
θ_i	(revolute) joint (i) displacement
μ	mean of a random variable (RV)

σ_x^2	variance of RV x
τ	n-vector of joint actuation torques (which may include forces)
τ^*	joint torques compensated for potential load
τ^{**}	joint torques compensated for potential load and contact force
Υ	combined vector of kinematic parameters $\mathbf{k}$ and $\mathbf{q}$
ϕ	direction of correlation vector
ϕ_f	estimated direction of looseness
Φ_i	joint offset of link (i) (planar case)

Chapter 1

Introduction

If you know what you're doing, you're not doing research.

Bertram N. Brockhouse, Nobel Laureate

An industrial robot, like any other machine, requires regular maintenance. Although maintenance ensures that process quality remains adequate in producing a competitive product, maintenance has both service costs and an opportunity cost of lost production. It is therefore necessary to have strategies to minimise the costs of robot maintenance [39].

The maintenance process is one of **Inspection** to monitor process quality and machinery condition, **Fault Diagnosis** to identify a problem with a machine, and **Correction** to remedy the fault in a timely way. Much effort has been expended in developing procedures to repair damage once it has occurred. Further effort has gone into developing inspection and condition monitoring techniques. But fault diagnosis is the key step to effective maintenance: timely identification of problems is what makes maintenance pay.

This work presents a strategy for diagnosing looseness faults in robotic manipulators.

The rest of this introductory chapter gives the scope of the problem of concern, the need for the work that was undertaken, and possible applications of the results.

The chapter concludes with an overview of the rest of the chapters in the present work.

1.1 Background Situation

Three maintenance strategies are in common practice: breakdown maintenance, preventive maintenance, and predictive maintenance.

Breakdown maintenance is simple: run the machine until it breaks. It requires little understanding of the process, although long outages are avoided if components are readily available to replace those with a short Mean Time Between Failures (MTBF).

Preventive maintenance involves checking a system at regular intervals and fixing whatever may soon be in need of repair [50]. The inspection interval is the Mean Time Between Inspections (MTBI), and the service interval is the Mean Time Between Servicing (MTBS). The probability that the system will not break down is low if the system runs with MTBF longer than MTBS[1]. The inspection interval MTBI and the anticipatory maintenance interval MTBS are each based on previous experience, the maintenance history, and remaining life models.

In predictive maintenance, equipment is monitored so that remaining life is predicted. There is no set service interval. If remaining life exceeds that of MTBI, then the equipment need not be serviced at the present time.

1.1.1 Nature of the Problem

Factories employing industrial robots typically use preventive maintenance to avoid unscheduled downtime [111].

This downtime could be significantly reduced by introducing predictive maintenance schemes, particularly in environments where it is hazardous or costly to have

[1]To ensure that MTBF is longer than MTBS, the system must run in one of two conditions: for all components, MTBF is greater than MTBS; or MTBF of a subsystem of parallel components exceeds MTBS. The present work does not consider robots with redundant systems.

humans doing inspections [94]. Equipment operating in such environments demands inspections and diagnostic routines that are remote—or even autonomous [119]. Such remote performance assessment and fault diagnosis leads to more efficient maintenance.

Users of industrial robots therefore need predictive maintenance strategies to make their robots more reliable [48].

1.1.2 Diagnostic Problem of Interest

Robots comprise a dynamic system with a mechanism, actuators to drive it, sensors to monitor its state, and a controller to command the dynamical system to achieve a desired state [133].

A diagnosis relates the effect of a problem in the system to the fault that is its cause. All elements of the robot system fall prey to faults, but some faults are more likely than others. To make the present work relevant, it is important to choose a problem that is of interest to robot maintainers and designers.

Robotic mechanisms have a number of flanged bolted connections, bearing seats, keyways, and other areas of mating parts that carry load. Increased compliance can degrade robot performance. There are reliability models that make general predictions as to how often fastened connections fail in service, but structural diagnostic tools for robot maintainers do not exist [39].

The problem of concern is that users of robots are not able to identify the location and the severity of looseness within the robot structure. This type of fault is of concern both to robot users and to robot manufacturers: each wants improved robot reliability.

1.2 Objective of the Present Work

The present work describes a method for identifying looseness and backlash faults in serial-link robotic manipulators. The method includes not only a technique for

recognising that a fault is present, but also a technique for determining the location of the fault on the mechanism.

Since most robotic manipulators are open kinematic chains, the focus is on open, serial link mechanisms with only one looseness fault at any time. The fault can be anywhere on the mechanism with no *a priori* knowledge of its location, and looseness motions need not be large.

Relevant previous work and diagnostic issues are discussed, solution techniques are proposed, simulation and experimental cases are presented, and the merits and limitations of the work are discussed with recommendations for future work.

1.3 Overview of Contents

The following chapters present a literature review of previous work, methodology for the investigation, implementation of the method, simulation results, experimental results, conclusions, and recommendations.

1.3.1 Literature Review

The review of the literature describes previous research efforts in supporting fields that contribute to the present work.

1.3.2 Methodology

The methodology chapter presents the scope of the present research, based on the gap between the problem and established solutions, and develops a methodology for solving the problem.

This chapter offers a set of hypotheses to be validated in the present work and discusses alternatives for tackling the problem. The methodology then focuses on the specific issues of exploiting the effect of random joint motions on end effector motions: locating extra degrees of freedom in a manipulator after searching for self-excited motions in the end effector.

1.3.3 Implementation

The implementation chapter describes how the hypotheses were validated. Specific strategies are discussed for implementing two methods of identifying structural looseness in a serial mechanism, first in simulation, and then by experiment.

1.3.4 Simulations

This chapter gives results of kinematic simulations of robot looseness faults. Simulated looseness motion distributions were used for preliminary assessment of looseness identification methods. There is a discussion of the modeling limitations that led to experimental studies to verify the simulation results.

1.3.5 Experiments

The chapter on experimental results considers the experimental aspect of the present work. Two multi-body rigs were built to investigate looseness motions. One unique feature of the present work is the use of the recursive Newton-Euler equations of motion in design iterations of sizing robot manipulator joint actuators.

A progressive set of experiments examined how end effector planar accelerations changed with looseness or backlash in the mechanism. Each of the experiments is described, including the experiment goal, method, equipment, and results.

Finally, this chapter interprets the experimental results and discusses how well the results achieved the desired goal of looseness identification.

1.3.6 Conclusions

The chapter of conclusions examines the merits and limitations of the looseness identification methods, assesses how well the methods addressed the stated problem, and summarises the original contributions of this work.

1.3.7 Recommendations

The final chapter recommends areas of further development of robot fault diagnosis methods for industrial implementation, and ends with speculation about the future of machinery diagnostics for robots.

Chapter 2

Literature Review

Nature, to be commanded, must be obeyed. *Francis Bacon*

This chapter reviews the robotics literature pertinent to looseness diagnostics, identifies issues in diagnosing faults in robotic systems, describes previous solutions, and notes the limitations of existing solutions for the present problem of looseness identification.

After a brief look at the general field of machinery diagnostics, the discussion turns to robot diagnostics. Performance criteria for manipulators are reviewed. Methods for assessing reliability of robot subsystems are discussed. Robot calibration is considered, with its emphasis on robot modeling and parameter estimation. Methods of analysing robot end effector motions are reviewed, both for structural analysis and rigid body analysis. Manipulability, the estimation of kinematic parameters from the Jacobian, and the concept of error envelopes lead to the methodology for identifying robot looseness faults.

2.1 Machinery Diagnostics

This section discusses the need for an effective quantitative monitoring strategy for robots and the requirements for a monitoring system for looseness.

2.1.1 The Need for a Monitoring Strategy

Industrial robots are not typically accessible for routine inspections and calibration checks, because the equipment operates at a high production rate in an environment hazardous to humans.

A typical practitioner of industrial robot maintenance is General Motors Canada, which does preventive maintenance of hydraulic power systems and breakdown maintenance of electric power, mechanical, and control systems. Chrysler Canada uses one-thousand hour preventive maintenance checks and daily checks of weld patterns to determine whether spot welding robots are maintaining product quality [111]. These maintenance strategies show that maintainers are not yet able to anticipate failures in most robot systems, despite the demand of the automotive industry for very high robot availability [90]. The robot maintenance philosophy is one of optimising breakdown maintenance to improve availability, and then using any emerging maintenance history to set preventive maintenance schedules.

The preferred strategy of predictive maintenance tracks equipment performance to anticipate its degradation. In robotic operations, tasks are structured with leeway in the manufacturing process for minor positional errors or vibration at the end effector [81].

Observing declining robot performance, however, requires measurements of outputs that represent the robot state as it affects task performance. But the goal of diagnostics must go beyond evaluating robot performance to identifying the cause of deficiencies in robots when they do not perform to specification.

Requirements for a Robot Monitoring System

Robot monitoring should not interfere with regular operation, and so inspection data should be collected remotely by a process integrated into the regular machine cycle. Monitoring priorities are categorised on two criteria: probability of failure for a given component, and impact on the robot system (and therefore product quality) should the failure occur. A fault severity index for each component is based on both criteria.

Probability of failure for an individual component is empirical information that comes from one of three sources: vendor tests to destruction, user tests to destruction, or in-service maintenance history that includes MTBF (and failure mode, for components that fail in more than one way) [50]. Expert systems have been used effectively in other fields [44], with the diagnostic system presenting either a single diagnosis or a set of possibilities with their respective probabilities. The result is based on the given *a priori* information (rules) and *a posteriori* information of present condition.

Assessment of the effect of a fault on the system comes from system analysis, and is machine dependent. Redundancy in the system with error correction capacity in the controller can reduce the severity index [50], but error correction is only possible if the robot is able to sense degradation in its own performance.

Since robots comprise actuation, sensing, and computer control subsystems driving a mechanism, faults in any subsystem affect robot performance. Auxiliary systems, such as power supplies (electrical or hydraulic), also contribute to performance. Moore [85] has also described the requirements of a robot health monitoring system, and Graham and Guan [49] described an approach for developing a knowledge-based robot diagnostic system. Neither was based on a system implementation.

The only experimental robot fault diagnostic work found in the literature was that of Tzou *et al* [117], who used an autoregressive model on time-series data of end-effector acceleration to identify a machine fault by pattern recognition of an archived fault signature. The present work, in contrast, concentrates on mechanical aspects of manipulator performance where model-based analysis is employed in the absence of records of fault signatures.

2.1.2 System Identification

Machinery diagnostics falls within the general field of system identification. The system identification problem is that of describing dynamic systems and estimating models of those systems [80]. Systems with little or no empirical maintenance history

rely on model-based analysis for fault models.

Both parametric and nonparametric system identification techniques are used, in time and frequency domains, but parametric methods have been preferred [29, 87], because robot mechanisms naturally lend themselves to lumped-parameter modeling. Adding appropriate parameters improves the fidelity of the model [73].

Nonparametric Methods

A nonparametric model description is not defined in terms of an equation with a finite number of parameters. Rather, it gives a representation of how the system responds using graphs, tables, or a range of the frequency spectrum.

The system response is based on an estimate of the output/input relationship, also called the transfer function. In a linear, time-invariant system, the system response in the Laplace domain is the transfer function. One transfer function estimation method is the power spectral density (PSD). The PSD gives a distribution of power with respect to frequency [29]. For stationary signals, the PSD is related to the autocorrelation $R_{xx}(t)$. The mapping from time to frequency is the Fourier transform, and the inverse Fourier transform of the PSD is the autocorrelation [52].

For diagnostic systems implemented on digital computers, data are discrete. A practical implementation of the Discrete Fourier Transform is the Fast Fourier Transform (FFT), which is an estimate of the power spectrum of a linear system. The data in the series are weighted (windowed) to satisfy the assumption of periodicity, and low-pass filtered below one-half the sampling frequency to avoid aliasing [75].

Nonparametric modeling techniques are appropriate for dynamic systems where there is no predefined dynamic model. Applications in robotics are presented in Section 2.3.1.

Parametric System Identification Methods

In a parametric system identification method, the system is approximated by equations of the state variables of a lumped-parameter model [37].

Appropriate modeling of robot kinematics or dynamics depends on the type of manipulator. An industrial robot, with its stiff links and tight joints, lends itself to parametric modeling.

Parameters are estimated using least-squares estimation, which minimises the merit-of-fit function that is the sum of squares of the residual between the data and a model of the data. For independent, normally distributed measurement errors with equal variance, the least-squares measure is a maximum likelihood estimator [56].

Models can be linear or nonlinear functions of the parameters. Parameters in nonlinear models are estimated using a nonlinear estimator such as the Levenberg-Marquardt method. This algorithm uses steepest descent parameter estimation when far from the minimum of the merit function, and continuously switches to an inverse-Hessian method when close to a minimum [87, 99].

2.2 Robot Diagnostics

Robot diagnostics work comprises measuring performance, scrutinising manipulator subsystems by modeling and analysis, and correcting a general model of the manipulator by calibration.

In developing a diagnostic system for a robot, the maintainer chooses systems of interest and appropriate system parameters to measure. The measurement method depends on the parameters and how they vary with time.

2.2.1 Robot Performance Criteria

The preliminary diagnostic procedure determines system performance against a standard. For industrial robots, accuracy and repeatability are the standards specified in the ANSI/RIA R15.05 and ISO/9283 Standards [55] and National Institute for Standards and Testing (NIST)[1] Designation F 1034-86 [1].

[1]The National Bureau of Standards (NBS) has been renamed the National Institute for Standards and Technology.

Alternative criteria have been proposed by Van Brusell [118] and Rivin [104]. Because the choice of performance specification is critical to gathering information about robot performance, measuring to a faulty standard would give an operator a false impression of adequate performance. Performance criteria appropriate for robots include: load (including moments of inertia for eccentric loads); velocity (path velocity of centre point of end effector or tool); accuracy of path; repeatability of path; fluctuation from path; acceleration (of joints or of end effector); positioning time (including stabilisation and settling time); and work space (including end effector orientation) [118].

The ANSI/RIA R15.05 Robot Performance Test Standard has attempted to standardise robot performance to the following criteria: static position accuracy, cycle time, overshoot, settling time, compliance, and point-to-point repeatability. There is no provision for testing path repeatability, path accuracy, or force control performance. Mooring and Pack describe a method for determining repeatability experimentally, with caveats about including the entire work space (including orientations) in the specification [88].

The ISO/9283 Standard describes performance tests inside a cubic workspace of the manipulator, including: unidirectional and multidirectional pose accuracy and repeatability, accuracy variation, cornering deviations, and static compliance at 100% of rated load [55].

There are a number of other robot testing standards [39]. Most measure static path errors across the entire workspace. The Ford method looks for duty cycle limitations by tracking the end effector in a cycling test of individual axes at full payload.

The position error of the robot end effector is the sum of the static and dynamic pose errors. Causes of static pose error include: digitisation error (finite encoder resolution); calibration error in joint offsets at home position and in joint gains; deterministic kinematic errors in geometric parameters; stochastic kinematic errors (imperfections such as friction and backlash imply that the joint angle can be any

value within one encoder unit of resolution [89]); and environmental effects (e.g. thermal expansion). Dynamic pose errors come from links and joints that are imperfectly rigid, inertia and/or gravity, and unmodeled dynamic effects such as friction and stiction.

Performance criteria presently do not consider the environmental impedance of the work space, except gravity fields, because the great majority of manipulators are positioning devices.

Looseness affects such performance criteria as pose repeatability and accuracy, trajectory variations, and structural stiffness.

Pose Measurement Tools and Methods

Pose repeatability is tested with a precision artifact (such as a cube) positioned in the workspace. A probe with sensors is held by the robot to measure the relative pose errors between trials.

Pose accuracy is more difficult to measure. The artifact method works when the position of the artifact is well known. Other methods for measuring end effector absolute position include stereo triangulation, laser tracking, ball-bar testing, and a test structure built around the robot.

Stereo triangulation uses two cameras located a fixed distance from each other detecting an illuminated target. Some systems use position sensitive devices to detect the centre of a point of light on a linear electro-optical array[2]. Cameras require precalibration; and the limit of accuracy is on the order of 1% of the range [137]. Range vision using stereo intensity images is an area of active research, but results to date are not accurate enough for measuring small looseness motions.

Theodolites have been used for tracking [125]. Although the measuring accuracy is excellent, the process is tedious. In a triangulation method, no direct length measurement is done. Laser tracking systems using triangulation and time-of-flight for ranging can locate targets accurately and automatically.

[2]These systems are also used for motion studies in biomechanics.

The Ford method uses a vision system to track the end effector in cycling tests. The NIST method continuously controls the angles of a laser beam projection so that the beam impinges on a target mirror on the robot wrist. Chesapeake Laser Systems uses a retro-reflector on the end effector aimed by three split-beam lasers to acquire three length measurements by interferometry; from this information the spatial position is calculated from triangulation data [39]. Although such systems are expensive and have limited depth of field and bandwidth, development efforts are producing higher performance systems at lower cost. Laser interferometry shows promise for measuring vibrations without contact at a distance.

Coordinate measuring machines (CMM) are instrumented mechanisms with multiple degrees of freedom (DOFs). When the tip contacts a target on the end effector, the robot and CMM form a closed kinematic chain by connecting the end effector to ground [87]. The disadvantage to a CMM is bringing it to the robot and having it large enough to span a significant portion of the robot workspace.

A single-pose position check is an automatic method to monitor performance. The manipulator occasionally stops regular operations to reach toward a sensor within its workspace. The sensor measures the positional accuracy of that particular motion [87]. This performance criterion simplistically assumes that if the manipulator can reach the sensor location accurately, then the robot works properly in the entire workspace. The single-pose accuracy check does, however, determine whether a kinematic calibration is still valid, for at least a subset of the kinematic parameters.

Although looseness contributes to manipulator positional inaccuracy, no method for identifying looseness from change in end effector position has been described.

Trajectory Variations

Bennekers and Teal [21] implemented a runaway protection system that permits a finite variation from the nominal joint trajectory before shutting down the manipulator. But this diagnostic criterion is based in joint space, not task space, and so any errors in mapping from joint space to task space go unmonitored. As well, the

variation in task space for a given variation in joint space depends on the dynamics in a given pose. In looseness, trajectory variations in task space are expected, because of the uncontrolled DOF that looseness adds. Visinsky *et al* used the nominal equations of rigid-body motion to weight the allowable error in acceleration given the manipulator state, where the fault was a static change in a dynamic parameter [121].

Other Observable Robot Parameters

System outputs other than motions can be measured as well, such as bearing temperatures, actuator power consumption (e.g. motor current and voltage), and sound emissions from the manipulator. The monitoring strategy demands that the measured parameters relate to possible faults. The next section discusses whether these parameters can be applied to diagnosing robot looseness faults.

2.2.2 Subsystem Analysis

Mechanical problems can plague bearings, power transmission elements, actuators, and the structure itself [16]. Some measurable outputs from the robot system are useful for robot looseness diagnostics.

Monroe [84] implemented diagnostic programs based on vibrations of PRAB FA600 robot components that remain nominally fixed, such as the hydraulic unit. He also relied on hydraulic fluid temperature measurements, another robot parameter that is relatively stable when a hydraulic robot is operating normally. Looseness faults were not investigated.

Bearing condition can be monitored by temperature or vibration measurement. Temperature thresholds indicate poor performance, as do peaks in power spectra of vibration signals that correspond to bearing kinematics [76]. Measurements are made at the bearing block [83], requiring one sensor for every bearing. Vibration analysis relies on the transmission of bearing noise through a structure to a transducer [6]. Although a vibration is measurable at a distance, the structure affects the signal,

especially for changing robot poses.

Looseness can develop in a journal or rolling-element bearing, and so vibration monitoring is an appropriate diagnostic technique, particularly if transducers are mounted close to the bearing of concern.

Gear faults, such as backlash and misalignment, can be found by analysis of gearbox vibrations. Gear meshing frequency components are enhanced by cepstrum processing [52, 102, 76]. Damage to gear teeth or bearings can be found by ferrography in gearboxes with circulated lubricant; the composition of metal filings filtered from the lubricant determines the worn component. Ferrography is not appropriate for robot gear train diagnostics, because lubricants are not circulated.

Looseness in the drive train of a robot causes torque variations. An electric motor can itself act as a torque transducer, because it generates a back electromotive force (EMF) when subjected to mechanical load. Kryter and Haynes [66] measured torque variations via current fluctuations on motor-operated valves, which, like robots, have a time-varying operation cycle. The advantage of this method is that motor current can be measured remotely along the motor power cables using standard current probes with no additional instrumentation on the robot. DC servomotor current measurements have been used for torque-based control, but not yet for robot diagnostics [74]. The potential problem with motor-current analysis is that the energy dissipated by the load due to damage may be so small that the motor current may be only slightly affected—analogous to the attenuation of vibration signals through the structure.

Other power transmission elements used in robots can also be examined by vibration analysis or transmission torque measurements: couplings, belts, clutches and chain drives.

Robot diagnostic systems based on acoustic signals have been proposed [86]. Such a system would have to be able to identify damage-related sounds and separate that information from ambient noise.

In any monitoring effort, the measured system parameter must be affected by the

fault of concern: looseness.

Statistical Reliability Analysis

The methods described in the previous section use a deterministic relationship between the measurement of a parameter representing a fault and the root cause, from which comes a diagnosis for predictive maintenance.

The alternative is to use a probabilistic approach. Čačko [33] noted that few deterministic signals can be collected from mechanical structures, and that a probabilistic model would include differential equations describing the dynamic structural behaviour, service experience, theoretical and experimental analyses of strength of components, dynamic analyses of structures (modal analyses), and reliability models. Cempel [34] used a Weibull distribution to model a group of machines (fans, not robots) to calculate the breakdown rate.

Dhillon [39] described several models for robot maintenance, all relying on having either foreknowledge of the reliability of the robot components, or a probability density function of the time between failures, or the failure rate of the overall subsystem of concern. Such failure data and analysis are useful for estimating the reliability, availability, and failure rate of the robot system or its components. From that comes the maintenance requirements and a determination of any deficiencies on the design. Such a method requires a failure reporting and documenting system (a maintenance history archive) that must be error-free and easy to use.

Dhillon noted that bearing failures (which can cause general looseness at a joint) range from 0.1 to 207 failures in 10^6 hours of general machine operation, as opposed to 3 to 5 failures of gears in 10^6 hours (which causes backlash). The failure rate of properly installed bolted connections was 4.8 failures per million hours; there were 600 failures per million hours due to improper installation. Performance unreliability in torquing was only 0.0048. Backlash modeling is thus more important for control than for maintenance.

Liégeois [69] discussed refining error models by incorporating data on statistics of

causes of errors at joint variables and an overall model of disturbances to a manipulator. The need for occasional calibrations to correct for faults in the mechanism is mentioned with no method. The goal was to compensate for errors without modeling error locations, by measuring end effector motions. This method was extended by Whitney *et al* for robot kinematic calibration [125].

Although a reliability analysis is a useful approach, much of the necessary probabilistic data will not be available for a given machine. Reliability data sources can provide approximate data for reliability of generic parts, by combining information from the literature, laboratory tests, event data banks, field failure data collection, and expert judgments. But the confidence interval of a diagnosis may not be acceptable if the information is too general and has too high a variance.

2.2.3 Robot Calibration

The diagnostic focus for robotic manipulators has been calibration. Robot calibration is the process of estimating parameters of a rigid-body robot model, usually from a model relating joint and end effector displacements. Good discussions of robot manipulator calibration are found in Mooring [87] and others [106, 58, 24], focusing on kinematic calibration.

Calibration includes four steps: choosing the model, measuring the behaviour of the system, analysing the data to extract good estimates of the actual parameters, and correcting the model with the new parameters. Incorporating estimates of the real kinematic and dynamic parameters of the robot mechanism, the improved model more closely emulates the actual behaviour of the robot.

Improved models benefit both offline programming and diagnostics, although the thrust of work in calibration has been increasing accuracy of manipulators, not diagnosing faults. Because robots of the same type are not truly interchangeable, each robot must be calibrated individually [87]. For diagnostics, periodic recalibrations track changes in a manipulator as it ages. Everett [24] does mention that actuators wear out and gears wear down, but offers no strategy for identifying the presence of

such errors in a manipulator.

Levels of Calibration

There are three progressive levels of model validation in robot calibration: sensor/actuator kinematics and dynamics, manipulator mechanism kinematics, and manipulator dynamics [106]. The majority of robot calibration work has focused on manipulator kinematics, finding the geometric parameters that define the robot kinematics [58]. Dynamic calibration is an area of active research, particularly for flexible robots.

Component Calibration

The first category of calibration is a straightforward estimate of terms of the function

$$q = f(q_a), \tag{2.1}$$

where q_a is the component input and q is the output. For a linear sensor, Equation(2.1) becomes

$$q = k_0 + k_1 q_a, \tag{2.2}$$

where k_0 is the offset and k_1 is the gain. Sensors and actuators are usually chosen to be approximately linear, and seldom require recalibration unless a highly accurate model is demanded.

Hughes and Ranganathan [59] examined robot sensor reliability by considering sensor performance over time compared to other sensors while a robot was operating. They used a Kalman filter to estimate how sensor data should relate to robot activities being measured by other sensors.

Kinematic Calibration

The second level of robot calibration has received the most attention [87, 58]. The static accuracy of the manipulator is of concern: given a vector of joint variables $\mathbf{q} = [q_1, q_2, \ldots, q_n]^T$, how closely does the modeled manipulator end effector position $\mathbf{p}_{\text{model}}$ come to the measured position $\mathbf{p}_{\text{actual}}$?

End effector position is a function of joint displacement variables and geometric parameters. There are two types of kinematic error: dimensional errors in the links, and joint variable errors. Dimensional errors are the result of manufacturing tolerances, thermal expansion, and other distortions [82]. A level-one calibration may not reveal all aspects of joint errors, because linkages between sensor motion and joint motion may have errors themselves.

Kinematic Modeling

To describe the kinematic motion of a manipulator includes determining the position of each link with respect to an inertial coordinate frame (w). The manipulator may be modeled as a series of spatial displacements of rigid bodies[3].

A spatial displacement in three-dimensional Euclidean space generally requires six independent parameters [105]. The standard formulation for a spatial displacement in robotics is the homogeneous transformation [36, 97, 81], because homogeneous transformations obey the rules of linear algebra. A finite screw is an equivalent formulation [107]. Ohwovoriole [92] extended screw theory to include ranges of motion where infinitesimal displacements can break contact with the surface of contact; the repelling screw [105] could be applied describing rigid-body motion due to looseness.

Figure 2.1 shows one description for the displacements from link to link. The position of the tool frame (t) on link (n) with respect to the world frame (w) is described by the homogeneous transformation

$$ {}^{w}_{t}\mathbf{T} = {}^{w}_{0}\mathbf{T}\,{}^{0}_{1}\mathbf{T}\cdots{}^{n-1}_{n}\mathbf{T}\,{}^{n}_{t}\mathbf{T}. \tag{2.3} $$

If the frame is located *arbitrarily* in the link, at least six parameters are required for the spatial displacement [78]. Denavit and Hartenberg [53] reduced the required number of parameters to four, by aligning one of the unit vectors of a rigid link frame

[3]The convention used is this work is Craig's method [36] of attaching a coordinate frame to the proximal end of each link. This approach has two advantages: it includes a base frame (0), and it has frame (i) coincide with joint (i). Paul's notation [97] fixes the frame (i) to the distal end of link (i) at joint ($i+1$), so that the tool frame is frame (n).

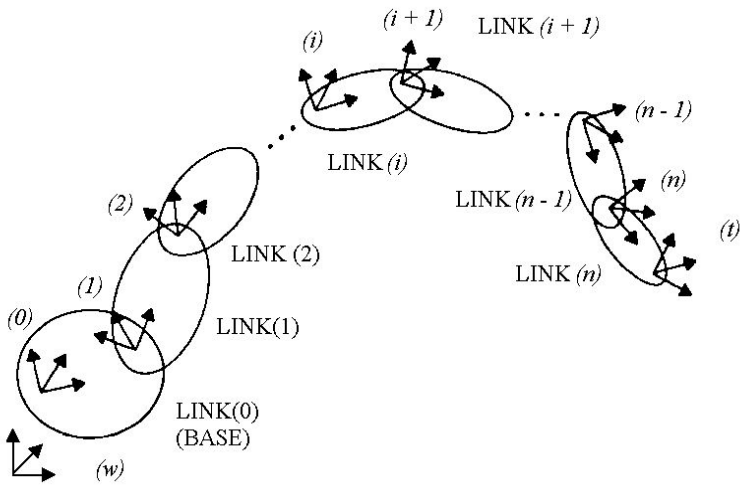

Figure 2.1: Serial link manipulator frames

in the direction of the associated lower-pair joint axis[4].

A Denavit-Hartenberg (D-H) formulation [53, 97, 138] completely describes the position and orientation of link (i) with respect to its neighbour with the following four parameters: α_i, the twist in link (i); a_i, the length of link (i) from joint axis (i) to axis $(i+1)$; s_{i+1}, the offset at axis $(i+1)$ from the common normal along which a_i is measured; and θ_{i+1}, the angle of joint $(i+1)$. In the case of a prismatic joint, where no rotation is involved, two parameters suffice.

Everett and Mooring [45] defined characteristics that a kinematic model must have: completeness, equivalence, and proportionality.

Completeness demands that the end-effector location with respect to a fixed reference frame can be described using only the parameters of the model. The minimum number of parameters for a kinematic model of a spatial mechanism with revolute and prismatic joints is

$$N_{\text{para}} = 4R + 2P + 6 \tag{2.4}$$

where N_{para} is the number of parameters, R is the number of revolute joints, and P is the number of prismatic joints, and the world frame is coincident with the first

[4]Higher-pair joints can be modeled as combinations of links with lower-pair joints [41].

joint frame when there is no joint motion. Six additional parameters are included to locate the position and orientation of the end effector on the most distal link.

Equivalence requires that a model can be transformed into another model with a different parameterisation. Complete models are equivalent.

Proportionality requires that small changes in position result in only small changes in the geometric parameters. The D-H method is inordinately sensitive to errors of alignment between adjacent parallel (or nearly parallel) joints. When adjacent axes are nearly parallel, small changes in alignment between the axes result in large changes in the location of the common normal (the offset s). Hayati [54] added a fifth parameter to maintain proportional changes in link parameters for small geometric errors in for the near-parallel case. This specific model still has four parameters, with proportionality. It would be important in adding looseness to a kinematic model that other parameters not be grossly affected.

Other model conventions have been proposed. Mooring [87] employed Rodrigues's equation [78], which uses a much different parameter set than the D-H formulation, defining each joint axis by a point through which the axis passes (in say, a plane perpendicular to the current axis) and a unit vector along the new axis, for a total of four parameters.

Stone, Sanderson, and Newman [114, 115] developed the S model, with five geometric parameters and one joint variable, in a set of equations that can be manipulated to extract the D-H parameters. Encoder calibration errors, machining tolerances, and assembly errors were assumed to be static and to have Gaussian distributions. Compliance in joints and links was assumed to be negligible. This approach was appropriate for calibration, but not for looseness diagnosis.

A number of researchers have examined the effect of errors in the model. Their results are pertinent because looseness is a time-varying kinematic error.

Ibarra and Perreira [62] related small variations in end effector pose to differential change in geometric parameters and joint variables, as did Driels and Pathre [42]. Paul developed a similar method to generate equations for control [97]. Menq and

Borm examined the sensitivity of end-effector accuracy to normal random errors in kinematic parameters [82], and they went on to determine optimal measurement configurations based on an observability measure [28]. Everett [24] noted, however, that as the observability measure increased, so did the measurement error, and so he suggested using weighted least-squares estimation to account for the range of work space measurement variances. Kumar and Waldron [67] looked at the effects of joint errors on static end effector position. They developed a method for finding probability contours of accuracy at locations inside the manipulator workspace to build a map of positioning accuracy.

Chen and Chao [35] used Sheth and Uicker's nominal transform (with six parameters) to model geometric errors in the link proximal to the joint. A second transform models geometric errors as a differential displacement after the nominal transform, and joint displacement appears in a third transform. Since axis variation is included in the differential displacement transform, the model maintains proportionality in the angle of axis variation. Everett [46] derived the error function for differential changes in the parameters from Sheth and Uicker's formulation. Driels and Pathre [41] extended the method of software error correction for coordinate measuring machines to compensate for geometric position errors and thermal effects and applied it to robot modeling. Their model allowed revolute and prismatic axes, including bearing eccentricity.

These researches support the conjecture that the fault can be modeled kinematically by considering looseness as an unactuated joint added to the mechanism.

Kinematic Calibration Schemes

Four types of kinematic calibration for robots have been described in the literature: differential-movement parameter estimation, pose-correction compensation, independent-axis analysis, and parameter estimation with kinematic loop closure [87, 118]. In all cases, the parameters to be estimated are the actual values of joint variables $\mathbf{q}$ and geometric parameters of the links $\mathbf{k}$.

In the method of **differential movements**, the actual end effector position is measured in the workspace. The error between the actual position and the desired one is considered a differential movement [97].

Wu [127] used the D-H model with geometric parameters as variables. By assuming that the trial kinematic parameters were close to the actual ones, he needed only to keep the first order terms of differential deviations of the D-H parameters to generate a linear least squares estimation approach. To first-order accuracy, the error in end effector position $\Delta\mathbf{p} = \mathbf{p}_{\text{actual}} - \mathbf{p}_{model}$ caused by errors in $\mathbf{q}$ and $\mathbf{k}$ is

$$\Delta\mathbf{p} = \mathbf{J}_{\text{id}}\ \Delta\tilde{\Upsilon}, \tag{2.5}$$

where $\mathbf{J}_{\text{id}}$ is the identification Jacobian relating changes in end effector position to changes in kinematic parameters, and $\tilde{\Upsilon} = (\mathbf{q}^T, \mathbf{k}^T)^T$. Later, Veitschegger and Wu [120] extended this model by including second-order terms.

Because $\Delta\mathbf{p}$ is a 6-element vector (at most) and $\Delta\tilde{\Upsilon}$ is an N_{para}-element vector, $\mathbf{J}_{\text{id}}$ is underdetermined. Multiple poses generate a sufficient number of equations to solve for $\Delta\tilde{\Upsilon}$ [54].

To find the best estimate of $\tilde{\Upsilon}$, the change in parameters $\Delta\tilde{\Upsilon}$ can be added directly to the current guess for the actual parameters until convergence occurs. Such an iterative method works well in linear least-squares estimation if errors in the parameters are small [87]. Kalman filtering has also been used to estimate parameters recursively as the pose set is generated [87]. When it is possible that errors in parameters may be large, a nonlinear estimator is used [99].

The **pose correction method** is referred to as inverse calibration. Shamma [109] used a set of measurements of errors between actual and desired pose to produce a correction function of the encoder values. During operation, the controller calculated nominal encoder angles based on the nominal (approximately correct) inverse kinematic model. The controller added a correction to the angles to bring the manipulator closer to the desired pose. This approach could be used diagnostically to augment a runaway protection system, with allowable motion variance as a function of task-space variables.

Stone [114, 115] developed the **direct axis measurement method**, which locates each axis in space. This is done by moving individual joints and measuring the end effector motion during each motion using a nonlinear estimation algorithm. The geometric parameters are then extracted directly from the axis line equations without the need for a nominal set of parameters [118]. The user can use any desired convention, guaranteeing that the model will be complete and equivalent to any other complete model [87] (although the location of the base with respect to the world frame (w) and the sensor location with respect to frame (n) must be established by other means). The versatility of this approach is a considerable advantage for looseness diagnostics, because it may be possible to find the line equation of a looseness joint and thus find its location on the mechanism. But detection of the unactuated looseness joint would require external excitation.

Bennett and Hollerbach [22] used the **kinematic loop-closure method**, incorporating a passive mechanism to close the kinematic chain from the end effector to ground. Using the displacement equation of the resulting closed-loop mechanism, parameters are extracted by nonlinear estimation without an external measurement technique. Because passive kinematic constraints locate the end effector, autonomous calibration can be performed much faster than methods requiring pose measurements. The passive constraint must, however, be well located and cover a reasonable portion of the workspace, and the manipulator must be able to move with the passive mechanism while the calibration takes place. We observe that looseness would make it easier for the manipulator to move with the constraint, because of the extra DOF. A loop-closure method would also require some means to account for the motion due to the unexpected DOF of looseness.

Recently, kinematic relationships other than displacement have been applied to robot calibration. Bennett and others [23] proposed kinematic calibration of a nonredundant revolute manipulator by extracting kinematic parameters from the Jacobian, using velocity and static force equations; and Canepa and others [31] used triaxial accelerometers to calibrate a revolute manipulator. These approaches require

that all joint motions be known, which is not possible with looseness.

Limitations for Looseness Diagnostics

There are limitations to manipulator kinematic calibration where looseness is concerned.

Kinematic calibration is concerned only with time-invariant parameters of the robot. Even repeatability studies look for the static positional error after a manipulator has stopped moving [87, 101], and are not suited for finding non-kinematic errors, which are also called nongeometric errors. If non-kinematic errors are detected, then a kinematic model attempts to reconcile the data in the kinematic parameter fit.

Faults producing nongeometric kinematic errors can not be resolved with static kinematic calibration techniques; nongeometric fault parameters must be included *a priori* into augmented kinematic models. Looseness errors are nongeometric errors.

Consider a single DOF revolute manipulator with backlash in joint (i), that is, looseness between power-transmission elements that results in a joint error. For a nominal value of q_i, the joint displacement can lie in the range from $q_i + \Delta q_i$ to $q_i - \Delta q_i$. It is not possible to resolve the error in terms of static equations involving kinematic parameters that are assumed to be time invariant.

Level Three: Dynamic Calibration

The highest level of robot calibration estimates parameters for a dynamic model of a manipulator. As well as inertial terms, the model may include such non-kinematic effects as backlash, link flexibility, and friction. Although rigid-body dynamical models suffice for robots with stiff links and non-compliant joints, robots with flexible links require terms to account for flexible modes in the links. Joint compliance also introduces a need for extra terms [125].

Whitney, Lozinski, and Rourke [125] included nongeometric errors (joint compliance, gear eccentricity, and backlash) in their manipulator model. They accounted

for nongeometric errors by testing for (or assuming) the form of the error and including coefficients of the model in the calibration scheme.

Tuttle and Seering [116] modeled a harmonic-drive gear transmission, a high-reduction type common in electric-motor driven manipulators. The models of friction, compliance and kinematic error were dependent on position and velocity. Numerical simulations of velocity step-response curves for the non-linear, second-order model compared favourably with experimental results.

Including nongeometric terms in the manipulator model is an effective method for diagnosing a set of faults that are modeled. But any fault not included in the set would not be detectable.

The controller and the working environment also contribute to the dynamic calibration problem. Controllers can contribute to non-kinematic errors because the Jacobian is updated at a slower rate than that of servoing, and velocities are assumed to change linearly between commands, which is not the case [136]. Hogan investigated how the working environment affects manipulator performance [57]. Payload mass lowers natural frequencies [26, 104], and liquid environments increase damping, also affecting frequency response. A manipulator in contact with an object may have a very different frequency response than a free-standing one. When monitoring, the manipulator should therefore be in its usual working environment with no payload.

Few researchers have tackled the problems of dynamic calibration, no doubt daunted by the number of parameters required for even a simple manipulator with rigid links [106]. One exception is the work of Atkeson, An, and Hollerbach [14], who recast the Newton-Euler equations of motion into a set of equations

$$\mathbf{w}_{ij} =_{ij} \mathbf{A}\kappa_j. \tag{2.6}$$

The 10-vector κ_j is a 10-vector of unknown inertial parameters of link j, ${}_{ij}\mathbf{A}$ is a 6×10 matrix of link (j) motions with respect to joint (i), and $\mathbf{w}_{ij}$ is the 6-element wrench at joint (i) due to motion of joint (j) alone. Each wrench can be transmitted across neighbouring links geometrically. Changes in the inertial parameters between tests would indicate that the mechanism had changed. But it would not be possible

to decide in advance where to include the looseness in the model. This method requires measurements of joint motions and torques. Motion of a looseness joint is unobservable unless instrumentation is installed at every possible looseness location, which is impractical.

2.3 Analysis of Robot Motions

Since the end effector motion is of diagnostic concern, the analysis of structural motions and of motions from joint actuations is of interest.

2.3.1 Structural Motions

Modal analysis is used to estimate the flexible modes of a structure. Linear analysis methods are well known and reliable [29, 52]. But modal analyses of robotic manipulators are made difficult by the nonlinearities inherent in the mechanism: each robot pose forms a different structure.

Modal analyses of robots have qualitatively shown that changes in the robot structure do change the structural dynamics of a manipulator [104]. Attempts by Kolhatkar [65] and by Van Brusell [118] to perform experimental modal analysis were restricted to single poses, but the results were in good agreement with mode shapes derived from finite-element models.

Dakalakis [38] showed that the coherence of the vibration with respect to the joint excitation is sensitive to the condition of the manipulator, and Bicker and Daadbin [26] showed that payload, backlash, and configuration affected vibration spectra at the wrist. No attempts were made to diagnose a fault based on vibration data only.

One limitation of applying modal analysis to robot looseness diagnostics lies in the nonlinear nature of the structure [134]. Nonlinear systems have modes that change with state: each different pose of a manipulator has a different inertia matrix. The other limitation for looseness diagnostics is developing a good model of the looseness of concern within the mechanism without necessarily knowing the geometry and

material properties in advance.

Some work [20] has been done in including nonlinear elements in modal models; the behaviour of the nonlinear element must be known *a priori*, a condition that is not met in most diagnostic situations. Unlike linear modal analysis, it is difficult to relate the identified parameters from a nonlinear modal analysis to the physical structure.

Xingui and others [131] examined coupling effects in a manipulator model with two flexible links. They considered the excitation of the structure to be velocity sources at the joints, but without experimental results. Zati and ElMaraghy [135] used a flexible link model for control. Youfang [134] recast the problem as a multiple-DOF vibration problem with forced excitation and parameter excitation to eliminate the coupling effects of rigidity and flexibility in the kinematic chain. Wyckaert and others [128] focused on the behaviour of a single flexible link, whereas Wang [124] modeled flexible robot links using transfer functions.

El-Saeidy [43] developed a detailed finite-element model of a geared joint with roller bearings (but no clearances). Xiaojiang and others [130] examined the frequency response function of a bearing assembly, and noted the nonlinear response as clearance developed. Mannan [77] investigated cracks (which may include flaws, cracks, looseness, and improper assembly), but only in otherwise solid, homogeneous pieces.

In some robotics applications, joint structural dynamics are of more concern than flexibility of links [104]. Readman used perturbation methods to isolate the high-frequency response of flexible joints modeled as second-order systems. Backlash was mentioned as a possible fault of concern, but it was not included in the model [103].

Vibroimpact studies have developed analytical models of impact regimes and limit cycles [74, 112] for harmonic excitations given quasistatic contact (no bounce) with linear contact stiffness. Natsiavas [91] developed a more representative model of an oscillator that allowed bounce at contact and stiffness and damping during free motion.

Because the limit cycle introduces a gap in the mechanism where there is free travel and zero stiffness, the stiffness function is nonlinear. This nonlinearity means that a number of different harmonic responses can not be superimposed to glean the response to an excitation with several frequency components. Although it is possible to model a pair of vibrating bodies with clearance, the resulting impact models are dependent on contact stiffness, gap size, and coefficient of restitution, which are difficult to estimate in most robot looseness situations. Some finite-element analysis packages now include nonlinear contact-dynamics analysis. Relating the modeled looseness motion to end-effector motion could then be done by modal analysis, but such work has not been found in the literature.

Vibration monitoring has been very successful in diagnosing faults with process machinery operating in steady state [29, 76, 83]. This analysis method offers promising advantages for robot monitoring, including remote assessment of performance before removing a machine from service, fewer fixtures, and less downtime for inspection.

Vibration monitoring has not been fully assessed for its usefulness in manipulator looseness diagnostics, since robots have changing configurations and do not operate in steady-state. The influence of looseness on manipulator vibrations is also not known. Analysis of transient end-effector motions using wavelet or Wigner-Ville transforms has not been reported.

Since most robots will not have detailed vibration-analysis information in the maintenance history, model-based analysis is necessary, particularly in factories wishing to use off-line programming. In that situation, an accurate robot model is essential. Practically, however, it may be difficult to produce and verify a sufficiently accurate model of the robot structure.

2.3.2 Rigid Body Analysis

Rigid-body analysis may offer a sufficiently faithful dynamic model for relating looseness to changes in the manipulator at the end effector without the demands of struc-

tural analysis.

Manipulability Measures

Manipulability is a measure of the ability of a manipulator to move its end effector within the workspace [133]. It is related to the condition number of the Jacobian. For a manipulator with n joints that spans an m-dimensional workspace, normalised joint velocities allow end-effector motion in an m-dimensional ellipsoid, with the principal axis in the direction of fastest motion.

With extra motion from looseness, the manipulator gains an additional, passive DOF. This change in manipulator configuration affects the Jacobian, and with it the manipulability. Orin and Schrader [93] described methods for computing the Jacobian given the manipulator kinematic parameters, from which the manipulability measure can be found. But no method has been found in the literature for estimating manipulability experimentally, which could be applied to looseness identification.

Error Envelopes

A concept related to manipulability is the error envelope, the set of differential displacements caused by errors in kinematic parameters [82].

Independent, normally distributed errors in n parameters produce an n-dimensional ellipsoidal error envelope [95, 99]. If the differential displacement error caused by one parameter (or more than one) is not independent and normal-randomly distributed, then the envelope is not ellipsoidal.

The shape of the error envelope is thus the manifestation at the end effector of probabilistic changes in parameters. Parameters associated with looseness contribute to the error envelope [70], but the effect of looseness on error envelopes has not been investigated.

Estimation of Parameters from the Jacobian

The Jacobian matrix relates joint motions to end-effector motions, and it is a function of geometric parameters only. Knowing the joint and end-effector motions, then, allows the geometric parameters to be estimated for non-redundant serial manipulators with revolute joints [22, 61].

Since there are identifiable changes in end-effector kinematics with changes in parameters, and since there are mathematical relationships between end effector kinematics and those parameters, it is possible to use kinematic motion relationships to diagnose looseness faults in robots in terms of changes in kinematic parameters.

2.4 Summary of Previous Work

This chapter has given an overview of the theory and technology pertinent to robot diagnostics and to the problem of finding looseness in the robot mechanism.

System identification and machine monitoring techniques are of concern, with specific attention to modeling manipulators for calibration, vibration and modal analysis, vibroimpact models, manipulability, the concept of error envelopes, and schemes for kinematic parameter estimation using the Jacobian relationship between joint motions and end-effector motions.

Limitations in Diagnosing Robot Faults

There are limitations in existing analysis methods for diagnosing structural faults with robotic manipulators.

The major effort in robot modeling to date has been in rigid-body kinematic and dynamics models [58, 87]. While diagnostic models will include such models, they may also include other relationships between system inputs and outputs.

There has been little effort to weigh the merits and demerits of different input/output combinations for validating robot models. The sensitivity of different modeling techniques to looseness has not been addressed. In the present context,

there is a need to evaluate different models of manipulators to find single looseness faults from observable robot variables, preferably at the joints and at the end effector. With an effective modeling and analysis strategy, a methodology for identifying robot looseness faults can be developed.

Chapter 3

Methodology

The function of geometry is to draw us away from the world of the senses and of corruption, to the world of the intellect and the eternal. — *Plutarch*

This chapter develops a technique for identifying looseness in robotic manipulators. The hypotheses to be validated are presented, a methodology for testing the hypotheses is suggested, and an overview is given of the theoretical development necessary to fulfill that methodology.

An examination of alternatives for modeling the system with looseness led to the choice of a kinematic model. The effect of looseness on the model was considered, along with options for locating the source of looseness in the mechanism. The limitation of recursive geometric parameter identification was uncovered, and a strategy was developed for using pose sets to find the link where looseness occurred.

The link identification strategy required an estimate of the direction of looseness motion at the end effector. Three alternatives were evaluated, and two were chosen for implementation.

3.1 Hypotheses

Three hypotheses address the problem of diagnosing structural faults in robots:

1. faults have observable effects that are repeatable;

2. the effects can be measured; and

3. the effects can be related to their respective origin using model-based analysis.

Each subsequent hypothesis relies on the validation of the previous hypothesis. Without theoretical and experimental support for all of the three, it would not be possible to establish the diagnostic connection between faults and their effects.

3.1.1 Looseness Identification Requirements

A diagnostic method has to have the following characteristics: a repeatable effect exists that relates to the fault of concern; the effect is measurable; and a relationship is established between the measured effect and the root cause.

The looseness identification method had to meet all three criteria, and so it was necessary to validate all of the hypotheses to meet the diagnostic criteria. The first criterion depended on the system of concern: either a causal diagnostic relationship existed or it did not. The second and third criteria defined the two steps of the method: motion caused by looseness was measured, and that motion was related to the location on the manipulator where the looseness existed.

3.2 Modeling Looseness for Diagnostics

Two desired characteristics of a looseness identification method were that little *a priori* information was required to identify a fault, and that few extra parameters were added to a model in order to describe the fault. An alternative to the second characteristic was the existence of an uncomplicated nonparametric fault signature.

3.2.1 Error Envelope Modeling Alternatives

To calibrate a physical system, parameters of a lumped-parameter model change to produce a minimum value of a goodness-of-fit criterion (usually minimum mean-

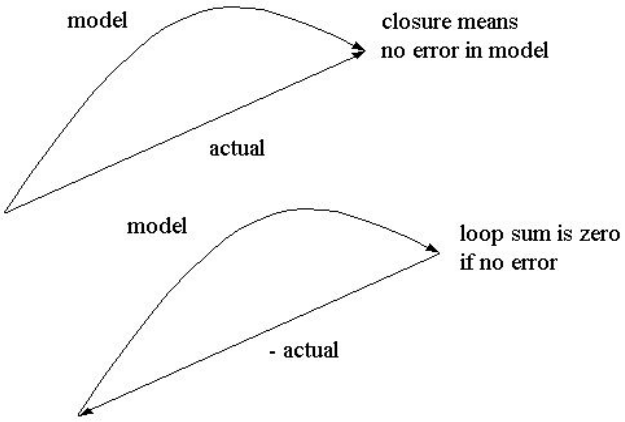

Figure 3.1: Modeled values and actual values ideally summing to zero

square error) between the value produced by the system and the values expected from the model (or from a known standard) [87, 106]. When there is no error, the difference between the actual values and the model values is zero. This concept is illustrated in Figure 3.1.

The seven modeling alternatives for mechanism calibration equations are:

1. displacement,
2. velocity,
3. acceleration,
4. static force,
5. unconstrained dynamics,
6. lumped-parameter, flexible-body dynamics, and
7. constrained dynamics.

Each alternative is based on a different set of modeling assumptions about the physical system.

In static-force balance equations, force is a node variable and displacement is a loop variable[1]. Time derivatives of displacement—velocity and acceleration—are also loop variables. In kinematics, these are the motion variables used to build descriptions of the motion of each part of a mechanism. The assumptions of static-force balance and kinematics are that bodies are rigid, and forces do not produce motions.

Any valid set of loop or node equations can be used to model the system. The model choice is driven by the parameters of concern.

In dynamics, force is also called an effort variable; the complementary variable is a flow variable. A dynamical system can have several combinations of efforts and flows: a hydraulic robot may have subsystems described by force and velocity, pressure and fluid flow, voltage and current, and temperature and heat transfer rate [37].

Rigid-body dynamics expressions may describe free motion in space. Such unconstrained equations of motion neglect the impedance of the environment [57]. Lumped-parameter, flexible-body equations of motion attempt to include flexible modes of the bodies. Including the dynamics of the environment in the model leads to constrained equations of motion.

The seven alternatives are presented with an assessment of which alternative is most appropriate for looseness diagnostics.

[1]A node variable is so named because the equation pertains to a sum of variables at a point; loop variables sum around a set of system elements. A constitutive relationship exists within each element between the two variables [37].

Position

As discussed in Chapter Two, there are a number of methods for finding geometric parameters $\mathbf{k}$ from the spatial displacement[2] relationship

$$ {}^0\mathbf{p} = {}^0_t\mathbf{T}(\mathbf{q},\ \mathbf{k})\ {}^t\mathbf{p}, \tag{3.1} $$

where ${}^0_t\mathbf{T}(\bullet)$ is the transformation from the origin of the end effector frame ${}^t\mathbf{p}_t$ to the world coordinate frame ${}^0\mathbf{p}_0$. This loop-closure alternative is illustrated in Figure 3.2.

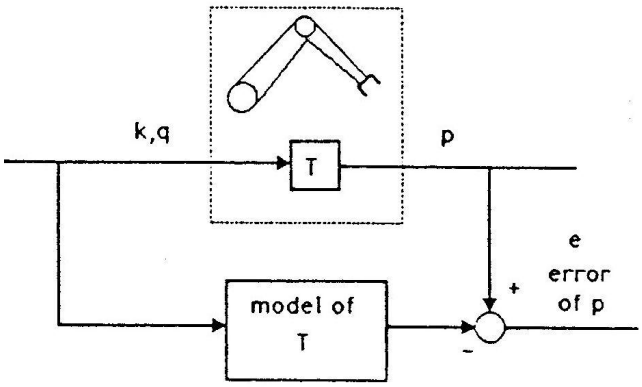

Figure 3.2: Displacement model

Almost every robot calibration scheme has focused on geometric parameters only, neglecting nongeometric effects such as looseness. The disadvantage of position-based methods is the need for absolute end-effector position measurement devices or constraint jigs that cover multiple locations in the work space.

Velocity

The relation (neglecting higher order terms) between the vector of joint velocities $\dot{\mathbf{q}}$ and the vector of end effector velocities $\dot{\mathbf{p}}$ is the Jacobian $\mathbf{J}$ [133], a function of static

[2]Displacement and position vectors are generally six-element vectors that include linear and angular terms. Similarly, force is generally a six-vector of forces and moments. In screw theory, position is a finite twist, and force is a wrench.

kinematic parameters and the joint vector $\mathbf{q}$:

$$\begin{aligned} \mathbf{J} &= [\frac{\partial \mathbf{p}}{\partial q_1}, \ldots, \frac{\partial \mathbf{p}}{\partial q_n}] \\ &= [\mathbf{J}_1, \ldots, \mathbf{J}_n] \\ &\approx \frac{\partial \mathbf{p}}{\partial \mathbf{q}^T}, \end{aligned} \tag{3.2}$$

which yields

$$\dot{\mathbf{p}} = \mathbf{J}\dot{\mathbf{q}}. \tag{3.3}$$

The velocity model is illustrated in Figure 3.3.

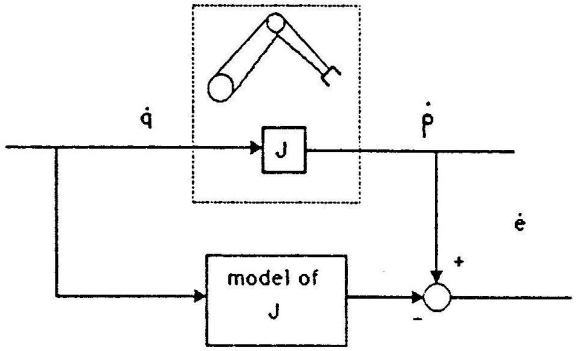

Figure 3.3: Velocity model

The Jacobian is a function of joint displacements $\mathbf{q}$ and geometric parameters $\mathbf{k}$:

$$\mathbf{J} = \mathbf{J}(\mathbf{q},\ \mathbf{k}). \tag{3.4}$$

From $\dot{\mathbf{p}}$, $\mathbf{q}$, and $\dot{\mathbf{q}}$, the parameters $\mathbf{k}$ can be found by generalised least-squares estimation. For nonredundant revolute serial manipulators, velocity is a recursive relationship

$${}^{i+1}\dot{\mathbf{p}} = {}^{i}\ \dot{\mathbf{p}} + {}^{i}_{i+1}\ \dot{\mathbf{p}}, \tag{3.5}$$

where ${}^{i}_{i+1}\dot{\mathbf{p}}$ is the relative velocity of frame $(i+1)$ with respect to frame (i), which, coupled with the location of neighbouring links, gives a recursive method for identifying kinematic parameters directly in a nonredundant, revolute-joint manipulator [23].

The Jacobian is a linear operator (although the functions of $\mathbf{q}$ in $\mathbf{J}$ may be nonlinear). The linearity of $\mathbf{J}$ means that joint velocities produce independent end-effector motions. The effect of looseness motion on the Jacobian is discussed shortly.

Acceleration

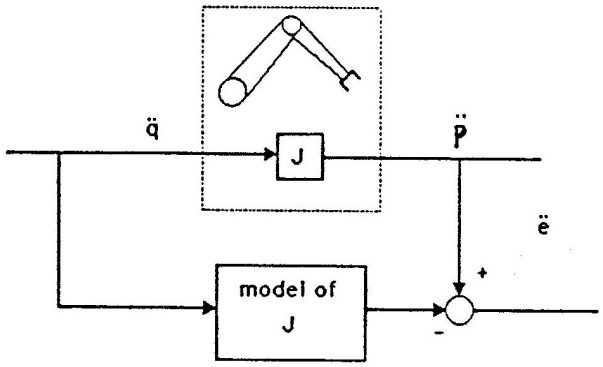

Figure 3.4: Acceleration model

The acceleration model of rigid-body motions is shown in Figure 3.4. The relation between the vector of joint velocities $\dot{\mathbf{q}}$, joint accelerations $\ddot{\mathbf{q}}$, and the vector of end effector accelerations $\ddot{\mathbf{p}}$ includes both the Jacobian $\mathbf{J}$ and its time derivative $\dot{\mathbf{J}}$:

$$\ddot{\mathbf{p}} = \mathbf{J}\ddot{\mathbf{q}} + \dot{\mathbf{J}}\dot{\mathbf{q}}, \tag{3.6}$$

where

$$\dot{\mathbf{J}} = \dot{\mathbf{J}}(\mathbf{q}, \dot{\mathbf{q}}, \mathbf{k}). \tag{3.7}$$

The second term on the right-hand side of Equation (3.6) is <u>not</u> a linear function of $\dot{\mathbf{q}}$. If $\mathbf{q}$, $\dot{\mathbf{q}}$, and $\ddot{\mathbf{p}}$ are known, then the parameters $\mathbf{k}$ can be estimated by generalized least squares from the nonlinear relation in Equation (3.6).

Since acceleration is a recursive relationship

$$^{i+1}\ddot{\mathbf{p}} = {}^{i}\ddot{\mathbf{p}} + {}^{i}_{i+1}\ddot{\mathbf{p}}, \tag{3.8}$$

where ${}^{i}_{i+1}\ddot{\mathbf{p}}$ is the relative acceleration of frame $(i+1)$ with respect to frame (i), the terms of $\mathbf{J}$ can be found from the recursive velocity relationship, the terms of $\dot{\mathbf{J}}$ can

be found from the acceleration relationship, and the parameters can be estimated by least squares for revolute serial manipulators [31]. This is a considerable effort, considering that there are no additional kinematic parameters in $\dot{\mathbf{J}}$ that are not already in $\mathbf{J}$.

For small joint velocities, $\dot{\mathbf{q}} = \vec{0}$, and the acceleration equation simplifies to

$$\ddot{\mathbf{p}} = \mathbf{J}\ddot{\mathbf{q}}, \tag{3.9}$$

leaving $\ddot{\mathbf{p}}$ a linear function of $\ddot{\mathbf{q}}$.

Static Forces

When a manipulator is statically loaded at the end effector, the joints are not moving and the only joint torques are those resisting the applied load. The relation between the vector of end effector static forces $\mathbf{f}$ and joint actuator static torques[3] τ is the transpose of the Jacobian:

$$\tau = \mathbf{J}^T\mathbf{f}, \tag{3.10}$$

which is again a linear relation, this time between end effector forces $\mathbf{f}$ and joint

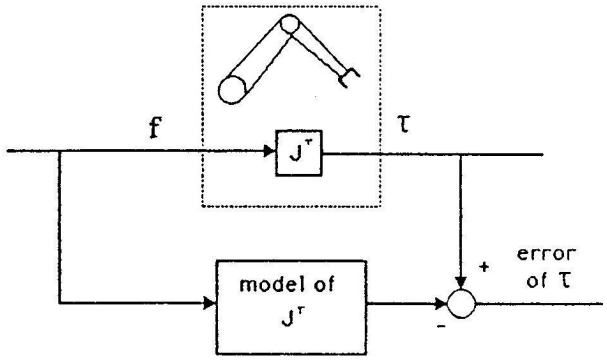

Figure 3.5: Static force model

torques τ. The static force model is shown in Figure 3.5.

[3]Force $\mathbf{f}$ is a six-vector of forces and moments; the vector of joint torques τ is an n-vector of actuator forces, called torques for convenience because most manipulators use revolute joints.

Since this is a static relation, measurements can be made using similar techniques as for kinematic calibrations, with measurements from stiffly supported locations across the workspace. The recursive nature of the Jacobian can be used for identification of kinematic parameters in a nonredundant revolute-joint serial-link manipulator [23].

Rigid-Body Dynamics with Free End Effector

The relation between the vector of joint actuator static torques τ and the vector of end effector accelerations $\ddot{\mathbf{p}}$ comes from the equation of motion

$$\mathbf{M}(\mathbf{q},\ \mathbf{k}_d,\ t)\{\ddot{\mathbf{q}}\} + \mathbf{C}(\mathbf{q},\ \dot{\mathbf{q}},\ \mathbf{k}_d,\ t) + \mathbf{K}(\mathbf{q},\ \mathbf{k}_d,\ t) = \mathbf{F}(t). \tag{3.11}$$

The inertia matrix $\mathbf{M}(\bullet)$ is a function of joint variables $\mathbf{q}$, dynamic parameters of the links $\mathbf{k}_d$ (which includes the kinematic parameters $\mathbf{k}$), and time (because $\mathbf{q}$ changes with time). The centripetal and Coriolis terms are contained in $\mathbf{C}(\bullet)$; and the potential terms are in $\mathbf{K}(\bullet)$. The vector of forcing functions is $\mathbf{F}(t)$, which, in the free dynamics case, is the set of actuator torques:

$$\mathbf{F} = \tau. \tag{3.12}$$

The torques are, of course, functions of the controller type. An open-loop controller produces joint torques that are functions of time only. A closed-loop controller produces a torque vector that is a function of the robot state, typically defined by $\mathbf{q}$ and $\dot{\mathbf{q}}$ for rigid-link manipulators.

If $\dot{\mathbf{q}} = \vec{0}$, the equation of motion reduces to

$$\tau = \mathbf{M}\ddot{\mathbf{q}} + \mathbf{K}. \tag{3.13}$$

This affine transformation is simplified by assuming that there is only a small change in the potential term caused by looseness: $\mathbf{K}(\mathbf{q}_{\text{loose}}) \approx \mathbf{K}(\mathbf{q}_{\text{nominal}})$. Because there is almost no motion, $\mathbf{K}$ is effectively constant for small motions about a nominal pose, assuming that any potential forces from the looseness are negligible. For a torque vector compensated for potential loads, τ^*,

$$\tau^* = \tau - \mathbf{K}, \tag{3.14}$$

the joint accelerations become

$$\ddot{\mathbf{q}} = \mathbf{M}^{-1}\tau^*. \tag{3.15}$$

Since $\dot{\mathbf{q}} = \vec{0}$,

$$\ddot{\mathbf{p}} = \mathbf{J}\ddot{\mathbf{q}}, \tag{3.16}$$

and the end-effector accelerations resulting from applied torques are

$$\ddot{\mathbf{p}} = \mathbf{J}\mathbf{M}^{-1}\tau^*. \tag{3.17}$$

The rigid-body dynamics model is shown in Figure 3.6.

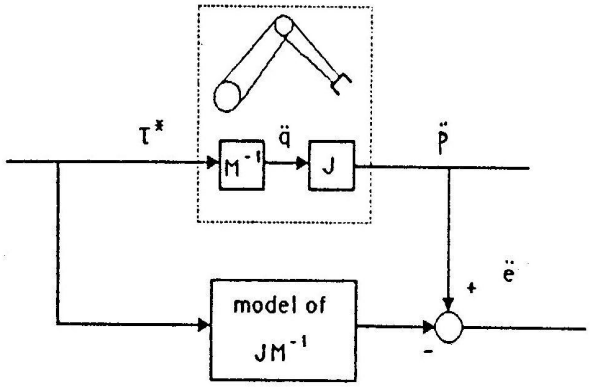

Figure 3.6: Free dynamics model

This model gives a closer approximation to the actual system behaviour than a kinematic model, given good estimates of the dynamic parameters. But now, in addition to $\mathbf{J}$, the inertia matrix $\mathbf{M}$ is involved. For a manipulator with n links, $\mathbf{M}$ is an $(n \times n)$ positive-definite matrix. If looseness appears, $\mathbf{M}$ becomes $(n+1 \times n+1)$, but remains positive definite. The effect of looseness on the inertia matrix is discussed in more detail in a subsequent section.

Lumped-Parameter Flexible-Body Dynamics

Modal analysis examines the frequency response of a structure modeled linearly as a lumped-mass, multiple degree-of-freedom system. Estimates of mass, stiffness, and damping are made for each element of the model, and the eigenvectors of the solution

describes the modal vectors. The model is typically validated using an experimental modal analysis that compares the response of the model at specific locations against that of the model at the same locations [52]. The advantage of this method is that the analyst no longer has to assume rigid-body motions. Removing this assumption, however, complicates the modeling process, demands that more data be acquired for model validation, and greatly increases the computational complexity of the model.

It is possible to construct an element that models looseness; the model may be linear or nonlinear. It may be difficult to find close estimates of the parameters of the element model, because it may not be possible to validate the looseness model independently. Although adding elements to finite element models shows promise for applying modal analysis to robotic manipulators, the manipulator modal analysis requires the looseness element to be included in the model at the proper location. The most likely diagnostic strategies would be to analyse a set of likely fault locations using analytical models of contact stiffness and damping, or to catalogue experimental modal analyses that are related empirically to faults from the maintenance history. Reconciling analysis results against the theoretical results requires considerable interpretation, which makes such an analysis unattractive for industrial implementation.

Constrained Rigid-Body Dynamics

In the constrained rigid-body dynamics case, the end effector has external forces applied to it while the robot moves. These forces are a reaction to motion through an environment with impedance [57]. The constrained rigid-body dynamics model is shown in Figure 3.7.

The equation of motion is now

$$\mathbf{M}(\mathbf{q},\ \mathbf{k}_d,\ t)\ddot{\mathbf{q}} + \mathbf{C}(\mathbf{q},\ \dot{\mathbf{q}},\ \mathbf{k}_d,\ t) + \mathbf{K}(\mathbf{q},\ \mathbf{k}_d,\ t) = \mathbf{F}(\mathbf{p},\ \dot{\mathbf{p}},\ t), \tag{3.18}$$

with the forcing function

$$\mathbf{F} = \tau_t + \tau_c. \tag{3.19}$$

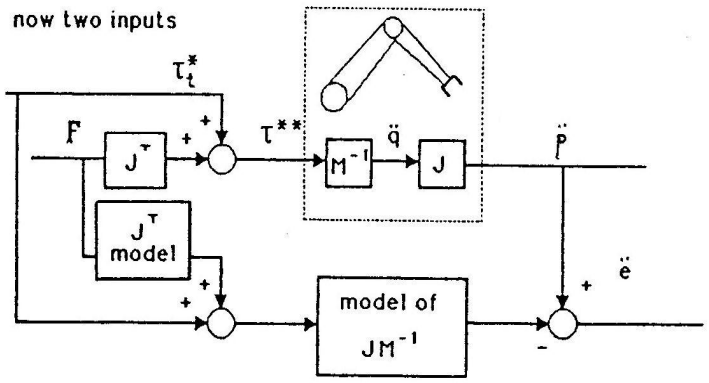

Figure 3.7: Constrained dynamics model

The vector of end effector accelerations $\ddot{\mathbf{p}}$ is still a function of joint torques. The actual joint torques include an extra component: not only is there torque τ_t for motion, but there is also torque τ_c required to apply a resisting end effector force against the force constraint on the end effector.

If $\dot{\mathbf{q}} = \vec{0}$, the equation of motion reduces to

$$\tau^{**} = \mathbf{M}\ddot{\mathbf{q}}, \tag{3.20}$$

where

$$\begin{aligned} \tau^{**} &= \tau_t + \tau_c - \mathbf{K} \\ &= \tau_t^* + \tau_c. \end{aligned} \tag{3.21}$$

From this equation comes the solution for the joint accelerations:

$$\ddot{\mathbf{q}} = \mathbf{M}^{-1}\tau^{**}. \tag{3.22}$$

From

$$\ddot{\mathbf{p}} = \mathbf{J}\ddot{\mathbf{q}}, \tag{3.23}$$

the end effector accelerations resulting from applied torques and end effector constraints are

$$\ddot{\mathbf{p}} = \mathbf{J}\mathbf{M}^{-1}\tau^{**}$$

$$
\begin{aligned}
&= \mathbf{J}\mathbf{M}^{-1}(\tau_t^* + \tau_c) \\
&= \mathbf{J}\underbrace{\mathbf{M}^{-1}\tau_t^*}_{\ddot{\mathbf{q}}_t} + \mathbf{J}\underbrace{\mathbf{M}^{-1}\mathbf{J}^T\mathbf{f}}_{\ddot{\mathbf{q}}_c},
\end{aligned} \tag{3.24}
$$

where $\ddot{\mathbf{q}}_t$ is the vector of actual joint accelerations caused by τ_t^*, and $\ddot{\mathbf{q}}_c$ is the vector of joint accelerations that occur under the torque vector τ_c if there is no force constraint. If the end effector is fully constrained, $\dot{\mathbf{q}} = \vec{0}$, $\ddot{\mathbf{q}} = \vec{0}$, and

$$
\begin{aligned}
\ddot{\mathbf{p}} &= \mathbf{J}\mathbf{M}^{-1}(\tau^{**}) \\
&= \vec{0}.
\end{aligned} \tag{3.25}
$$

This is the static-force case: the manipulator joints are not moving. If $\ddot{\mathbf{p}} = \vec{0}$ but $\ddot{\mathbf{q}} \neq \vec{0}$, then $\mathbf{J}$ is rank-deficient: there is an extra degree of freedom (DOF), and $\mathbf{J}$ is an $(m \times \ n+1)$ matrix, where $m \leq 6$.

Since compliance can be modeled as a set of six screws [96], a nonredundant manipulator will provide an end-effector compliance comprised of up to six screws. The static-force method can thus be used to find extra unactuated DOFs. By constraining the end effector of a nonredundant manipulator, any joint motion that occurs during joint actuation is an extra screw twist in the mechanism, which (for looseness) is associated with a wrench with zero amplitude.

Wiggling the manipulator while the end effector is fixed is therefore a viable method of identifying looseness, although fixing the end effector in a number of manipulator poses across the workspace presents a daunting implementation challenge.

If the end effector is not fully constrained, then there are nonzero components of $\ddot{\mathbf{p}}$. Whether an additional dimension of end effector motion appears will depend on the direction of looseness and whether the constraint allows motion in that direction.

3.2.2 Effect of Looseness on the Manipulator Model

Since looseness may occur between any two mating parts, looseness can be thought of as "backlash" between the parts, adding an extra DOF to the manipulator.

An extra degree of freedom changes the manipulator kinematics and dynamics, as the new DOF introduces an additional twist into the mechanism. It is necessary

to know the other twists, and the direction of the end-effector motion caused by the extra DOF at a given pose, to find the source of the additional twist.

Kinematic Modeling of a Looseness Fault

The motion is included in the kinematic model by considering each of the loose parts as a link and by placing an extra "joint" in the manipulator at the location of the loose connection between the parts. The joint variable of the new link represents the motion due to the flaw. There is looseness at joint (i) in Figure 3.8, and the

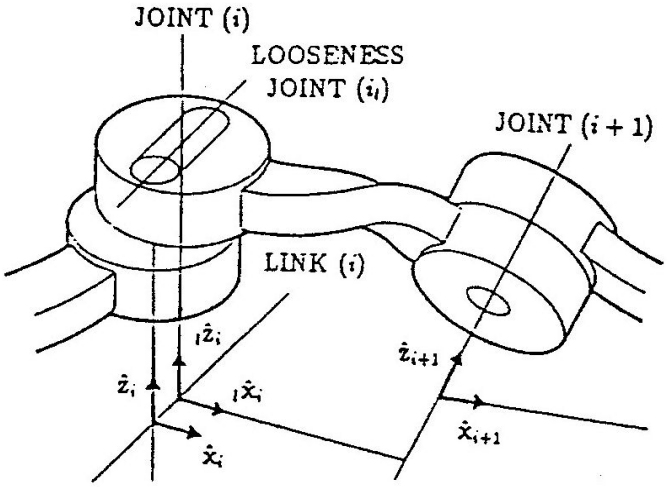

Figure 3.8: Looseness in joint (i)

looseness joint (i_l) describes that motion.

The kinematic assumptions in modeling the looseness joint are rigid links and lower-pair joints. Looseness fault models can represent various cases: gear backlash, sliding in an ostensibly revolute lower-pair joint, rotation in a prismatic joint, etc. Although the extra joint models only one additional DOF, the looseness motion may be either prismatic or revolute, in any orientation.

This extra DOF is assumed to act along a consistent direction, that is, the new joint is also a lower-pair revolute or prismatic joint. Two extra DOFs are needed to model an undersized pin at joint (i), because motion is possible along both the $\hat{\mathbf{x}}_i$

and $\hat{\mathbf{y}}_i$ directions. In general, six extra single-DOF joints are necessary to describe a completely loose joint [41].

The parameters of the Denavit-Hartenberg (D-H) formulation are sensitive to changes in relative position and orientation between coordinate frames. To avoid changing the D-H parameters in neighbouring links at a loose joint, an inverse rotation transforms the looseness joint frame (i_l) back to the orientation of the original undamaged joint. The series of transformations is

$$\begin{aligned} {}^{i}_{il}\mathbf{T} &= {}^{i}_{l}\mathbf{T}\,{}^{l}_{il}\mathbf{T} \\ &= \begin{bmatrix} {}^{i}_{l}\mathbf{R} & {}^{i}_{l}\mathbf{p} \\ 0\,0\,0 & 1 \end{bmatrix} \begin{bmatrix} & & 0 \\ {}^{l}_{il}\mathbf{R} & & 0 \\ & & 0 \\ 0\,0\,0 & & 1 \end{bmatrix}, \end{aligned} \tag{3.26}$$

where ${}^{l}_{il}\mathbf{R} = {}^{i}_{l}\mathbf{R}^{-1} = {}^{i}_{l}\mathbf{R}^{T}$ for orthonormal bases.

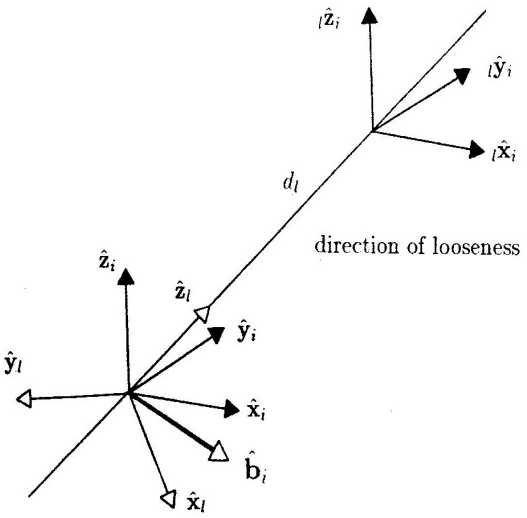

Figure 3.9: A homogeneous transformation for looseness

Figure 3.9 shows the transformation for a prismatic fault, a looseness slot in the $\hat{\mathbf{x}}_i$, $\hat{\mathbf{y}}_i$ plane of joint (i), perpendicular to a unit vector $\hat{\mathbf{b}}_i$ that lies in the plane, such that

$$\hat{\mathbf{z}}_l = \hat{\mathbf{z}}_i \times \hat{\mathbf{b}}_i, \tag{3.27}$$

where $\hat{z}_l$ is the direction of looseness. This transformation requires only two parameters: the angle of $\hat{\mathbf{b}}_i$ about $\hat{\mathbf{z}}_i$, and d_l, the translation along $\hat{\mathbf{z}}_l$. (If the coordinate axes are located less conveniently, it may require up to six parameters to describe the transformations.) The orientation of $\hat{\mathbf{b}}_i$ is dependent on θ_i if the slot is in the base of link (i) and not in the distal end of link $(i-1)$.

Effect of Looseness on the Jacobian

The Jacobian of an n-link serial manipulator is

$$\begin{aligned} {}_n\mathbf{J} &= [\frac{\partial \mathbf{p}}{\partial q_1}, \ldots, \frac{\partial \mathbf{p}}{\partial q_n}] \\ &= [{}_n\mathbf{J}_1, \ldots, {}_n\mathbf{J}_n], \end{aligned} \tag{3.28}$$

where the columns of ${}_n\mathbf{J}$ with respect to a world coordinate frame w are

$$\begin{aligned} {}_n\mathbf{J}_k &= \left\{ \begin{array}{c} {}^w_k\mathbf{R}\{{}^k\hat{\mathbf{z}}_k\} \times ({}^w_t\mathbf{R}\{\hat{\mathbf{0}}\} - {}^w_k\mathbf{R}\{\hat{\mathbf{0}}\}) \\ {}^w_k\mathbf{R}\{{}^k\hat{\mathbf{z}}_k\} \end{array} \right\}, \\ & k = 1, \ldots, n. \end{aligned} \tag{3.29}$$

By adding an extra joint to the kinematic model at joint (i), the Jacobian changes from ${}_n\mathbf{J}$ to ${}_{n+1}\mathbf{J}$, with an additional, unmeasurable joint variable ${}_l\dot{q}_i$:

$$\dot{\mathbf{p}}_l = {}_{n+1}\mathbf{J}\dot{\mathbf{q}}_l, \tag{3.30}$$

where $\dot{\mathbf{q}}_l = [\dot{q}_1, \ldots, \dot{q}_{i,l}\, \dot{q}_i, \ldots, \dot{q}_n]^T$. In the new Jacobian for the manipulator with $n+1$ links,

$$\begin{aligned} {}_{n+1}\mathbf{J} &= [\frac{\partial \mathbf{p}_l}{\partial q_1}, \ldots, \frac{\partial \mathbf{p}_l}{\partial q_i}, \frac{\partial \mathbf{p}_l}{\partial_l q_i}, \ldots \frac{\partial \mathbf{p}_l}{\partial q_n}] \\ &= [{}_{n+1}\mathbf{J}_1, \ldots, {}_{n+1}\mathbf{J}_{i,n+1}\mathbf{J}_{il}, \ldots, {}_{n+1}\mathbf{J}_n], \end{aligned} \tag{3.31}$$

where

$$\begin{aligned} {}_{n+1}\mathbf{J}_k &= \left\{ \begin{array}{c} {}^w_k\mathbf{R}_l\{{}^k\hat{\mathbf{z}}_k\} \times ({}^w_t\mathbf{R}_l\{\hat{\mathbf{0}}\} - {}^w_k\mathbf{R}_l\{\hat{\mathbf{0}}\}) \\ {}^w_k\mathbf{R}_l\{{}^k\hat{\mathbf{z}}_k\} \end{array} \right\}, \\ & k = 1, \ldots, i, i_l, i+1, \ldots, n. \end{aligned} \tag{3.32}$$

When the Jacobian is defined in world coordinates, there is no change in the proximal (left) columns until looseness appears:

$$\text{If} \quad k \leq i, \quad \text{then } {}^{w}_{k}\mathbf{R}_{l} = {}^{w}_{k}\mathbf{R}. \tag{3.33}$$

Conversely, when the Jacobian is defined in end effector coordinates, there is no change in distal (right) columns until looseness appears. The motion $\mathbf{p}_k$ does not change if the elements of the subset of joint variables $\{\dot{q}_{k+1}, \ldots, \dot{q}_n\}$ are invariant and the kinematic parameters for links $k+1$ to n are invariant.

The error vector $\dot{\mathbf{e}}$ is the difference between the actual velocities due to looseness $\dot{\mathbf{p}}_l$ and the velocities $\dot{\mathbf{p}}$ for the nominal n-link manipulator:

$$\begin{aligned} \dot{\mathbf{e}} &= \dot{\mathbf{p}}_l - \dot{\mathbf{p}} \\ &= {}_{n+1}\mathbf{J}\dot{\mathbf{q}}_l - {}_{n}\mathbf{J}\dot{\mathbf{q}}. \end{aligned} \tag{3.34}$$

To solve for parameters of ${}_{n+1}\mathbf{J}_l$ in Equation (3.34), the n-link Jacobian ${}_{n}\mathbf{J}$ must be well known in advance. The terms of ${}_{n+1}\mathbf{J}_l$ depend on where the looseness occurs; and ${}_{l}q_i$ is unknown.

If a kinematic calibration of the manipulator is done before looseness appears, then ${}_{n}\mathbf{J}$ is known.

Equation (3.33) indicates that any search for the looseness joint should begin at the most distal joint, where the fewest terms are affected. If the Jacobian is defined in the end-effector frame, then a change in the columns of the Jacobian reveals on which link the looseness has entered the mechanism. A strategy for determining the component of end effector motion caused by the looseness motion is considered in a later section.

In structural looseness, the direction of looseness does not generally lie along one of the principal axes of the nominal Jacobian. If $m < 6$, then structural looseness can increase the dimension of the space spanned by end effector motion by one. In backlash, the rank of the Jacobian does not change, because the looseness motion is superimposed onto the associated joint motion.

To construct the actual Jacobian with looseness requires knowledge of where the looseness occurs in the mechanism and where to put the additional column in the actual Jacobian. For the general case, the nominal and actual Jacobian is $6 \times (n+1)$, with all six DOFs of Euclidean 3-space and $(n+1)$ degrees of manipulator freedom included. Thus, in the absence of *a priori* knowledge about the effect of the extra degree of freedom, the Jacobian should be a $6 \times (n+1)$ matrix. If the rank of $\mathbf{J}$ is less than six, then some rows are dependent.

Inertia Matrix

In the dynamic case, the inertia matrix $\mathbf{M}$ is nominally $n \times n$ for a mechanism with n rigid bodies. But when looseness appears, the number of DOFs increases to $(n+1)$, and so $\mathbf{M}$ becomes $(n+1) \times (n+1)$.

If $\mathbf{M}$ is always $(n+1) \times (n+1)$, then $\mathbf{M}$ is ill-conditioned when there is no looseness. This ill-conditioning is an artifact of the two bodies joined by the looseness joint. When there is no looseness, the two bodies move as the one original body of the nominal case. The inertial properties of this body are split between the two new bodies bracketing the looseness joint. If most of the mass and inertia lumps into one body, then $\mathbf{M}$ becomes ill-conditioned. This would be the case for backlash, since a motor has much less inertia than the link it drives. The condition number of an estimated inertia matrix would therefore be an indicator of looseness.

Even in the looseness case, there is often contact between the bodies. This occurs whenever the loose body hits a bound of its travel in the looseness joint. When this happens, relative velocity between neighbouring loose bodies is zero. At one looseness boundary, the relative velocity is an inequality

$$_{\iota}\dot{q}_i \leq 0, \qquad q_{li} = q_{l\ \text{distal}}; \tag{3.35}$$

and at the other boundary,

$$_{\iota}\dot{q}_i \geq 0, \qquad q_{li} = q_{l\ \text{proximal}}. \tag{3.36}$$

Manipulator Rigid-Body Dynamics Example

As an example of the change in rigid-body dynamics, a planar articulated manipulator with looseness in the distal link is considered. Mechanical system rigid-body simulations use the inverse dynamic equations of motion for state variables $\ddot{\mathbf{q}}$ and $\ddot{\mathbf{q}}$, found from classical Newton-Euler methods, from Lagrangian dynamics, or—in serial-link mechanisms—from the recursive Newton-Euler method [36].

Letting the generalised coordinates be $\mathbf{q}$, the state variables are defined as

$$\mathbf{y}_1 = \mathbf{q}; \tag{3.37}$$

$$\mathbf{y}_2 = \dot{\mathbf{q}}. \tag{3.38}$$

The equations of motion are recast into the form

$$\mathbf{F}(\mathbf{y}_1,\ \mathbf{y}_2, t) = \mathbf{M}(\mathbf{y}_1,\ \mathbf{y}_2,\ t)\{\dot{\mathbf{y}}_2\} + \mathbf{C}(\mathbf{y}_1,\ \mathbf{y}_2, t) + \mathbf{K}(\mathbf{y}_1, t), \tag{3.39}$$

or, briefly,

$$\mathbf{F} = \mathbf{M}\{\dot{\mathbf{y}}_2\} + \mathbf{C} + \mathbf{K}. \tag{3.40}$$

The generalised coordinates for the equations of motion for the rigid-body dynamics of the nominal manipulator with no looseness are joint angles θ_1 and θ_2, and generalised forces were joint torques τ_1 and τ_2. State variables were $\theta_1,\ \theta_2,\ \dot{\theta}_1$, and $\dot{\theta}_2$. The plane of motion is perpendicular to gravity.

The joint forces and torques for the nominal manipulator are:

$$\begin{aligned}
\tau_1 = {} & (I_1 + m_2 l_{c1}^2)\ddot{\theta}_1 \\
& + l_1 m_2 [S_2(-l_{c2}\dot{\theta}_{12}^2 - C_2 l_1 \dot{\theta}_1^2 + S_2 l_1 \ddot{\theta}_1) \\
& + C_2(-l_{c2}\dot{\theta}_{12}^2 - C_2 l_1 \dot{\theta}_1^2 + S_2 l_1 \ddot{\theta}_1)] \\
& + l_{c2} m_2 [l_{c2}\ddot{\theta}_{12} + l_1(S_2\dot{\theta}_1^2 + C_2\ddot{\theta}_1)] + I_2\ddot{\theta}_{12};
\end{aligned} \tag{3.41}$$

$$\tau_2 = l_{c2} m_2 [l_{c2}\ddot{\theta}_{12} + l_1(S_2\dot{\theta}_1^2 + C_2\ddot{\theta}_1)] + I_2\ddot{\theta}_{12}. \tag{3.42}$$

When there is prismatic looseness d at the proximal end of link 2, the joint variable vector for the planar articulated manipulator (neglecting gravity and friction) is

$\mathbf{q} = [\theta_1,\ \theta_2,\ d]^T$. The generalised coordinates are

$$\mathbf{y}_1 = \left\{ \begin{array}{c} \theta_1 \\ \theta_2 \\ d \end{array} \right\}; \tag{3.43}$$

the accelerations are

$$\dot{\mathbf{y}}_2 = \left\{ \begin{array}{c} \ddot{\theta}_1 \\ \ddot{\theta}_2 \\ \ddot{d} \end{array} \right\}; \tag{3.44}$$

the generalised forces are

$$\mathbf{F} = \left\{ \begin{array}{c} \tau_1 \\ \tau_2 \\ 0 \end{array} \right\}; \tag{3.45}$$

and thus there are three equations of motion in Equation (3.40). The equation of

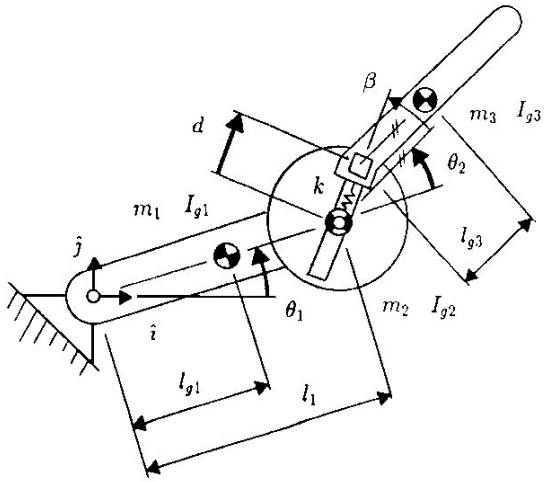

Figure 3.10: 3 DOF RRP manipulator representing looseness in distal link

motion for body one (the proximal link) is

$$\begin{aligned} \tau_1 \ = \ & \{m_1 l_{g1}^2 + m_2 l_1^2 + I_{g1} + I_{g2} + I_{g3} \\ & + m_3[l_1^2 + 2l_1(dC_{2\beta} + l_{g3}C_2) + d^2 + l_{g3}(2dC_\beta + l_{g3})]\}\ddot{\theta}_1 \\ & + \{I_{g2} + I_{g3} + m_3[l_1(dC_{2\beta} + l_{g3}C_2) + d^2 + l_{g3}(2dC_\beta + l_{g3})]\}\ddot{\theta}_2 \\ & + m_3(l_1 S_{2\beta} + l_{g3}S_\beta)\ddot{d} \end{aligned}$$

$$+m_3[2d\dot{\theta}_{12}(l_1C_{2\beta}+l_{g3}C_\beta+d)-l_1\dot{\theta}_2(dS_{2\beta}+l_{g3}S_2)(2\dot{\theta}_1+\dot{\theta}_2)]. \quad (3.46)$$

In the looseness case, the original body 2 splits into bodies 2 and 3. For the proximal body 2, which is not loose with respect to link 1, the equation of motion is

$$\begin{aligned}\tau_2 &= \{I_{g2}+I_{g3}+m_3[l_{g3}(l_1C_2+l_{g3})+d(l_1C_{2\beta}+2l_{g3}C_\beta+d)]\}\ddot{\theta}_1\\ &\quad +\{I_{g2}+I_{g3}+m_3[l_{g3}(2dC_\beta+l_{g3})+d^2]\}\ddot{\theta}_2\\ &\quad +(m_3l_{g3}S_\beta)\ddot{d}\\ &\quad +m_3[2d\dot{\theta}_{12}(d+l_{g3}C_\beta)+l_1\dot{\theta}_1^2(dS_{2\beta}+l_{g3}S_2]. \quad (3.47)\end{aligned}$$

For body 3, which is loose with respect to body 2, the equation of motion is

$$\begin{aligned}0 &= m_3(l_1S_{2\beta}+l_{g3}S_\beta)\ddot{\theta}_1+(m_3l_{g3}S_\beta)\ddot{\theta}_2\\ &\quad +m_3\ddot{d}-m_3[l_1\dot{\theta}_1^2C_{2\beta}+\dot{\theta}_{12}^2(d+l_{g3}C_\beta)]\\ &\quad +kd+c\dot{d}. \quad (3.48)\end{aligned}$$

The inertia tensor $\mathbf{M}$ has gone from a (2×2) matrix to (3×3), and $\mathbf{C}$, $\mathbf{K}$, and $\mathbf{F}$ have become 3-element vectors.

The zero element in $\mathbf{F}$ represents the unactuated looseness joint. Reaction forces during contact are accommodated by the contact stiffness k and damping c, nonlinear functions that are equal to zero in the region of free motion. The model assumes that there is no bounce and bodies remain in contact during a given time step. The unactuated prismatic joint between body 2 and body 3 moves according to the equations of motion. The effective stiffness of the mechanical stops is estimated from the contact geometry and material properties of the manipulator of interest, or from experimental data. A more representative joint model may also include stiffness and damping in the free-motion region [91].

3.2.3 Choice of Modeling Alternative

To avoid the additional modeling complication of the dynamics cases, this study concentrated on kinematic models. The intent of this strategy was to examine the

usefulness of a simple model before considering more realistic (and complicated) models.

Motion variables were chosen because motion transducers could be more readily used on industrial robots than force-torque sensors coupled with support jigs in the workspace.

To find the looseness, two conditions had to be met. The contribution of looseness to end-effector motion had to be known, and a relationship had to exist for finding the location on the mechanism from which that motion originated. It was not necessary to find all of the robot kinematic parameters to diagnose a looseness fault, if the manipulator was kinematically calibrated before looseness appeared.

Linear models relating end-effector motion to joint motion were preferred, because the contributions to motion could be separated into components. Thus, velocity modeling and acceleration modeling with low velocity were the approaches considered in this study.

3.3 Locating a Looseness Fault within a Serial Mechanism

This section describes the development of a method for locating a looseness fault on a serial-link manipulator. A recursive method was used to find geometric link parameters for serial-link revolute manipulators from velocities, as first proposed by Bennett [23].

Limitations were found with the method for manipulators with prismatic joints (including an unactuated looseness joint), and so a strategy was developed for using different poses of the manipulator to find the link which the prismatic joint actuates.

In the case of a looseness joint, identifying the link on which it appeared satisfied the first of the requirements for diagnosing the looseness fault. The other requirement was to isolate the component of end-effector motion caused by the fault. A method for isolating looseness motion is described in a subsequent section.

Assumptions for the Looseness Link Finding Method were:

1. looseness was prismatic, but no *a priori* assumption was made about the location of the looseness;

2. the component of end-effector motion from each joint was known, including the contribution from looseness;

3. the location of the end-effector motion sensors was known with respect to the most distal joint;

4. only linear velocities were known.

3.3.1 Recursive Identification Method

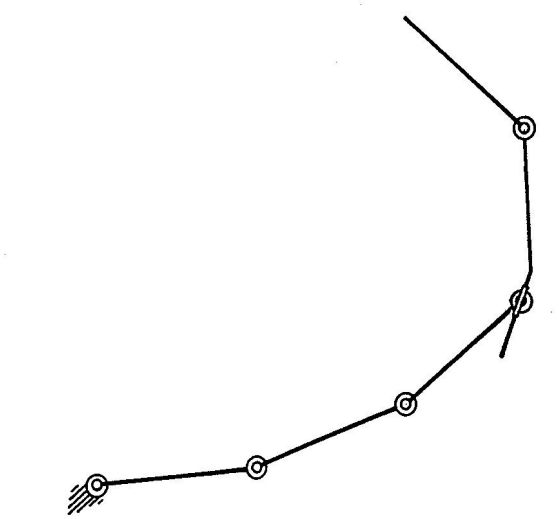

Figure 3.11: General serial mechanism with revolute and prismatic joints

A planar serial-link, open-chain mechanism with revolute joints and a single prismatic joint is illustrated in Figure 3.11. The prismatic joint axis intersects the axis of the neighbouring proximal revolute joint. The advantage of this model construction is explained below.

Figure 3.12 shows the assignment of relative coordinate frames: the origin of frame (i) lies on the axis of joint (i), at the proximal end of link (i). The displacement

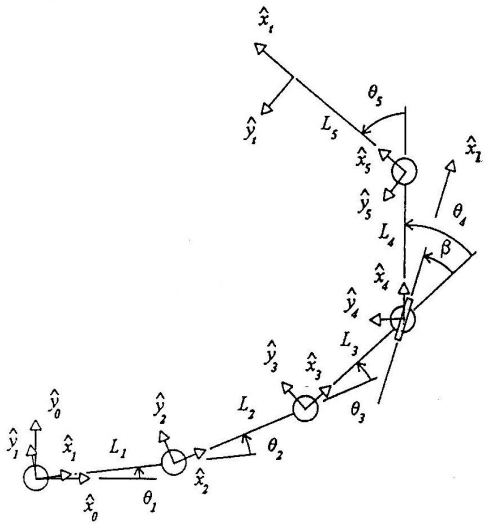

Figure 3.12: Frame assignments and kinematic parameters

vector from frame (i) to frame $(i+1)$ is ${}_i\mathbf{p}_{i+1}$. In the planar case,

$$ {}_i\mathbf{p}_{i+1} = L_i \hat{\mathbf{x}}_i, \tag{3.49} $$

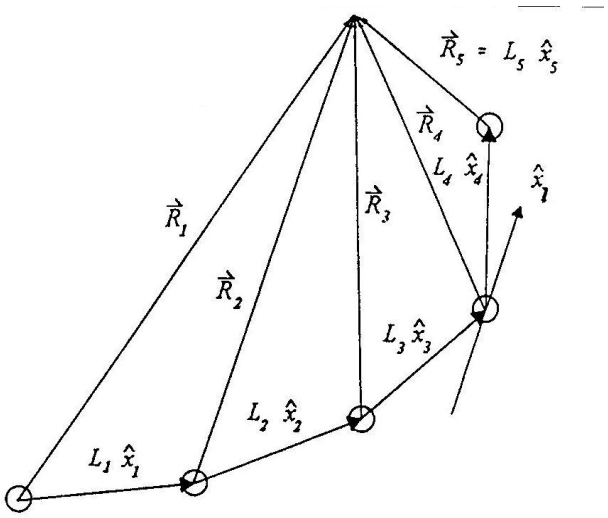

Figure 3.13: Vectors from frames to end effector

If, as in figure 3.13, a vector $\vec{R}_i$ is drawn from the origin of each frame (i) to the end effector, then the recursive relationship

$$ \vec{R}_i =_i \mathbf{p}_{i+1} + \vec{R}_{i+1} \tag{3.50} $$

holds.

For an n-DOF manipulator, the velocity of joint (i), $\dot{q}_i$, produces an end effector velocity component $\dot{\mathbf{p}}_i$:

$$\dot{\mathbf{p}}_i = \mathbf{J}_i \dot{q}_i \tag{3.51}$$

$$= \mathbf{J}\,{}_n\mathbf{I}_i \dot{\mathbf{q}}, \tag{3.52}$$

where $\mathbf{J}_i$ is the ith column of the Jacobian, and ${}_n\mathbf{I}_i$ is an $n \times n$ diagonal matrix with element i equal to one and all other elements equal to zero, and $\dot{\mathbf{q}}$ is the vector of joint motions. Each velocity-vector component $\dot{\mathbf{p}}_i$ contributes linearly to the overall end effector velocity:

$$\dot{\mathbf{p}} = \sum_{i=0}^{n} \dot{\mathbf{p}}_i. \tag{3.53}$$

There is also a recursive velocity relationship from link to link.

The end-effector velocity vectors can be expressed either in tool space with respect to frame (n) or in world space frame (0). But the orientation of the velocity vectors must be known with respect to the most distal link.

Revolute and prismatic joints are more common in robotic manipulators than other types of lower-pair joints, and so the discussion focuses on manipulators with those joint types[4].

For revolute joints, end-effector velocity component $\dot{\mathbf{p}}_i$ is related to joint velocity $\dot{q}_i = \dot{\theta}_i$ by

$$\dot{\mathbf{p}}_i = \dot{\theta}_i \hat{\mathbf{z}}_i \times \vec{R}_i. \tag{3.54}$$

The linear velocity resulting from revolute joint velocity is thus related to the relative joint location $\vec{R}_i$, shown in Figure 3.14. Known quantities are the elements of velocity vector $\dot{\mathbf{p}}_i$ and the magnitude of the joint velocity $\dot{q}_i$.

For a prismatic joint, however, end-effector velocity component $\dot{\mathbf{p}}_i$ is related to joint velocity $\dot{q}_i = \dot{d}_i$ by

$$\dot{\mathbf{p}}_i = \dot{d}_i \hat{\mathbf{z}}_i. \tag{3.55}$$

[4]The other four types of lower-pair joints—the cylindrical, helical, planar, and spherical—can be resolved into revolute and/or prismatic joints, so this method applies to manipulators with other types of lower-pair joints as well.

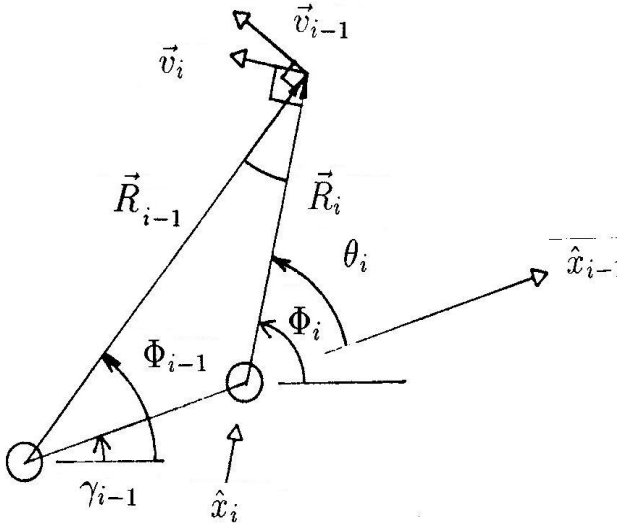

Figure 3.14: Joint velocities mapped into end effector velocities

In spatial manipulators, the direction of motion for a prismatic joint is typically chosen to be $\hat{\mathbf{z}}_i$. But in the planar case it is convenient to keep all relative frame transformations in the plane, with the result that

$$\hat{\mathbf{z}}_i = \hat{\mathbf{z}} \quad \text{for} \quad i = 0, \ldots, n, \tag{3.56}$$

where $\hat{\mathbf{z}}$ is a unit vector perpendicular to the plane. The end-effector velocity component of a prismatic joint (i) in a planar manipulator $\dot{\mathbf{p}}_i$ is related to joint velocity $\dot{q}_i = \dot{d}_i$ by

$$\dot{\mathbf{p}}_i = \dot{d}_i \hat{\mathbf{x}}_i. \tag{3.57}$$

Planar Revolute Manipulator Recursion

The recursion operation begins at joint n (the most distal joint) with $\vec{R}_{n+1} = 0$. The recursion has six steps working through successively proximal links. The set of neighbouring links around a joint of interest is shown in Figure 3.14 with the associated parameters.

Step one is to actuate (revolute) joint (i) with velocity $\dot{\theta}_i$. Step two is to measure the magnitude and direction of the resulting end effector velocity $\dot{\mathbf{p}}_i$. The third step is to find the direction perpendicular to the direction of $\dot{\mathbf{p}}_i$, and the length of the

rotation arm from the joint to the end effector $\vec{R}_i$. In the planar case for the (x, y) plane,

$$\dot{\mathbf{p}}_i = \dot{\theta}_i \hat{\mathbf{z}} \times \vec{R}_i, \tag{3.58}$$

which becomes

$$\begin{Bmatrix} {}_x v_i \\ {}_y v_i \\ 0 \end{Bmatrix} = \begin{Bmatrix} 0 \\ 0 \\ \dot{\theta}_i \end{Bmatrix} \times \begin{Bmatrix} {}_x R_i \\ {}_y R_i \\ 0 \end{Bmatrix}. \tag{3.59}$$

Expanding the cross product yields the components of $\vec{R}_i$:

$$\begin{Bmatrix} {}_x R_{i-1} \\ {}_y R_{i-1} \\ 0 \end{Bmatrix} = \begin{Bmatrix} {}_y v_{i-1}/\dot{\theta}_{i-1} \\ -{}_x v_{i-1}/\dot{\theta}_{i-1} \\ 0 \end{Bmatrix}. \tag{3.60}$$

The internal angle η_i between vectors $\vec{R}_i$ and $\vec{R}_{i+1}$ comes from the difference in their directions:

$$\Phi_i = \arctan \frac{{}_y R_i}{{}_x R_i}; \tag{3.61}$$

and

$$\eta_i = \Phi_{i+1} - \Phi_i. \tag{3.62}$$

The fifth step is to find the magnitude of the link vector $\vec{L}_i = L_i \hat{\mathbf{x}}_i$, which is a function of η_i and the magnitudes of the vectors,

$$L_i = [R_i^2 + R_{i+1}^2 - 2R_i R_{i+1} \cos \eta_i]^{\frac{1}{2}}. \tag{3.63}$$

The sixth step is to find the direction:

$$\hat{\mathbf{x}}_i = \frac{1}{L_i}[\vec{R}_i - \vec{R}_{i+1}]. \tag{3.64}$$

The distended angle θ_i is

$$\theta_i = \Phi_{i+1} - \gamma_i, \tag{3.65}$$

where

$$\gamma_i = \arctan \frac{{}^0_y \hat{\mathbf{x}}_i}{{}^0_x \hat{\mathbf{x}}_i}. \tag{3.66}$$

The arctangent comes from the components of $\hat{\mathbf{x}}_i$ with respect to a fixed frame of reference. In Equation (3.66), the frame is the world coordinate frame (0). The kinematic parameters being sought are link length L_i and joint offset ψ_i, where

$$\psi_i = \theta_i - q_i \tag{3.67}$$

for revolute joints.

The recursion can be done with respect to any fixed frame, be it the world frame (0), the end effector frame (t), or an intermediate frame. For an arbitrary world frame, there are three additional kinematic parameters that locate joint 1 and its angle offset in the plane. Those three parameters are static, and can not be found by a velocity method [23].

Parameters are gathered as the recursion continues for a single pose set. Once the set is finished, other poses may be chosen for parameter estimation.

Accommodating Backlash in the Model

When a looseness joint enters the mechanism, there is no *a priori* information where the looseness is, or whether it is prismatic or revolute. If it is revolute due to backlash in a revolute joint, then a looseness motion $\dot{\mathbf{p}}_l$ appears in the same direction as motion from an existing joint.

Accommodating Prismatic Looseness in the Model

The recursion is well suited for revolute-joint, serial mechanisms; if, however, the mechanism includes a prismatic joint, then the recursion fails.

There is no direct relationship associating translational velocity to a prismatic joint location on the mechanism, because linear velocity is a free vector. In Figure 3.15, the serial-link mechanism includes a prismatic joint as well as revolute joints[5]. Joint $(i-1)$ is a prismatic joint. The length of link $(i-1)$ is d_{i-1}, whereas the joint offset is β_{i-1}. For convenience, the prismatic looseness joint with displacement d_l is located at the distal end of the link on which it rides. It is assumed that

[5]The mechanism shown is planar, but the argument applies to spatial mechanisms as well.

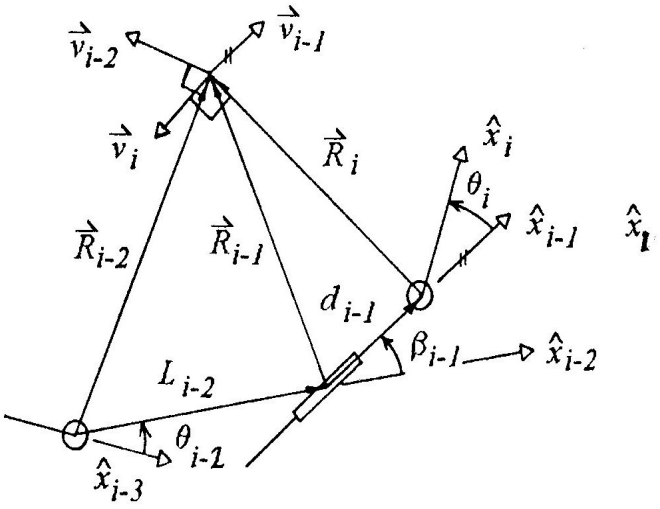

Figure 3.15: Serial mechanism with prismatic joint

small looseness motions occur such that d_l is small and has a mean of zero, which are realistic assumptions for structural looseness.

The component of end-effector velocity due to looseness is now $\dot{\mathbf{p}}_l$ parallel to $\hat{\mathbf{x}}_{i-1}$:

$$\dot{\mathbf{p}}_l = \dot{d}_{i-1}\hat{\mathbf{x}}_{i-1}. \tag{3.68}$$

The unit direction vector $\hat{\mathbf{x}}_{i-1}$ comes directly from

$$\hat{\mathbf{x}}_{i-1} = \frac{1}{\dot{d}_{i-1}}\dot{\mathbf{p}}_l. \tag{3.69}$$

The magnitude of looseness velocity is $\dot{d}_l$ in the direction $\hat{\mathbf{x}}_l$ parallel to $\dot{\mathbf{p}}_l$. But Equation (3.55) does not reveal the location of $\hat{\mathbf{x}}_l$ with respect to a link on the mechanism. Although the orientation of frame $(i-1)$ is known, there is no way from the given information to find the vector $\vec{R}_{i-1}$ that locates frame $(i-1)$. Since linear velocity is a free vector, not a line vector, velocity information alone is not enough to locate the axis of motion in space.

Because line motion is a free vector, the looseness prismatic joint can be placed at any convenient location on the link. The most convenient line for the prismatic joint intersects the axis of the revolute joint that moves that link, that is, the neighbouring proximal joint. With the assumption that the mean offset d is zero, the only

parameter to be identified in the planar case is the direction of the looseness motion $\hat{\mathbf{x}}_l$, which can be found from Equation (3.68).

It is necessary, however, to identify on which link the looseness exists.

Searching for the Link of Concern

In a given pose, there is no *a priori* information as to which link contains prismatic looseness.

One option for including looseness in the displacement model is to add a looseness joint to each of the links, and attempt a solution with a nonlinear parameter estimator. The initial parameter value of each looseness magnitude would be zero, since looseness magnitudes are small with respect to the displacements of actuated joints. But directions of looseness are not known, and so the trial values for direction parameters may be greatly in error. For that reason, this approach may fail.

A more appealing option is to use the order of poses to provide the additional information as to which link exhibits looseness.

If there is a prismatic joint in the serial mechanism, its location can not be found in a single pose. Multiple poses, however, determine the link on which a prismatic joint is located, by moving joints proximally until there is a change in the direction of the end effector motion.

Structuring how information is gathered thus provides extra information to the estimation process. The set of poses contributes the necessary additional information, because moving individual joints forms new poses and the change in prismatic looseness motion in task space changes between poses, depending on the pose.

Starting proximally to the base and working out distally, the task space looseness orientation does not change until the link of concern is moved with respect to the end effector, as illustrated in Figure 3.16.

The procedure is to change the most proximal element of the joint vector, and then to check for a change with respect to task space. If there is a change with respect to task space, then the source of the change lies in the section of the mechanism more

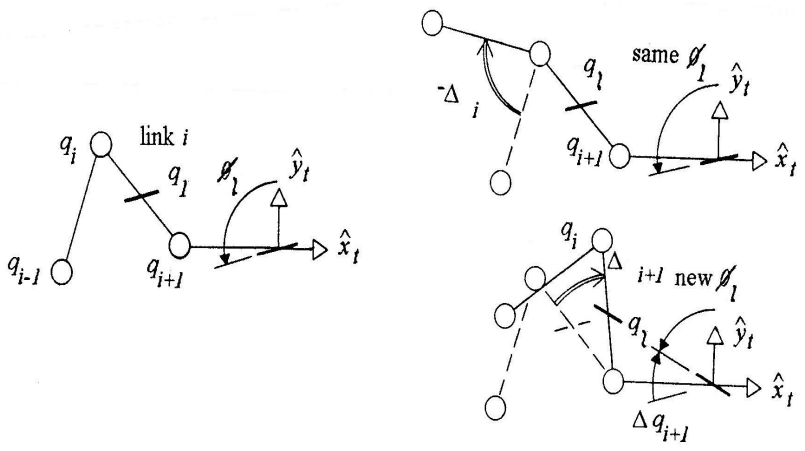

Figure 3.16: Looseness location identification

proximal than the joint element changed.

The pose set can also take advantage of the singularities of the mechanism to eliminate degrees of freedom that might contribute to the motion if the robot structure is compliant.

The result of the Looseness Link Finding Method with multiple pose sets is the identity of the link with looseness, and an estimate of the magnitude and direction of the looseness after a preliminary operation to identify the free vector amplitude and direction. The next section describes the process of identifying the component of end effector motion contributed by looseness.

3.4 Finding the Looseness Contribution to End Effector Motion

The strategy for finding the looseness in the mechanism depends on being able to find the motion at the end effector contributed by looseness. This section discusses how the direction of looseness motion is found when motions are random variables. The merits are weighed between multiple random excitation of joints and single excitation of a joint; and the merits of parametric and nonparametric search techniques are considered for finding the direction of looseness.

Solving Kinematic Parameters Using Random Variables

The proposed identification method differs from previous kinematic calibration schemes; the traditional approach is to take single end-effector position, velocity, or acceleration measurements at each pose, and to rely on many different poses to give an overdetermined system for a least-squares estimate of the kinematic parameters. In the present method, a measure of the quantity of looseness and its location in the manipulator comes from statistical features of end-effector motion resulting from random joint motions.

For zero-mean random variables (RVs), linear transformations result in new zero-mean random variables [95]. Further, if the original RVs are independent and Gaussian, then the new RVs are also independent and Gaussian. The autospectrum for each RV is flat with equal signal power at all frequencies[6]. Coherence between each spectrum is ideally one across all frequencies of interest.

If, however, the RVs are <u>not</u> all independent and Gaussian, then even linear transformations of RVs do not produce new independent, Gaussian RVs. The autospectrum of the non-Gaussian RV is no longer flat, and coherence drops from one at some or all frequencies [17].

The method for identifying the direction of motion from looseness assumes that independent, Gaussian joint motions can be produced in a manipulator, that the Jacobian remains approximately linear for small motions about a given pose, and that any resulting looseness motion in the unactuated joint is **not** a Gaussian RV.

For a two-dimensional probability density function (PDF) $f_{xy}(x, y)$, the marginal PDF of RV x, $f_x(x)$, is found by integrating the 2-dimensional PDF over the whole range of the other RV y. For a continuous PDF,

$$f_x(x) = \int_{-\infty}^{\infty} f_{xy}(x, y)dy. \tag{3.70}$$

The marginal PDF of a multi-dimensional PDF comes from integrating over the

[6]In fact, it is not possible to have equal power contribution to a signal across all frequencies, because that would require infinite power. In a finite bandwidth, however, power is finite, and the above argument holds.

range of each of the other RVs.

The presence of looseness therefore changes the probability distribution function (PDF) of the end-effector motion. Both the Gaussian RVs and the non-Gaussian RV of manipulator joint motions undergo a linear transformation to produce end effector motions. All RVs contribute to the PDF, and the marginal PDF of each RV can be extracted from the PDF.

A multi-dimensional PDF of independent, Gaussian RVs has probability contours that are ellipsoids in n-dimensional space [99]. Each of the marginal PDFs is Gaussian. Even if the basis is changed, marginal PDFs are still Gaussian. The projection of an n-dimensional ellipsoid onto m-dimensional space, where $m \leq n$, is an m-dimensional ellipsoid[7].

In the case of velocities, and in the case of accelerations with negligible velocities, if a manipulator makes only very small motions about a given pose $\mathbf{q}$, then the nominal Jacobian can be assumed to remain constant.

For the no-fault case, the random end effector velocity vector $\breve{\dot{\mathbf{p}}}$ due to a given set of random joint velocities $\breve{\dot{\mathbf{q}}}$ is

$$\breve{\dot{\mathbf{p}}} =_n \mathbf{J}\breve{\dot{\mathbf{q}}}, \tag{3.71}$$

If there is a looseness fault, then there is a corresponding change in $\breve{\dot{\mathbf{p}}}$.

An independent, low-power, zero-mean, normal-random (Gaussian) joint motion produces a normal-random end-effector motion in an ideal rigid-body manipulator. The mean motion error is zero, and the contour enclosing a space of equal error probability of a multi-dimensional distribution of independent Gaussian RVs is an ellipsoid, as shown in Figure 3.17[99]. The velocity ellipsoid is the time-varying case of the Cartesian error envelope described by Menq and Borm [82], and can be considered to be a statistical kinematic manipulability ellipsoid [133].

If, however, one of the random variables is non-Gaussian, then the multi-dimensional PDF has probability contours that are no longer ellipsoids. In an n-

[7]A physical interpretation for $n = 3$ and $m = 2$ is that an ellipsoid looks like an ellipse from every direction.

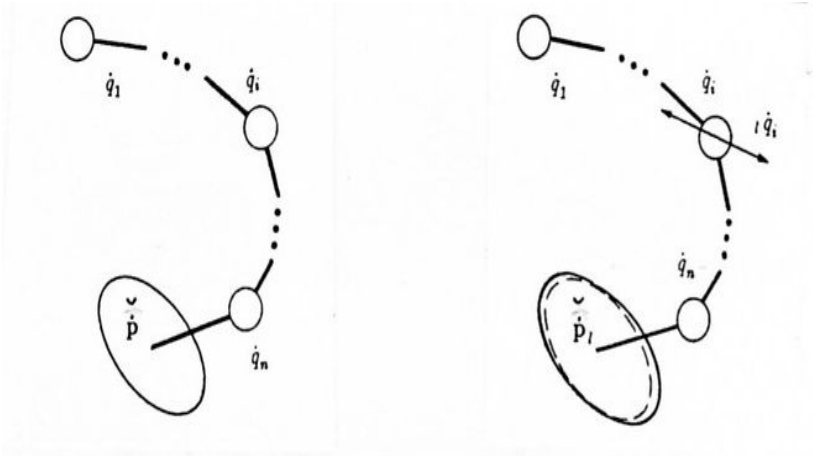

a) ideal motion b) nonlinear motion

Figure 3.17: Velocity error ellipsoid

dimensional PDF projected onto m-dimensional space, there are $(m-1)$ marginal PDFs that are normal-random; the mth marginal PDF is the PDF of the RV that is not normal random.

If all the other RVs in the system are independent and normal-random, then the non-normal RV is identifiable from the shape of its marginal PDF. This is the direction of motion caused by looseness joint motion that is non-Gaussian.

Because the assumed looseness motion is not normal random, the ellipsoid becomes misshapen, with a drop in coherence along the direction of the action of the looseness joint. The variance of the marginal PDF gives a measure of the amount of looseness that exists.

The identification problem reduces to one of finding the kinematic parameters that are most likely to produce the non-normal random motion in the different poses of the mechanism.

The identification method relies on generating random-variable joint motions to produce the end-effector motion due to looseness. All of the time-varying kinematic errors in the mechanism are assumed to combine to produce a non-normal random motion in the mechanism. The dynamics of the manipulator with this extra (uncontrolled) DOF dictate the motion at the region of looseness. The assumption is that

there is non-normal random looseness-joint motion, and that the end-effector motion due to other joints remains normal-random. Part of the experimental work in this project involved verifying that this assumption could be made.

There are two possible methods to generate these random motions. The first method is to perform single actuations, starting from the most distal joint. If the motion spans two dimensions, then spurious motion has occurred due to looseness in the mechanism, and the direction of lowest coherence is the direction of the looseness motion. If the motion spans only one dimension, but the motion distribution has become highly non-normal, then backlash has developed in the joint being actuated.

The second method is to perform multiple actuations at the same time. The only difference is that normal-random motions appear in more dimensions, making the search space larger. Multiple actuations with independent, normal random variables produce the same motions as the superposition of the single joint motions—except for the looseness motion, which, being nonlinear, does not obey superposition. Since the actuated joint motions are independent, they can be used just as independent deterministic joint motions were used in Bennett's method.

Finding the Direction of Lowest Coherence

One way to find the direction of motion that is not independent normal-random is to find the direction of lowest coherence with respect to the normal-random joint motions.

The direction of lowest coherence corresponds to the direction along which the most non-normal motions occur in a given pose, as illustrated in Figure 3.18.

Alternatives for finding this direction include: matching a parametric model of a distribution to the data; using the linear correlation coefficient between the end effector motion data in a given direction and the joint motion data; and looking for a non-uniform frequency spectrum of the motion data in a given direction.

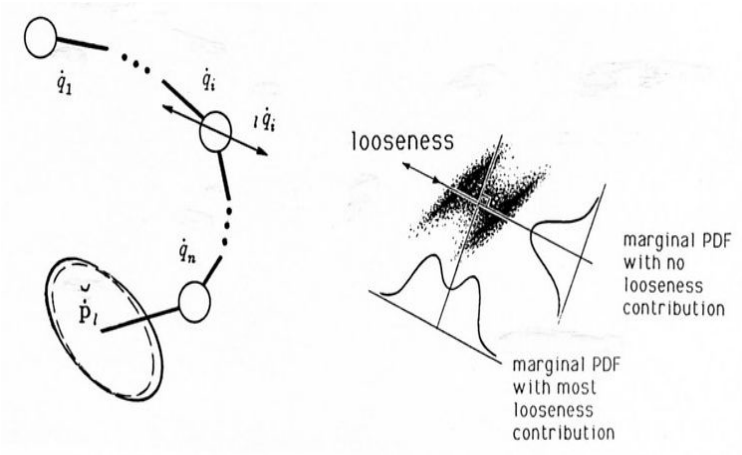

Figure 3.18: Finding the direction of lowest coherence

3.5 Summary of Methodology

It was recognised that looseness adds an unactuated, additional degree of freedom to the manipulator. Since the location of looseness in the manipulator mechanism is not known *a priori*, alternatives were sought to adding a looseness joint to each manipulator link. The limitation of kinematic parameter estimation for finding a prismatic looseness joint was described. End-effector motion (velocity and acceleration with low velocity) were chosen as diagnostic parameters of interest, because they are linearly related to joint motions, including that of looseness.

The methodology uses changes in manipulator end-effector motions that results from looseness. Independent, normal-random motions in the joints of a kinematic manipulator model produce independent normal-random end effector motions. When looseness appears, the direction of the non-normal component of end-effector motion is the direction of looseness.

The Looseness Link Finding Method uses a set of different poses, determining the direction of end-effector looseness motion in each pose. The method looks for a change in the direction of looseness motion at the end effector caused by the change in pose. Individual joints are moved to new poses, starting from the proximal end, until the link of concern changes orientation with respect to the end effector, causing a change in the direction of the looseness motion.

The next chapter examines how to implement a looseness identification method on robotic manipulators.

Chapter 4

Implementation

The ancestor of every action is a thought. *Emerson*

This chapter describes the implementation of the two steps in the looseness identification procedure.

The first step was to find the direction of motion due to looseness. Several methods were considered, including fitting curves to a bivariate distribution or to an ellipsoid function; examining the flatness of the power spectrum with respect to direction; and making correlations between the end-effector motion and the excitation motion.

The second step was to find the link responsible for the looseness by examining the change in looseness direction with changes in pose.

4.1 Finding the Direction of Looseness Motion

If the probability distribution of end-effector motions is m-dimensional, $1 \leq m \leq 6$, then finding the direction of looseness depends on $(m-1)$ marginal distributions being zero-mean and normal-random.

The search procedure for prismatic looseness motion requires at most three dimensions, because the looseness motion is a free line vector in space that passes through the point of measurement.

The search has one of two goals. It either finds the $(m-1)$ marginal distributions, such that looseness is found in the perpendicular direction; or the search finds the non-normal random distribution direction directly.

The first section covers parametric modeling to match $(m-1)$ normal marginal distributions to end-effector motions, and then describes the parametric estimation procedure. The second section describes a direct method for finding the direction of non-normal random motion nonparametrically using a correlation with joint motion.

4.1.1 Parametric Methods

Parametric methods were investigated for finding the direction of looseness motion by fitting a model of a normal distribution to a sampled motion distribution.

Three-Dimensional Model for Estimation

In the case of prismatic looseness motion in three-dimensional Cartesian space, the best fit is sought for a zero-mean, two-dimensional Gaussian distribution $N(x, y)$. There are six parameters to be found for this bivariate distribution in x and y: the marginal variances σ_x^2 and σ_y^2, the three parameters orienting the distribution in space, and a scaling parameter. Since a bivariate normal distribution has contours that are ellipsoids on a plane, the number of parameters required is that of an ellipsoid model.

The parameters defining an ellipse on a plane are: the location of the centre, the orientation of the major axis, the aspect, and the scale. But having the ellipse centered on the origin reduces the number of parameters by two. The relationship of the contour ellipse to the probability (the gain of the distribution) adds a fourth parameter. The parameters of a two-dimensional probability ellipse are illustrated in Figure 4.1.

The desired information is the orientation of the plane (i), spanning the two-dimensional subspace of $({}^{i}x,\ {}^{i}y)$ in three-dimensional space across which the data best fit a bivariate normal distribution. The line perpendicular to that plane is the

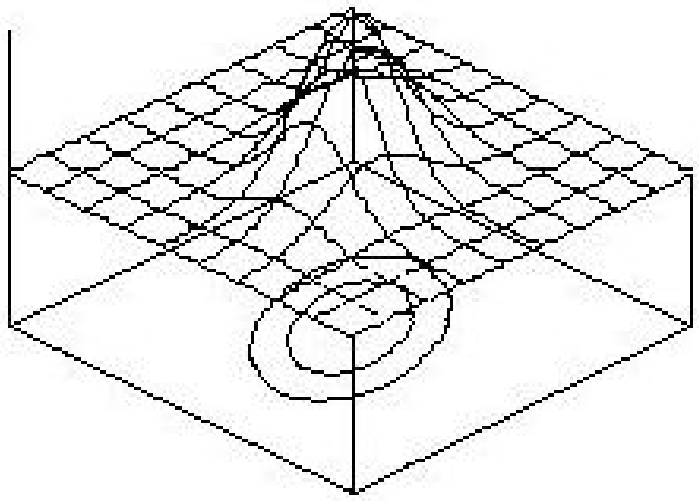

Figure 4.1: Parameters of 2D probability ellipse contours in 3D space

direction in which that data most poorly fit the normal distribution: this is the estimated direction of looseness.

One characterisation of the plane of interest uses azimuth and elevation $(\rho,\ \zeta)$. The vector of azimuth, elevation, and magnitude is $(\rho,\ \zeta, \gamma)$. The search objective is a set of good choices for parameters $(\rho,\ \zeta)$; and $(\rho^*,\ \zeta^*,\ 1)$ is the best-fit estimate of the unit vector perpendicular to the plane.

A set of three-dimensional data points $\{{}^0\vec{p}_j\},\ j = 1, \ldots, n$ then maps onto plane (i) with the best fit to a 2D Gaussian distribution. Each datum maps into plane (i) according to

$$ {}^i\vec{p}_j = {}^i_0\,\mathbf{R}(\rho,\ \zeta)\,{}^0\vec{p}_j, \tag{4.1} $$

or, in expanded form,

$$ \begin{Bmatrix} {}^ip_{jx} \\ {}^ip_{jy} \\ 0 \end{Bmatrix} = \begin{bmatrix} C_\rho C_\zeta & -S_\rho & C_\rho S_\zeta \\ S_\rho C_\zeta & C_\rho & S_\rho S_\zeta \\ -S_\zeta & 0 & C_\zeta \end{bmatrix} \begin{Bmatrix} {}^0p_{jx} \\ {}^0p_{jy} \\ {}^0p_{jz} \end{Bmatrix}. \tag{4.2} $$

After rotating data to frame i being tested, ${}^i\vec{p} = \mathbf{R}(\rho,\ \zeta)\,{}^0\vec{p}$, an estimator uses the linearly transformed $({}^ix,\ {}^iy)$ data to fit to a bivariate Gaussian distribution,

checks goodness of fit, and continues searching until the estimator finds the best fit of the data to the model. This is a nonlinear search, since the distribution model $N = f({}^{i}x,\ {}^{i}y)$ is a nonlinear function of parameters ρ and ζ that transform the original data $({}^{0}x\ {}^{0}y\ {}^{0}z)$. Because of the symmetry of the problem, the estimator can restrict the search range in each angular direction to $\pm\pi/4$ radians.

On the plane itself, the orientation of the $({}^{i}\hat{\mathbf{x}},\ {}^{i}\hat{\mathbf{y}})$ axes of the plane (i) coordinate frame themselves do not affect the goodness of fit, because projecting the data onto any line of the plane produces a single-dimensional Gaussian distribution. Marginal distributions $N({}^{i}x)$ and $N({}^{i}y)$ have different values for the parameters σ_x^2 and σ_y^2, depending on planar orientation. But the distributions themselves remain Gaussian, with zero-mean distributions.

On the plane of concern, a search for the angle of the largest-variance marginal distribution yields the orientation of the major axis of the probability contours for the bivariate distribution.

Since the probability contours are ellipsoids, the fit can also be done to a model of an ellipsoid on plane i, rather than fitting the data to a model of a Gaussian distribution.

Two-Dimensional Model for Estimation

For single joint excitation with only one source of looseness motion, local motion occurs in a plane. That plane may have any orientation in Cartesian 3D space; but, in cases where the orientation of the plane is known, a two-dimensional model on the plane is sufficient.

The planar estimation problem is considerably simpler than the three-dimensional problem. The joint distribution of motion is two-dimensional, but in the direction of looseness the marginal distribution is assumed to be non-normal. Perpendicular to that distribution is the one-dimensional normal distribution being sought.

The planar case again assumes that there is a direction along which the motion maintains a normal distribution. If the direction of that normally distributed data

line is ${}^{i}\hat{x}$, then the normal distribution is a function z of the magnitude of a vector along that line, ${}^{i}x$:

$$z = f({}^{i}x). \tag{4.3}$$

If the line along which the Gaussian distribution z acts is at an angle a_2 to the ${}^{0}x$ axis, the mapping of two-dimensional data $({}^{0}x,\ {}^{0}y)$ into ${}^{i}x$ is:

$${}^{i}x = \cos(\alpha){}^{0}x + \sin(\alpha){}^{0}y, \tag{4.4}$$

from which comes the equation for fitting data to a one-dimensional, zero-mean Gaussian distribution z with parameters $a_0,\ a_1,$ and a_2:

$$z = a_0 e^{a_1(\cos(a_2){}^{0}x + \sin(a_2){}^{0}y)^2}, \tag{4.5}$$

illustrated in Figure 4.1. This model assumes a uniform distribution in the direction of poorest fit to the normal distribution.

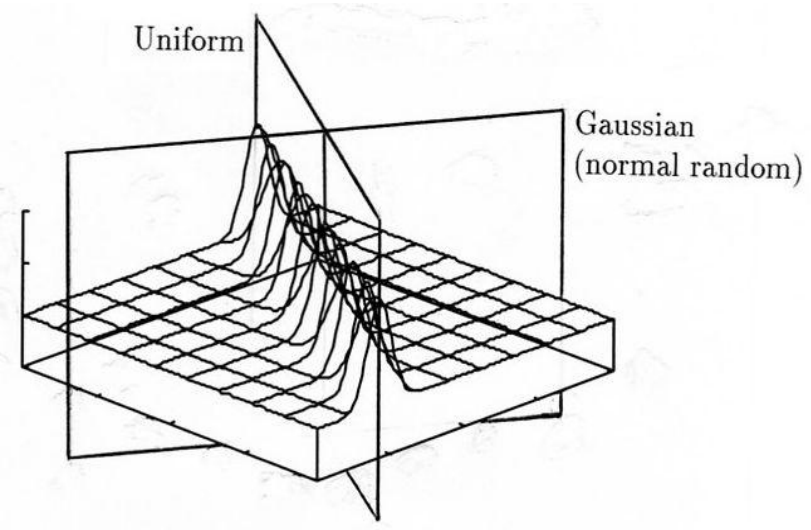

Figure 4.2: Two-dimensional normal-random and uniform distribution

Generating a Multi-Dimensional Distribution Estimate

An approximate probability distribution of the data in an $(m-1)$-dimensional subspace of the task space is an $(m-1)$-dimensional histogram. The histogram has

a rectangular grid, with bin sizes the same in each direction. The number of dimensions, number of bins (resolution) and number of data are all user-defined in a custom program with the following algorithm.

The histogram program opens a data file with $(m-1)$-dimensional data, and finds the range of data in each dimension. The largest range is used for display in all directions to preserve scale; each range is discretised into a user-defined resolution (e.g. 120×120). Sorting each datum into the discretised regions generates the histogram by incrementing the array element corresponding to the region into which the datum falls. After sorting the data into array elements corresponding to bins, the program saves the array containing the concentration of data in each region in a file compatible for orthogonal-distance regression to a curve.

For visual display, probability contours of the histogram are shown by layering the plot from the highest concentration to the lowest, to establish layers of the histogram. The current sum of all contributing layers divided by the total number of data is thus greater than or equal to the desired probability within the area plotted.

Parameter Estimation Method

In the planar case, the model has a single nonlinear function,

$$z = a_0 e^{a_1(\cos(a_2)^0 x + \sin(a_2)^0 y)^2}, \tag{4.6}$$

with three parameters to be estimated, a_0, a_1, and a_2. Figure 4.3 shows how parameter a_0 scales the distribution, a_1 scales the width of the distribution to give the variance, and a_2 is the angle of orientation of the normal distribution in the plane.

Orthogonal-Distance Regression

Although the distribution being sought is single-dimensional, there is more than one independent variable. The angle of orientation in the plane of concern produces a two-dimensional distribution function z that has two explanatory (independent) variables x and y. Single-dimensional parameter estimation algorithms are thus inappropriate for this problem [100].

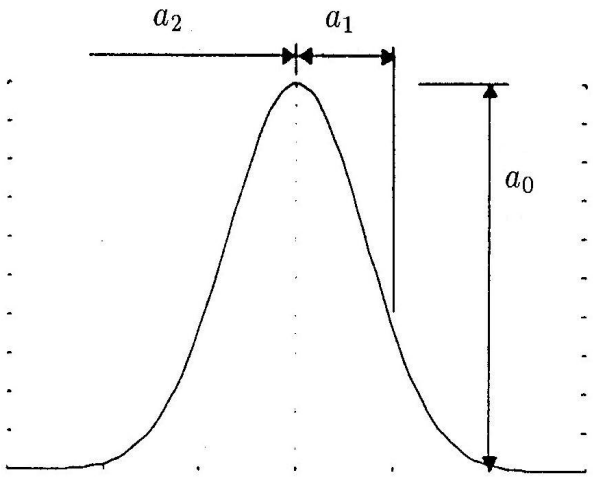

Figure 4.3: Parameters of 1D normal random distribution

Weighted orthogonal-distance regression is a method for estimating parameters in multi-dimensional nonlinear functions. The regression finds the parameters that minimise the sum of the squares of the orthogonal distances from the observed data to the curve (or surface) described by the model function; the orthogonal distances can also be weighted by the user. A Fortran driver routine FCN for version 2.01 of ODRPACK from NIST supplied the model function z. The SAMPLE function in ODRPACK was configured to estimate derivatives using forward-difference equations [27].

Trial Parameters

The estimator requires trial parameters for a_0, a_1, and a_2.

The trial scaling factor a_0 was set by finding the maximum bin value in the histogram. An alternative method is to take the volume of a histogram of data and then, assuming radial symmetry, find the area under a single-dimensional histogram for the trial value.

The variance a_1 is initially estimated by calculating the variance σ^2 of each of n points on the histogram. Point j in plane (i) has a discrete value ${}^{i}c_j$, and lies a distance ${}^{i}h_j$ from the expected value of the center of the joint distribution at $({}^{i}\overline{x}, {}^{i}\overline{y})$

on plane (i) (with a mean of zero, in this case), as illustrated in Figure 4.4. The trial

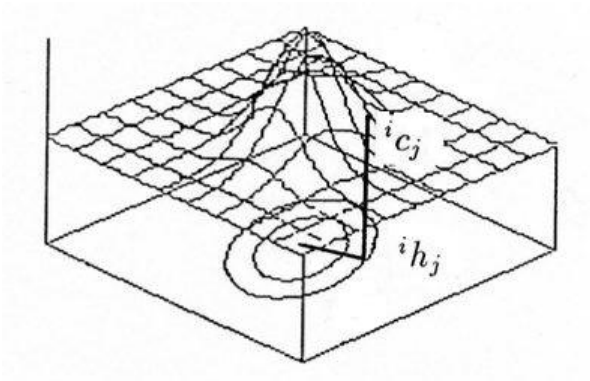

Figure 4.4: Variance calculation for joint distribution

estimate of the variance is thus

$$\sigma^{2*} = (\Sigma_{j=1}^{n} h_j^2 c_j)/2. \tag{4.7}$$

Because

$$a_1 = -\frac{1}{2\sigma^2}, \tag{4.8}$$

the trial value for a_1 is

$$a_1 = -(\Sigma_{j=1}^{n} h_j^2 c_j)^{-1}. \tag{4.9}$$

Since the square of that distance is the sum of the squares of the distances of components, the direction in which the components lie has no effect on the final value of the variance[1]. This is analogous to calculating the moment of inertia in a body [110].

With the assumption of a radially symmetrical distribution, the estimate of the variance of the marginal distribution is the same. Since there is no indication of asymmetries in the distribution without calculating marginal variances in different directions, symmetry was assumed.

The direction a_2 is not known. A strategy for choosing a trial value for a_2 is to choose a direction arbitrarily, and let the estimator converge if it can. If no

[1]In practice, a manipulator probably has only a small number of possible looseness failure modes. The trial value of looseness direction could be based on the direction of bolted joint connections on the link of interest.

convergence occurred, then a new trial direction is chosen and the estimation is run again. The choices should span the range of possible values for a_2.

The estimation program prompts the user for trial parameters and other information pertinent to the estimation: number of sets of data, number of explanatory variables, and number of functions in the model.

Order of Operations

The order of operations for locating the direction of looseness motion at the end effector for a given pose is

1. Generate excitation data at a given pose i for excited joint j;
2. Generate a multi-dimensional distribution histogram from the end effector motion data;
3. Estimate the direction of the normal distribution ${}^t a_2$ with respect to the end effector frame from the histogram;
4. Estimate the variance of the marginal distribution of looseness (this variance is a measure of the amount of looseness);
5. Pass the looseness direction and magnitude estimates to the second stage of evaluation (where subsequent poses are generated to determine the link upon which looseness exists).

4.1.2 Nonparametric Methods

This section describes a nonparametric method for finding the direction of looseness as the direction where the correlation between the end-effector motion and the excitation motion reaches a minimum. Descriptive statistics and power spectral density are also considered.

Linear Correlation Vector

Between n pairs of data $(x_i,\ y_i)$, $i = 1, \ldots, n$, the linear correlation coefficient is

$$r = \frac{\sum_{i=1}^{n}(x_i - \overline{x})(y_i - \overline{y})}{\sqrt{\sum_{i=1}^{n}(x_i - \overline{x})^2}\sqrt{\sum_{i=1}^{n}(y_i - \overline{y})^2}}, \tag{4.10}$$

where $\overline{x}$ is the mean of the $\{x_i\}$ data set, and $\overline{y}$ is the mean of the $\{y_i\}$ data set [99]. This data set $\{y_i\}$ is transformed. For a set of data $(v_i,\ w_i)$, $i = 1, \ldots, n$, which are a function of a parameter ϕ, y is a function of v and w,

$$y = f(v,\ w). \tag{4.11}$$

The effect of ϕ on x data is found by correlating x data with respect to a function y of ϕ and v and w data,

$$y_i = f(v_i,\ w_i,\ \phi), \tag{4.12}$$

in Equation (4.10).

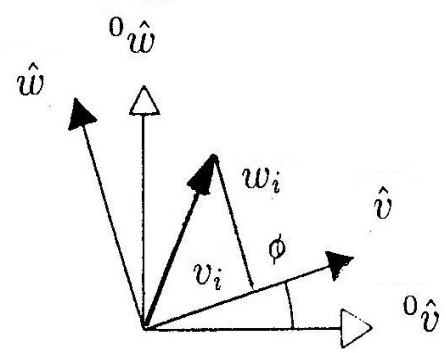

Figure 4.5: Rotating a vector basis

In the present case, v and w are the orthogonal-motion components of concern, and ϕ is the angle that the basis formed by $(\hat{v},\ \hat{w})$ makes with respect to a vector basis $(^0\hat{v},\ ^0\hat{w})$, shown in Figure 4.5. The w component with respect to frame (0) is:

$$^0w_i = \cos(\phi)v_i + \sin(\phi)w_i, \tag{4.13}$$

which is the transformed datum y_i. Successive correlation calculations with respect to ϕ produce a function of linear correlation r with respect to that parameter:

$$r = f(x,\ v,\ w,\ \phi). \tag{4.14}$$

In this case, parameter ϕ is a direction, and this correlation function is a vector with magnitude r and direction ϕ. The data $(v,\ w)$ are the end-effector motions correlated against joint motion x or against motion of a link that lies closer to the base of the manipulator than does the link of concern.

Finding Direction of Lowest Correlation

The correlation function is unique only in the range $0 < \phi \leq \pi$. From $\pi < \phi \leq 2\pi$, the magnitude of $\mathbf{r}$ is the negative of that of $\mathbf{r}$ between $0 < \phi \leq \pi$:

$$|\mathbf{r}(\phi)| = -|\mathbf{r}(\phi + \pi)|. \tag{4.15}$$

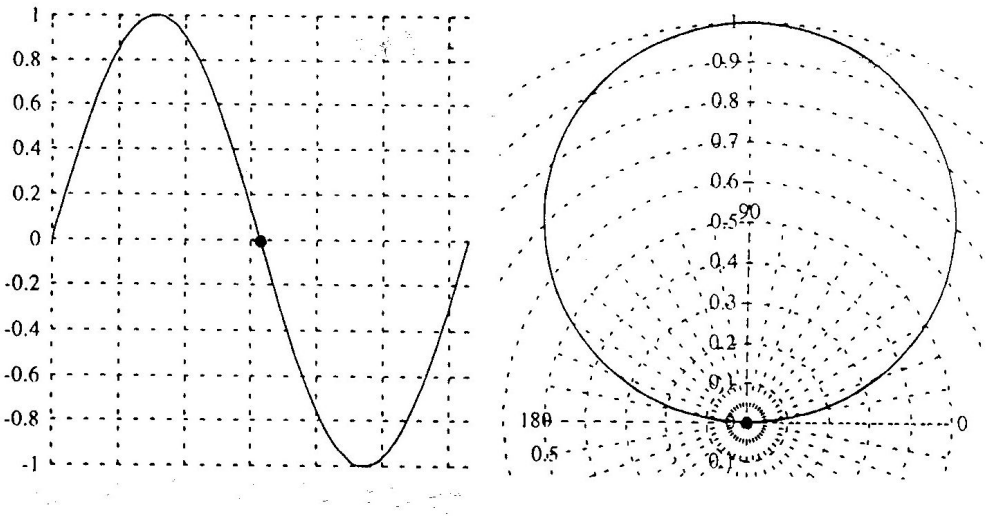

Figure 4.6: Polar plot of minimum correlation

This function is represented on a polar plot by a loop in only one half of the plane, as shown in Figure 4.6. The point at which the loop comes closest to the origin is in the direction of the lowest correlation. The correlation vector at its maximum is denoted as $\vec{C}$.

Since the magnitude of $\mathbf{r}$ changes sign at this point, the value of ϕ at which the minimum correlation occurs can be determined automatically within some predetermined angular precision, using a zero-crossing technique such as bisection.

Descriptive Statistics

The correlation function establishes a relationship between motions across the joint. When only the data of end-effector motion are available, the descriptive statistics can be used to describe the distribution of samples of the random variable.

Descriptive statistics for a set of independent data samples x include the expected value, the variance, the skewness, and the kurtosis. For multi-dimensional data, samples of data are generated by finding marginal distributions, as previously discussed.

The expected value is

$$E[X] = \sum_{j=1}^{n} x_j f(x_j), \tag{4.16}$$

where $f(x_j) = P(X = x_j)$. Here, $P(X = x_j) = 1/n$, so

$$E[X] = \sum_{j=1}^{n} x_j / n, \tag{4.17}$$

which is the arithmetic mean μ or $\overline{x}$.

The variance of the data σ^2 is

$$\sigma^2 = E[(X - \mu)^2], \tag{4.18}$$

where $\mu = E[X]$. The variance of signal data is an indication of the signal power [56].

Skewness is a measure of the asymmetry of the distribution:

$$\alpha_3 = E[(X - \mu)^3]/\sigma^3. \tag{4.19}$$

For the normal curve, $\alpha_3 = 0$, because the normal curve is symmetric [110].

Kurtosis is a measure of how the distribution peaks near the centre of the distribution:

$$\alpha_4 = (E[\frac{(X - \mu)}{\sigma}]^4) - 3. \tag{4.20}$$

The normal curve has $\alpha_4 = 0$. For other distributions, a negative value of kurtosis means that there are a large number of data away from the mean: the distribution has a flat peak compared to that of the normal distribution. A positive value of

kurtosis indicates a sharp peak. In a zero-mean case where average motion data value is zero, high kurtosis indicates that many values are close to zero, and low kurtosis is an indication that many motion samples have high values.

The descriptive statistics provide quantitative indications of the shape of the distribution, and act as indices of how non-normal the marginal distribution has become, as a function of ϕ, the direction.

Power Spectral Density

An alternative to measuring coherence is to examine the power spectral density of the signal component of interest. If the signal is Gaussian, then the power spectral density remains flat across the bandwidth of interest. Conversely, a power spectrum with peaks and valleys represents a non-Gaussian signal. One measure of the flatness of a power spectrum is to fit the magnitudes of the components of a Fast Fourier Transform to a polynomial. This approach was not pursued in the present work.

4.1.3 Excitation Methods

An analogue random-noise generator was chosen to provide external excitation of joints and shaker tables used in experiments.

In industrial implementation, the robot actuators themselves provide excitation of the mechanism, just as passive joints have been driven by dynamic coupling for point-to-point control [15]. A random component can be superimposed onto a controller signal in two ways: analogue or digital. The first method mixes a signal from a random noise generator into the analogue voltage signal coming from the D/A converter, using a summing amplifier. The second method overlays a random component onto the controller signal in software before D/A conversion, using the Box-Muller algorithm [99].

4.1.4 Measurement Methods

Practical aspects of measuring motion are discussed in this section.

General Measurement Issues

In the time domain, data acquisition is triggered at a specific robot state. Otherwise, the influence of the change in robot state due to the normal motion may obscure the motion of interest. Time averaging reduces the effect of noise in the process, but this averaging is only valid for data gathered in the same state.

In transient tests of repeatability, the sampling window has to be large enough for a good signal, but narrow enough that the robot state changes little over the course of a single measurement. Of course, this approach relies on the robot being repeatable enough to move "close to" the same state over repeated measurements. It is unnecessary for the robot error between the desired state and the actual state to be small, only that the error be repeatable.

Triggering is therefore an implementation issue for diagnostic data acquisition during *large* motions. If the robot controller is to be used to signal the beginning of the measurement period, then timing errors are possible. Any uncertainty in the trigger signal generates uncertainty as to whether the measurement made is really of the state of interest. If a time shift is of concern, then data can be synchronised after recording by one-dimensional pattern matching in the time domain.

The method of random variables uses small motions about a given pose, so there is little change in state. Data synchronisation is therefore not a concern in the present work, except in correlations between random variables.

When using absolute-motion transducers such as seismic accelerometers, the robot base either must be immobile with respect to an inertial frame, or it must move repeatably with respect to it. That is, compensation of base motion may be done: the vibration of the base of the structure can be measured and subtracted from the vibration of the point of interest. This assumption is valid if the base motion is repeatable and if measurement noise is normal random. If, however, there are spurious signal components from other sources (transient vibrations from other equipment, etc.), then measurements should be done simultaneously to maintain a reliable correlation between the base and distal signals.

The contribution of flexible motion of non-rigid bodies in the manipulator can be estimated by mounting strain gauges on the links. Since strain is related to displacement, dynamic strain measurements are compared to displacement data. It is more difficult to measure compliance in joints and in fastened connections. The cumulative effect of all motion due to compliance is the difference between the actual motion and the motion predicted by the rigid-body equation of motions (neglecting other modeling errors).

Velocity Measurement

Although the simplest linear relationship for manipulators is the velocity equation

$$\dot{\mathbf{p}} = \mathbf{J}\dot{\mathbf{q}}, \tag{4.21}$$

there are practical limitations on measuring $\dot{\mathbf{p}}$. Seismic velocity transducers are relatively massive (especially compared to smaller manipulators) and do not have good low frequency response.

Joint velocities $\dot{\mathbf{q}}$ are estimated by numerical differentiation of the joint angle data from joint displacement sensors, or measured directly with tachometers [81]. If the actuator for joint (i) is a DC motor, then the back EMF E_i may be used to estimate velocity:

$$E_i = {}_ik_e \, {}_i\dot{q}_a, \tag{4.22}$$

where ${}_ik_e$ is the constant of voltage per unit of angular velocity, and ${}_i\dot{q}_a$ is the actuator angular velocity [32]. For a sensor measuring $\dot{q}_i$ acting through a transmission ratio of ${}_ik_g$, the joint velocity is

$$\begin{aligned} \dot{q}_i &= {}_i\dot{q}_a / {}_ik_g \\ &= \frac{{}_ik_g}{{}_ik_e \, {}_i} \, \dot{q}_a. \end{aligned} \tag{4.23}$$

Any method using sensors measuring through a transmission must account for possible errors in ${}_ik_g$, including backlash.

Acceleration Measurement

The acceleration relation with small velocities is also linear:

$$\ddot{\mathbf{p}} = \mathbf{J}\ddot{\mathbf{q}}, \quad \dot{\mathbf{q}} = 0. \tag{4.24}$$

Measuring $\ddot{\mathbf{p}}$ in a fixed frame coincident with the tool frame is not difficult. Seismic accelerometers give excellent results, with good low frequency response, low transverse sensitivity, and low mass.

Because the method depends on relative accelerations between seismic accelerometers, it is important to match the accelerometer dynamics. Unless transducers are matched, large errors in angular acceleration estimates result [98].

No transducer for direct measurement of joint (angular) acceleration $\ddot{\mathbf{q}}$ was found, but $\ddot{\mathbf{q}}$ could be estimated by differentiating a tachometer signal $\dot{\mathbf{q}}$, or by twice differentiating $\mathbf{q}$, with some risk of noise amplification.

Joint Actuator Torques

The static-force method requires joint-torque measurements and end-effector force measurement, as does the method involving dynamics.

Joint torques can be measured directly by instrumenting the joint axes with strain gauges [74]. There is a tradeoff between torsional stiffness and sensitivity.

Provided the range of motion is not too large, the associated wiring can be physically protected. Telemetry using FM transmission of data is also possible. If the motor dynamics are known, the joint torque can be estimated from the input to the motor [64]. In the case of DC servomotors, the torque of motor i is approximately

$$_i\tau_m = \ _ik_\tau \ i_i, \tag{4.25}$$

where $_i\tau_m$ is the torque (Nm), $_ik_\tau$ is the torque constant (Nm/A), and i_i is current to the motor (A). For a transmission ratio of $_ik_g$, the joint torque is

$$\tau_i = \ _ik_g \ _i\tau_m. \tag{4.26}$$

Generally, ${}_ik_\tau$ is not a constant, but rather a function of joint angle q_i. Because of friction and temperature effects, the function may be quite complicated. Friction and hysteresis may cause problems in measuring forces accurately. Motor current can be measured nonintrusively using a clip-on transducer around the motor power conductor at any location, and so this method holds promise for industrial applications [86].

End Effector Force and Moment Measurement

Force-torque sensors (FTS) are available that can measure the three forces and three torques in a wrench (the general force six-element force vector). Less sophisticated and less expensive models measure in fewer than six directions.

An FTS may be mounted on the end effector or onto the anchoring point. End-effector mounting suits a manipulator employing force control, which already has an FTS at the base of the end effector [14]. For either mounting, the mating between the end effector and the fixture must be stiff, to prevent motion that would be mistaken for internal robot looseness.

End-effector mounting is acceptable for calibration provided that the end-effector kinematics and dynamics are well known. In constrained dynamics motions occur, and so accelerations are measured in the directions of FTS measurement. Although force is not controllable in a direction of motion, it is measurable by an accurate FTS. An FTS for force control may not be able to measure forces in direction $(m+1)$, if it should appear. In that case, an estimate of the environmental impedance can be used to calculate force based on accelerations in direction $(m+1)$ [57]. Because a force sensor has mass, the sensor also measures acceleration if motion occurs [79].

Using a force-torque sensor introduces again the limitations of pose measurement. The manipulator must attach itself to a rigid fixture, and the fixture must be relocated in a set of locations spanning the workspace. It would be a considerable technical challenge to build constraint fixtures that span the workspace and yet have stiff connections.

Choice of Variables

To have minimal sensor mass, seismic accelerometers were chosen for this study, with signals integrated to yield end-effector velocity. Joint displacements were differentiated to obtain joint velocities. Care had to be taken to measure all velocities as close to simultaneously as possible, and so a multiple-channel tape recorder was used to archive sensor signals.

4.2 Looseness Link Finding Method

Using seismic sensors, motion data are measured with respect to the end-effector frame (t). The orientation of frame (i) with respect to frame (t) is ${}^t_i\mathbf{R}$, which is a function of the joint displacements and kinematic parameters of link twists α_j, $j = i, \ldots, n$. The relative orientation of the frames is useful for locating the link on which looseness occurs.

4.2.1 Relating the Link with Looseness to the End Effector

From a fixed coordinate frame, such as frame (w) in Figure 4.7, the direction of loose-

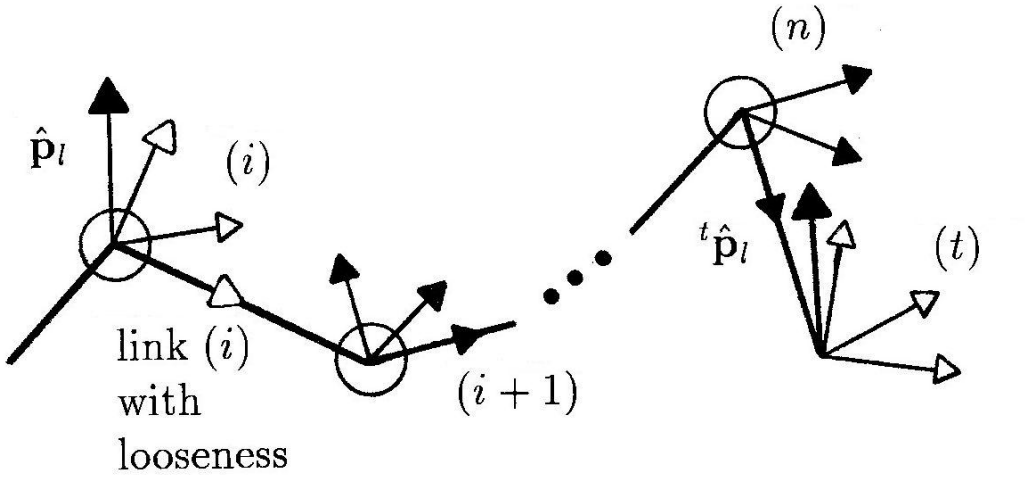

Figure 4.7: Looseness motion in different frames

ness motion at the looseness joint is the same as the direction at the end effector, because prismatic motion is a free vector. When there is a relative change in orientation between the looseness joint and the end effector, the direction of the looseness motion vector changes accordingly. The end-effector frame can also be used.

On a manipulator with revolute joints, the direction of the looseness vector changes if there is a change in joint displacement of any joint between the looseness location and the measurement location. For example, in Figure 4.8 there is

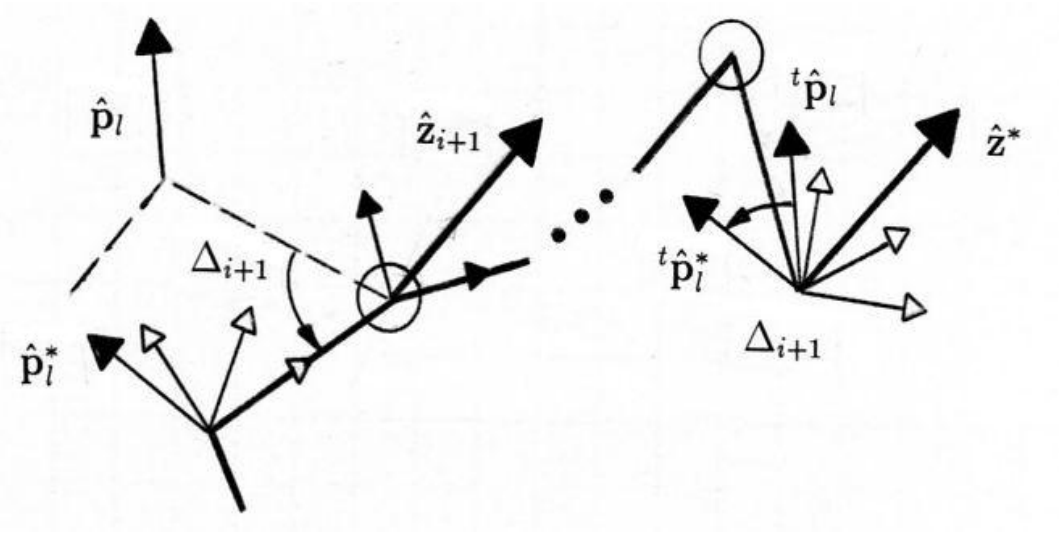

Figure 4.8: Finding the direction of looseness motion at the end effector

looseness in link i. The change in the looseness vector direction $\hat{\mathbf{p}}_l$ in the end effector frame (t) for a change Δ_{i+1} in revolute joint $i+1$ is

$$ {}^t\hat{\mathbf{p}}_l = {}^t_i\mathbf{R}\,{}^i\hat{\mathbf{p}}_l, \tag{4.27} $$

where the rotation comprises a concatenation of intermediate rotations:

$$ \begin{aligned} {}^t_i\mathbf{R} &= {}^t_n\mathbf{R}\,{}^n_{n-1}\mathbf{R}\ldots{}^{i+1}_i\mathbf{R} && (4.28)\\ &= {}^n_t\mathbf{R}(\alpha_n,\theta_t)^T\,{}^{n-1}_n\mathbf{R}(\alpha_{n-1},\theta_n)^T\ldots{}^i_{i+1}\mathbf{R}(\alpha_i,\theta_{i+1}+\Delta_{i+1})^T. && (4.29) \end{aligned} $$

All of the intermediate rotations are known, including the change in ${}^{i+1}_i\mathbf{R}$. That change in orientation from Δ_{i+1} is a rotation about $\hat{\mathbf{z}}_{i+1}$, which in the end effector frame is

$$ {}^t\hat{\mathbf{z}}_{i+1} = {}^t_{i+1}\mathbf{R}\,{}^{i+1}\hat{\mathbf{z}}_{i+1}, \tag{4.30} $$

where ${}^{i+1}\hat{\mathbf{z}}_{i+1} = (0\ 0\ 1)^T$. An estimate of the direction of rotation ${}^t\hat{\mathbf{z}}^*$ comes directly from the cross product of looseness direction unit vectors:

$${}^t\hat{\mathbf{z}}^* = \frac{{}^t\hat{\mathbf{p}}_l \times {}^t\hat{\mathbf{p}}_l^*}{\sin(-\Delta_{i+1})}. \tag{4.31}$$

The method thus searches for a match to a joint rotation axis. In a three-dimensional implementation, Δ_{i+1} is an angle on a sphere.

4.2.2 Order of Operations

The order of operations for locating the link with looseness is:

1. Let $i = 0$;
2. Generate a baseline case and find the direction of looseness with respect to the end effector (sensor) frame (t): ${}^t\hat{\mathbf{p}}_l$;
3. Move joint $i+1$ through some finite angle Δ_{i+1};
4. Generate a test case, and find the direction of looseness ${}^t\hat{\mathbf{p}}_l^*$;
5. Calculate
$${}^t\hat{\mathbf{z}}^* = \frac{{}^t\hat{\mathbf{p}}_l \times {}^t\hat{\mathbf{p}}_l^*}{\sin(-\Delta_{i+1})};$$
6. If ($|{}^t\hat{\mathbf{z}}^*| < \epsilon_{min}$), where ϵ_{min} is a predetermined threshold of whether the two vectors are close to being in the same direction, then increment i and move to the next distal joint (go to Step 2);
7. If ($|{}^t\hat{\mathbf{z}}_{i+1} - {}^t\hat{\mathbf{z}}^*| < \epsilon_{max}$), where ϵ_{max} is a second predetermined threshold for a close match to the actual direction of rotation, then return the value of i as the number of the link with looseness;
8. If, however, there is no definite decision, choose a new Δ_{i+1} and go to Step 3 to repeat the trial.

4.2.3 Choosing Pose Sets

The discussion now turns to the criteria for choosing pose sets.

One approach is to examine reaction forces on a link of interest when a force or torque is applied to the manipulator. The applied wrench comes from the joints. In a pose that is useful for exciting looseness in link (j), the combined set of wrenches should be able to provide a net reaction force to link (j) in three dimensions. A good pose set has large angles through which all joints are moved between poses, so that Δ is large. When Δ is large, errors in the estimates of the direction of looseness motion have less effect on the solution.

Reaction forces occur on link (j) when joint torque is applied to joint (i) in a given manipulator pose; this torque is the wrench that induces motion in the manipulator distal to link $(i-1)$. If the wrench is reciprocal to the twist of looseness motion, then looseness motion does not occur. There is also a gravity wrench: the reaction at link (j) of the part of the manipulator distal to link (j). The gravity wrench has to be compensated during excitation.

A location is chosen on link (j) at which to calculate reaction forces. For convenience, the centre of gravity can be chosen, or the site of a bolted connection of interest on link (j).

If there is no assumed direction in which the looseness may act, then a good pose is one in which three reciprocal wrenches can be applied to the link of interest. In this way, the link of interest experiences a component of loading that is not reciprocal to the direction of possible looseness. The wrenches should be normalised with respect to the energy imparted to links (j) through (n) [40]. In joints proximal to joint (j), this approach is equivalent to a manipulability measure based on minimum energy for a manipulator with j joints that has an end effector comprising links j to n. Each pose is then evaluated for its ability to produce reaction forces in three dimensions on the link of interest, using Chebyshev spacing to search the space spanned by the joint vectors. From a set of candidate poses, the pose set is chosen to be the set that has the largest differences in the elements of the n-vector of joint displacements.

4.3 Summary of Implementation

This section summarises how manipulator joint and end effector motion data is reduced for looseness diagnosis and for display.

The time-domain data represent a sample of random variables of the manipulator joints and the end effector. The probability distribution of end-effector motion is approximated by a discrete PDF—a multi-dimensional histogram.

The marginal PDFs are found either by transforming the original data and then doing a single-dimensional histogram, or by postprocessing the multi-dimensional histogram. The first alternative is more attractive, because no resolution of the data has been lost in the original signal processing needed to develop the histogram. The histogram is, however, useful for displaying the distribution of motions, and it could be used by an inspector to choose trial parameters for estimation.

Two methods of finding looseness motion were implemented: the Marginal Distribution Matching Method and the Correlation Vector Method.

In the Marginal Distribution Matching Method, the normality of a given marginal PDF is assessed by a nonlinear curve fit to the equation of the normal distribution [99]. For a rigid-body manipulator undergoing normal random motions in its actuated joints, the direction of non-normal random motion is the direction of looseness. (Descriptive statistics of the marginal distribution also assess whether the distribution is closely normal-random.)

The Correlation Vector Method relates the motion of the mechanism distal to the area of interest to the motion proximally. The component of motion that has the poorest correlation to the proximal motion is the direction of looseness.

Having found the direction of looseness, the next step is to identify the link on which the looseness occurs using the Looseness Link Finding Method. Multiple poses, moving one revolute joint at a time, determine the link where looseness is present. The identification criterion is a change in the direction of the looseness motion at the end effector when the orientation of the link with looseness changes with respect to the end-effector frame.

Chapter 5

Simulations

Prudens quæstio dimidium scientiæ.
(To know what to ask is already to know half.) *Aristotle*
(attributed)

This chapter describes attempts to model a robotic manipulator with looseness: a planar articulated manipulator with two revolute joints and a prismatic looseness joint in the distal link.

Kinematic models generated end-effector motion distributions in Monte Carlo simulations using artificially assumed looseness motion distributions. The simulation results were used to test the effectiveness of the two looseness direction-finding methods. The Correlation Vector Method produced better estimates than the Marginal Distribution Matching Method.

The difficulty in generating appropriate motion distributions supported the need for experiments to validate the hypothesis that the looseness motion would manifest itself in the end-effector motion in a recognisable way.

5.1 Monte Carlo Simulations

A planar articulated manipulator was simulated with prismatic looseness in the distal link. With looseness, the manipulator gained an uncontrolled degree of freedom and had three joints and three links.

Kinematic Monte Carlo simulations used artificial joint-motion distributions to generate end-effector motions. Two approaches were examined. Differential displacement simulations approximated the velocity case, using assumed displacement distributions, whereas simulations based on velocity equations used displacement and velocity distributions.

Actuated joint-motion distributions were independent and normal-random. The looseness motion distribution was based on assumptions about contact motions.

The resulting end-effector motions were processed to generate a multi-dimensional histogram approximating the actual motion distribution; this histogram showed the effect of looseness motion on the end-effector motion distribution.

5.1.1 Estimating the Distribution of a Random Variable

Monte Carlo simulation is a method for examining system behaviour when the distribution of a random variable is of concern rather than a deterministic solution [51, 99]. In Monte Carlo solutions, the probability distribution for one random variable is estimated using approximate distributions for each of the other random variables.

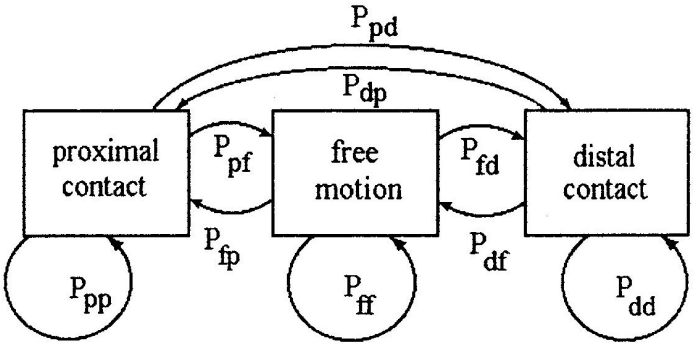

Figure 5.1: Transitions between regions

The system may pass from one region to another, with different system behaviour in each region, as shown in Figure 5.1. To estimate the distribution of the random variable of interest, the simulation thus requires the probability distribution of the other random variables within each region and the transitional probabilities between

regions.

Looseness Motion Distributions

In the case of looseness, the regions were defined by displacement: the contact point at the proximal stop; the free motion region between stops; and the contact point at the distal stop. The transitional probabilities were therefore based on displacement,

P_{pp}	P_{pf}	P_{pd}	(sum = P_{p*});
P_{fp}	P_{ff}	P_{fd}	(sum = P_{f*});
P_{dp}	P_{df}	P_{dd}	(sum = P_{d*});
(sum = P_{*p})	(sum = P_{*f})	(sum = P_{*d})	(sum = 1).

Table 5.1: Displacement transitional probabilities

as shown in Table 5.1.

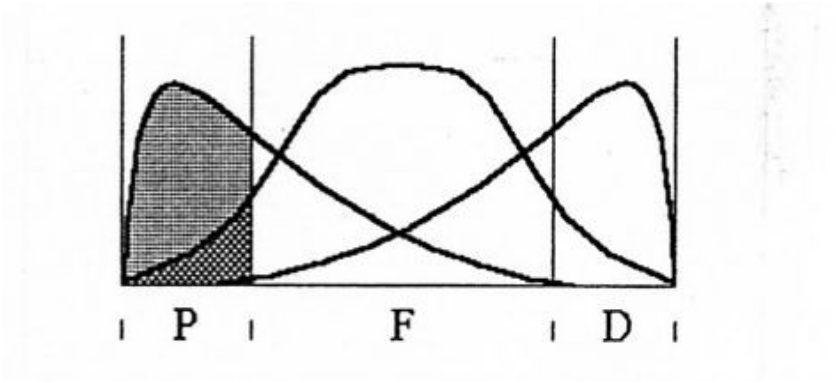

Figure 5.2: Probability distributions of displacement

Figure 5.2 shows three probability distributions of looseness displacement. The shaded area represents the conditional probability distribution given that the previous state of displacement was that in region P of proximal contact: P_{*p}. The middle area represents the displacement probability given that the previous state was in the free region F: P_{*f}. The right-hand area illustrates the displacement probability given that a previous state was in the distal contact region D: P_{*d}.

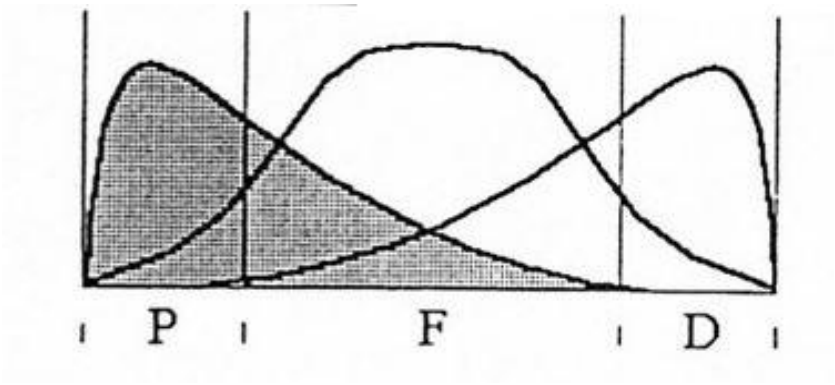

Figure 5.3: Probability of displacement being in region P

The probability that the displacement lay in region P is illustrated in Figure 5.3. This probability was

$$P_{p*} = P_{pp} + P_{pf} + P_{pd}. \tag{5.1}$$

Probabilities in other regions followed similar relationships, so the probability that the event lay in one of the three sets of displacements was

$$P_{p*} + P_{f*} + P_{d*} = 1. \tag{5.2}$$

The contact probabilities were point probabilities that two bodies were in contact. The distribution of motion in the region of free motion could be estimated by experiment[1]. It was also possible to construct probability distributions for velocity and acceleration from the displacement distribution. The bounds on velocity were the minimum and maximum velocities that could occur during a time step $(t - t_0)$ without producing displacements outside the set of displacements $x(t) \leq x_{\max}$. Similarly, the minimum and maximum accelerations were those which did not produce excessive velocities. The velocity and acceleration distributions were therefore bounded by the displacement.

[1]Estimates for P_{p*}, P_{f*} and P_{d*} displacement distributions for real systems come directly from displacement measurements or by double integrating accelerometer signals. Of course, in a diagnostic situation, actual looseness motion is not measurable unless a looseness location is instrumented in advance.

In velocity and acceleration distributions, probability distributions for each region could not be measured unless the displacement was also known, because the conditions (bounds that uniquely defined the regions) were displacement based. The intersection of displacement sets was a null space, but velocity sets could intersect for distributions in different displacement regions, as could acceleration sets. For example, there could be positive velocity at both the proximal contact point and in the free-motion region.

In the present work, it was necessary only that the motion distribution was different from the normal distribution.

5.1.2 Simulation Algorithm

The simulation algorithm comprised a loop with two activities. For a finite number of trials the loop generated values for each of the three random variables (two actuated joints and a looseness joint), and substituted the values into the equation relating end-effector motion to joint motion. The transformation of random variables through this equation produced a population with a discrete multi-dimensional distribution that, with a large number of trials, approached that of the end-effector motion distribution for the given multi-dimensional motion distributions.

Generating Random Variables

Pseudo-random numbers with uniform and normal deviates (distributions) were generated in software.

The uniform deviate used a seed value to produce a pseudo-random value uniformly distributed between two user-defined values. For the point-probability values at the stops, a wider range of the uniform distribution was used and the values produced outside the range of interest (in free motion) were lumped into the impulse probability. This method is illustrated in Figure 5.4 for a uniform probability with cumulative probability of 0.5 with point probabilities of 0.25 on each end. Point probabilities represented the likelihood that there was contact; the value of the point

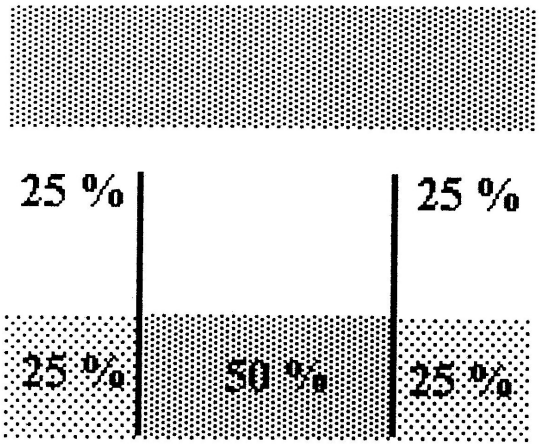

Figure 5.4: Generating point probability from uniform distribution

probability of contact was chosen arbitrarily. The uniform distribution was deemed to be a good approximation of free looseness motion between stops produced by a narrow-band random force input at either stop. The distribution was symmetrical because it was assumed that the looseness dynamics were the same in each direction of looseness motion.

The Box-Muller algorithm used two uniform deviates (distributions) with a range from -1 to 1 to produce a pair of pseudo-random variables, each independent and normally distributed with zero mean and unity variance [99].

Transformation of Random Variables

Three kinematic relationships were used in transforming random joint motions to end-effector motions: differential displacements, velocities, and accelerations with small velocities.

5.1.3 Differential Displacement

For the first kinematic simulations, a first-order approximation to velocity was a differential displacement per unit time.

In the planar articulated manipulator with looseness in the second link at an

angle β to the ${}^2\hat{\mathbf{x}}$ axis, the position of the end-effector in world coordinates (${}^0\hat{\mathbf{x}}$, ${}^0\hat{\mathbf{y}}$) was

$$\begin{aligned} {}^0\mathbf{p} &= (l_1C_1 + dC_{12\beta} + l_2C_{12}){}^0\hat{\mathbf{x}} \\ &+ (l_1S_1 + dS_{12\beta} + l_2S_{12}){}^0\hat{\mathbf{y}}. \end{aligned} \tag{5.3}$$

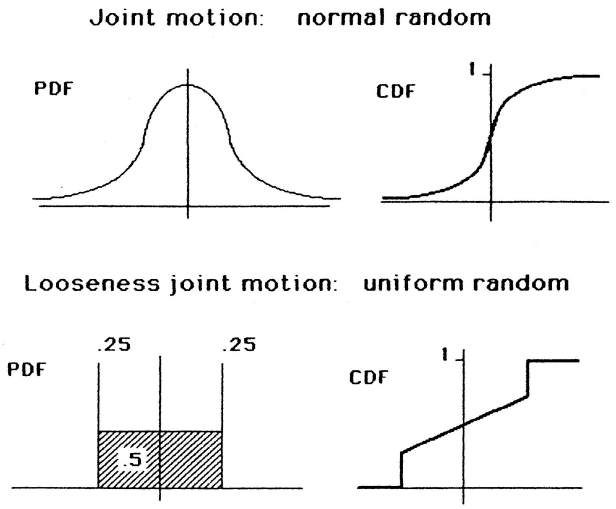

Figure 5.5: Assumed looseness-displacement distribution

The assumed looseness distribution is shown in Figure 5.5. The position of looseness was uniformly distributed along the zone of free motion 50% of the time, with the joint in contact with each stop 25% of the time.

The assumed differential displacement for each revolute joint was normal-random, with a mean about the nominal joint angle; both distributions had the same variance.

Figure 5.6 shows differential motions in two manipulator poses; angles were measured CCW from $\hat{\mathbf{x}}$. Motions were normal distributions in joints and uniform looseness in the looseness joint at the proximal end of link 2. The distributions are magnified for clarity.

The distributions had an ellipsoidal shape in the no-looseness case, and the contours became more ellipsoidal as the number of trials in the random variable sequence increased.

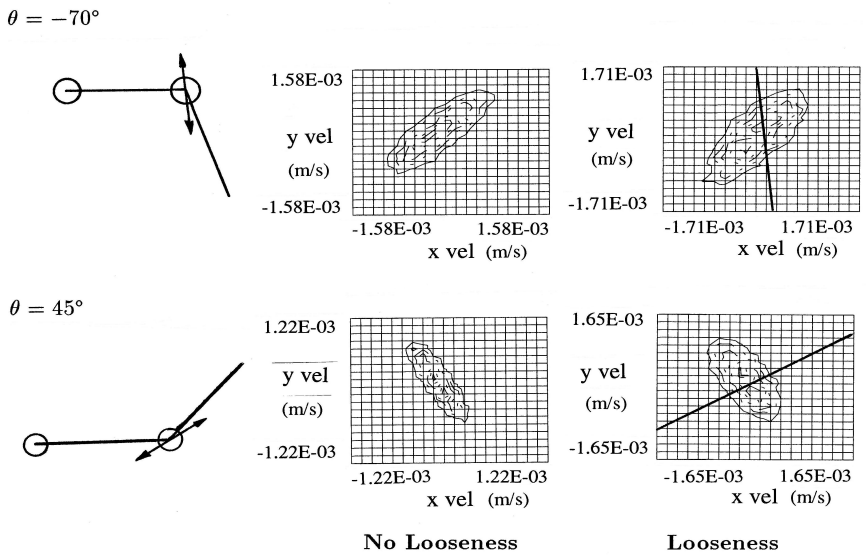

Figure 5.6: End-effector differential-displacement distribution

5.1.4 Velocity

The linear velocity of the manipulator end effector with link 2 looseness with respect to frame (0) was

$$\begin{aligned} {}^0\dot{\mathbf{p}} &= [-\dot{\theta}_1 l_1 S_1 + \dot{d}C_{12\beta} - \dot{\theta}_{12}(dS_{12\beta} + l_2 S_{12})]{}^0\hat{\mathbf{x}} \\ &\quad +[\dot{\theta}_1 l_1 C_1 + \dot{d}S_{12\beta} + \dot{\theta}_{12}(dC_{12\beta} + l_2 C_{12})]{}^0\hat{\mathbf{y}}. \end{aligned} \tag{5.4}$$

The angular velocity of the looseness link ${}^0\vec{\omega}_3$ was the same as that of the link proximal to the looseness link ${}^0\vec{\omega}_2$:

$${}^0\vec{\omega}_3 = {}^0\vec{\omega}_2 = (\dot{\theta}_1 + \dot{\theta}_2){}^0\hat{\mathbf{z}}. \tag{5.5}$$

The looseness distribution approximation is shown in Figure 5.7. There were three distributions, one for each zone. In proximal contact there could be no motion deeper into the stop, so there was either velocity in the direction of free motion or no motion (zero velocity). Conversely, against the distal stop, there could only be zero velocity or negative velocity into the free-motion zone. In free motion, the velocity distribution was assumed to be uniform with a mean of zero. In all cases,

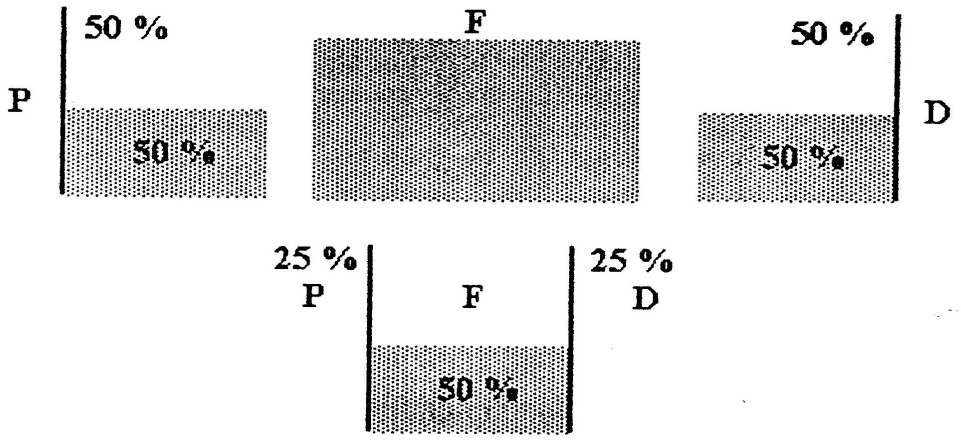

Figure 5.7: Assumed looseness-velocity distribution

the maximum positive and negative velocity were assumed to be those which carried the link across the looseness gap in one time interval.

The displacement could be evaluated in one of two ways. Either a displacement distribution could be used, or a series of samples from the velocity distributions could be integrated to produce a displacement distribution[2]. If the velocity distributions were symmetrical and had means of zero, then the expected value of the multi-dimensional end-effector velocity was zero because the velocity transformation was linear. In the present case, the displacement distribution used was the same as that of the differential-motion case.

The actual velocity equations produced an end-effector velocity distribution that did not suffer from the first-order accuracy limitation of differential displacements. Figure 5.8 shows the end-effector velocity distribution in several poses. Results were very similar to results of simulations with differential displacements, except for a change in the looseness gap related to the scale of looseness motion used.

[2]Integrating a series of samples from a random process assumed that velocity samples were from a time sequence and each trial was an event of equal probability.

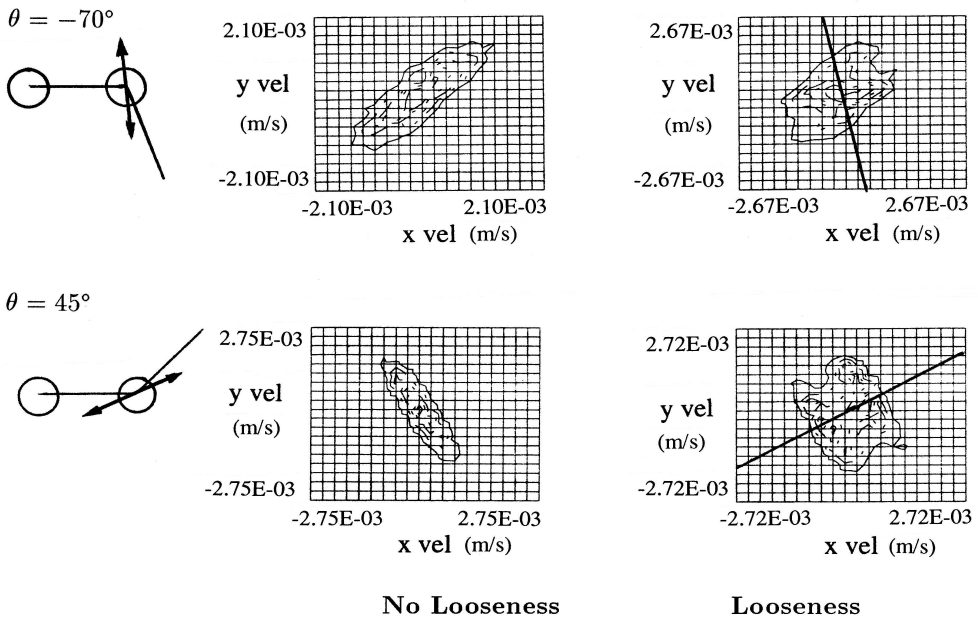

Figure 5.8: End-effector velocity distribution

5.1.5 Acceleration

Rather than using differential velocities to generate end-effector accelerations, a more accurate approach was to use the acceleration equations directly:

$$\begin{aligned} {}^0\ddot{\mathbf{p}} &= [-l_1(\dot{\theta}_1^2 C_1 + \ddot{\theta}_1 S_1) - d(\dot{\theta}_{12}^2 C_{12\beta} + \ddot{\theta}_{12} S_{12\beta}) \\ &\quad -l_2(\dot{\theta}_{12}^2 C_{12} + \ddot{\theta}_{12} S_{12}) + \ddot{d} C_{12\beta} - 2\dot{d}\dot{\theta}_{12} S_{12\beta}]^0\hat{\mathbf{x}} \\ &\quad +[l_1(-\dot{\theta}_1^2 S_1 + \ddot{\theta}_1 C_1) + d(-\dot{\theta}_{12}^2 S_{12\beta} + \ddot{\theta}_{12} C_{12\beta}) \\ &\quad +l_2(-\dot{\theta}_{12}^2 S_{12} + \ddot{\theta}_{12} C_{12}) + \ddot{d} S_{12\beta} + 2\dot{d}\dot{\theta}_{12} C_{12\beta}]^0\hat{\mathbf{y}}. \end{aligned} \tag{5.6}$$

The looseness acceleration distribution had the same three-part structure as the velocity distribution, with different acceleration distributions for proximal contact, free motion, and distal contact. Transitional probabilities depended on having displacement and velocity distributions.

In the case of accelerations with negligible velocities, the acceleration results were the same as in the velocity case, provided that the looseness acceleration distribution was the same as the looseness velocity distribution.

5.1.6 Rigid-Body Dynamics

Although the methods described for locating looseness are based on kinematics, the implementation relies on dynamic coupling between links to produce relative motion in the unactuated looseness joint. The working hypothesis is that a non-normal motion results that allows identification of the looseness location. But the looseness motion itself is not known, and the assumed uniform-random motion distributions in the kinematic simulations above may not have been realistic.

Dynamics simulations would have been more realistic approximations of the physical system. In a kinematic simulation, the random variables of concern are joint values and end-effector displacements and their derivatives. In a rigid-body dynamics simulation, the equation of concern is

$$\mathbf{F} = \mathbf{M}\ddot{\mathbf{y}} + \mathbf{C}(\mathbf{y},\ \dot{\mathbf{y}}) + \mathbf{K}(\mathbf{y},\ \dot{\mathbf{y}}), \tag{5.7}$$

where $\mathbf{M}(\bullet)$ is the inertia tensor, $\mathbf{C}(\bullet)$ is the vector of centripetal and Coriolis terms, $\mathbf{K}(\bullet)$ is the vector of potential terms, and $\mathbf{F}$ is the vector of generalised forces on the system. The random variables are the elements of vectors $\mathbf{F}$, $\mathbf{y}$, $\dot{\mathbf{y}}$, and $\ddot{\mathbf{y}}$. The distribution of $\ddot{\mathbf{y}}$ thus depends on the distributions of $\mathbf{F}$, $\mathbf{y}$, and $\dot{\mathbf{y}}$:

$$\ddot{\mathbf{y}} = \mathbf{M}^{-1}[\mathbf{F} - (\mathbf{C} + \mathbf{K})]. \tag{5.8}$$

For a given set of equations of motions, by knowing the distribution of the input variables it is possible to transform the variables to approximate the distribution of the variable of concern. From input distributions of force, displacement, and velocity, the rigid-body equations of motion produce acceleration distributions. Because these distributions, the conditional probabilities for transitions between sets of equations of motion, and the dynamic parameters of looseness may be uncertain, dynamic Monte Carlo simulations were not pursued in verifying the kinematic method of looseness identification.

5.1.7 Summary of Monte Carlo Simulation Results

Kinematic simulations of the effect of looseness supported the conjecture that the presence of non-normal random looseness motion distorted the statistical manipulability ellipsoid. Larger sets of data made distribution probability contours better defined. The results of all these simulations were, however, dependent on the assumed looseness motion distribution.

Because the Monte Carlo method was uncertain without good knowledge of the probability distributions, there was a need for experimental investigation of the nature of the change in motion from looseness.

5.2 RR Manipulator Rigid-Body Joint Forces

In the present work, the rigid-body equations of motion were useful for manipulator design, and for indicating where looseness might appear.

The recursive Newton-Euler equations of motion were used to generate the joint forces and torques required for a specified rigid-body motion of the nominal planar articulated (RR) manipulator.

The range of motion in joint space was $-90^\circ \leq \theta_2 \leq 90^\circ$. Four sets of joint velocity and acceleration criteria were used. The simulation results were used to specify the torque requirements of the actuated joints. This manipulator design tool is described in detail in Chapter 6.

The highest joint forces acted in the tangential direction of the proximal link. This result indicated that there was a likely place to look for looseness in the RR manipulator moving perpendicular to gravity: in the tangential direction at the distal end of a link.

5.3 Verification of Looseness Direction Finding Methods

Simulated motion distributions were used to evaluate the two methods for finding the direction of looseness.

5.3.1 Direction Search Using the Marginal Distribution Matching Method

Simulated data were processed into a multi-dimensional histogram. The bin values of the histogram were the data used to verify the performance of the nonlinear parameter estimator of direction of the normal distribution.

Bivariate Distribution

A bivariate distribution was used to verify the estimator performance. A normal-random data set $\{x\}$ was generated with unit variance, and $\{x\}$ was a set of data trials from a uniform distribution. The data pairs were then transformed by a rotation ϕ to produce two-dimensional data, with the marginal normal distribution in the direction ϕ with respect to a fixed direction $\hat{\mathbf{x}}$.

Histogram Processing

To verify the estimator performance, a custom program generated data using the bivariate distribution. One hundred trials were performed, and the resulting data sets were sorted into a two-dimensional histogram with an equal number of bins in each direction. The program then collected those data points and generated a file to be read by the ODRPACK nonlinear curve-fitting package.

Results

The estimator was able to find the three parameters to within 0.1% , provided that the trial values were within 10% of the correct answer. If initial parameters were

excessively different from the actual parameters, then the estimator did not converge to close estimates. In such a case, the ODRPACK program reported that the square of the residual exceeded the convergence threshold, indicating that the estimates did not fit the model well.

This method offered no way to home in on the direction of looseness motion, because the trial value of the direction a_2 had to be chosen arbitrarily. An alternative strategy would have been to do multiple trials, with the trial value of a_2 evenly spaced in the range from 0 to π radians, choosing the solution with the lowest residual.

5.3.2 Direction Search using the Correlation Vector Method

The next simulation examined the effectiveness of the correlation vector method for finding the direction of looseness.

The modeled data of a bivariate distribution came from samples of a normal distribution and a uniform distribution, each with six thousand points. No trial values were used for the motion direction. A set of correlation vectors with respect to the normal distribution was generated for motion components at angles spaced uniformly from 0 to π radians.

The first simulation investigated the effect of scaling a sequence of samples of a bivariate normal distribution that was then correlated against one of the sequences of data unscaled. The ratio of variance between the distributions ranged from 0.1 to 10.

The second simulation correlated a normal-random sequence against a sequence of uniformly distributed data. Again, the ratio of normal distribution variance to the width of the uniform distribution varied between 0.1 and 10.

Results

Figure 5.9 shows the vector plot for normally distributed data correlated against itself when rotated through an angle. When the angle was 0, the correlation was 1; at right angles, the correlation was 0. This was, in effect, the cosine function plotted

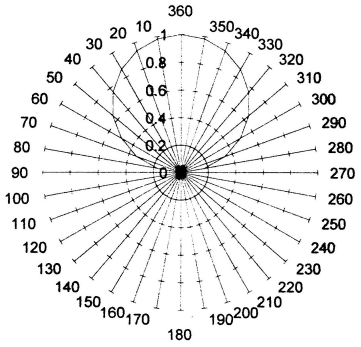

Figure 5.9: Correlation plot for normal distribution

in polar coordinates.

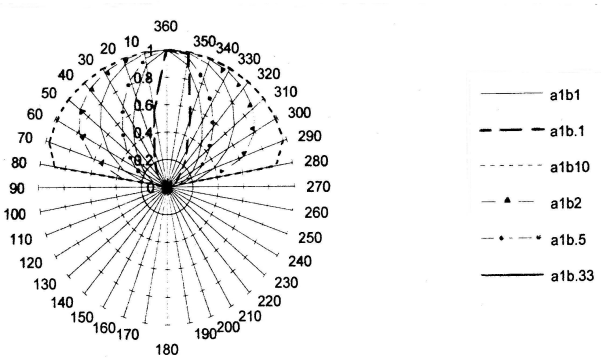

Figure 5.10: Correlation plot for scaled normal distribution

The effect of scaling on the correlation vector is shown in Figure 5.10. The aspect ratio of the correlation vector plot changed according to the scaling of the normal distribution, but the direction of minimum correlation remained the same.

Because the two normal RVs in the bivariate distribution were independent, the second normal distribution did not affect the correlation with respect to the RV of concern: the other data were rejected as noise. There was an effect of scaling on the correlation of the rotated RV with respect to itself. At ratio 1:1, the aspect ratio was unchanged. Attenuating the RV narrowed the plot, which made the curvature near the minimum high. In contrast, the aspect ratio flattened when the RV was amplified. Amplification made the curvature low near the minimum, which improved

the resolution where the minimum occurred. It was therefore preferable in practice to amplify the end-effector signal with respect to the joint signal when searching for the looseness direction.

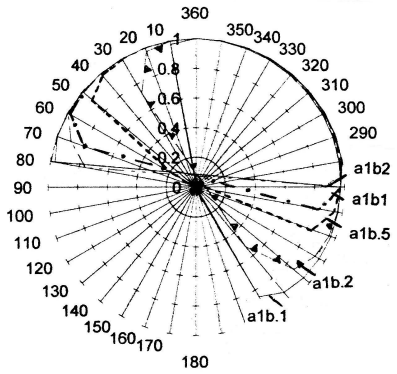

Figure 5.11: Correlation plot for normal distribution and uniform distribution

Figure 5.11 shows a correlation plot of a bivariate distribution for a Gaussian RV in the direction 0° and a uniform RV perpendicular to the Gaussian RV. The correlation was with respect to the Gaussian RV. The legend gives the ratio of the width ω of the uniformly distributed RV to the variance σ^2 of the normally distributed RV[3]; the notation a1b5 represents $\omega : \sigma^2 = 1 : 5$.

When the ratio of uniform-distribution width to variance of the normal-random variable was high, the minimum correlation direction approached the direction of the normal-random component. The correlation was dominated by the uniform distribution.

Conversely, when the ratio of uniform-distribution width to variance of the normal-random variable was low, the correlation vector tended to have its minimum close to the expected value of 270°. The normal-random distribution dominated the correlation.

The correlation was done against the normal-random variable only. Also, the power in the non-normal random signal was less than that of the normal-random component of the bivariate distribution. If those conditions were met, then the

[3]For a uniform RV range of 5, width ω is 2.5.

direction of most non-normal motion could be found with no need for a trial direction.

5.4 Summary of Simulation Results

The Monte Carlo kinematic simulations generated good results based on uncertain assumptions. The rigid-body dynamics equations of motion were, however, useful for designing the experimental manipulator.

The Correlation Vector Method of locating the direction of looseness worked well, while the Marginal Distribution Matching Method required good trial parameters to converge on the correct solution.

5.4.1 Monte Carlo Kinematic Simulations

Kinematic simulations showed that non-normal multi-variate motion distributions resulted when a non-normal random joint motion was introduced with other joint motions that were independent and normal-random. The nature of the looseness motion distribution was contrived, and so actual multi-variate motions could not be simulated.

Monte Carlo simulations of the rigid-body dynamics were not attempted, because they depended on accurate estimates of the distributions for random joint forces, displacements, velocities, and accelerations.

5.4.2 Verification of the Looseness Direction Finding Techniques

The Marginal Distribution Matching Method searched for the direction in which histogram data best matched a normal-random distribution. The search failed whenever there were poor initial choices of trial parameters. Trial estimates were made of variance and scale parameters, but there was no way to make a good preliminary guess of the direction parameter. The Marginal Distribution Matching Method did not perform well without *a priori* information about the direction.

The Correlation Vector Method was successful at finding the direction of looseness motion when components of the distal motion in different orientations were correlated against the proximal excitation motion. This method assumed good transmission of the excitation motion and looseness motion through the structure to the end effector.

5.4.3 Rationale for Pursuing Experimental Study

The motivation for experimental studies was a desire to produce actual looseness motion distributions. The present simulations used idealised distributions that most likely did not reflect actual conditions.

Experimental studies allowed investigation of the practical aspects of implementing the looseness identification method: how to generate random joint motions, how to measure motions at the end effector, and whether joint motion was transmitted well through the manipulator structure.

Chapter 6

Experiments

Facts don't come with points of view.
Facts don't do what I want them to. *Talking Heads*

Chapter Three introduced the concept that a viable method for identifying looseness in robots validates three hypotheses:

1. faults have observable effects that are repeatable;

2. the effects can be measured; and

3. the effects can be related to their respective origin using model-based analysis.

A model-based analysis approach was developed in Chapter Four for relating fault effects to their origins, which laid the groundwork for validating the third hypothesis. But the first and second hypotheses had to be validated by experiment for the method to be viable.

This chapter describes experiments that showed that a stochastic relationship existed through manipulator kinematics between joint and end-effector motions, and that this relationship was sensitive to structural looseness in an identifiable way.

6.1 Experimental Plan

To demonstrate the proof of the concept of locating structural looseness in robotic manipulators, a progressive series of six experiments was undertaken.

The first experiment tested the first hypothesis, that robots produce repeatable, observable end-effector motions.

Subsequent experiments tested the second hypothesis that looseness effects could be measured. The second experiment tested whether planar accelerations could be well represented by perpendicular accelerometers. The third experiment established whether the kinematic relationship between joint motions and link motions would survive the dynamic effects of a physical system when the motions were stochastic.

The fourth experiment examined the effect of looseness on the correlation vector and on the descriptive statistics of planar acceleration components in the direction of prismatic looseness.

The fifth experiment assessed the dependence of manipulator pose on the method for locating a looseness fault in a planar revolute-joint manipulator. The final experiment assessed the dependence of pose for locating a backlash fault seeded into the manipulator.

6.1.1 Experimental Rigs

Three experimental rigs were used in this study. The first apparatus was a cylindrical-coordinate industrial manipulator. The second apparatus was a slide with a detachable prismatic joint with adjustable looseness. The third rig was a planar revolute articulated manipulator upon which the looseness joint could be mounted; this apparatus was dubbed VERA, the Variable Estimation Robot Arm.

Motivation for Rig Development

The industrial manipulator available at the beginning of the project did not have known dynamic parameters, nor was it easy to induce reproducible looseness faults.

Experimental rigs were designed with simple but nontrivial kinematics and dynamics (with measurable parameters), and each rig could incorporate reproducible looseness faults.

Two kinds of looseness were of concern: structural looseness and backlash. A special linear joint was designed to be added to the linear rig, or to the proximal end of VERA link one or link two. The looseness joint had variable looseness-gap adjustment screws, space for stops of different stiffness, and additional mounting holes to permit adjustment of the looseness angle with respect to the link. Backlash was added by adjusting the gear-mesh gap of the joint-motor pinions.

6.1.2 Robot Design

Design Methodology

The robot was designed to have the following characteristics:

1. Multiple degrees of freedom, because selecting the pose set for locating the fault was part of the scope of the present work.

2. Simple dynamics.

3. Modularity, allowing variable kinematic parameters for multiple trials.

4. Expandability, for installation of end effectors, instrumentation, and extra degrees of freedom.

5. Changeable configurations, so that kinematics could be altered to suit the task at hand.

6. Bench-sized, for an economical implementation and laboratory usefulness after the project.

7. Maximal use of off-the-shelf components.

8. Maximal use of in-house equipment.

9. Structured computer code, in C.

The design of the manipulator followed seven steps: specification choices, kinematic design, dynamics design, actuator selection, sensor selection, controller implementation, and performance checking to ensure that specifications were met. All steps required attention to mechanical, electrical, and control-system design[72]. These design steps were iterative, as Figure 6.1 shows, and within this cycle, the

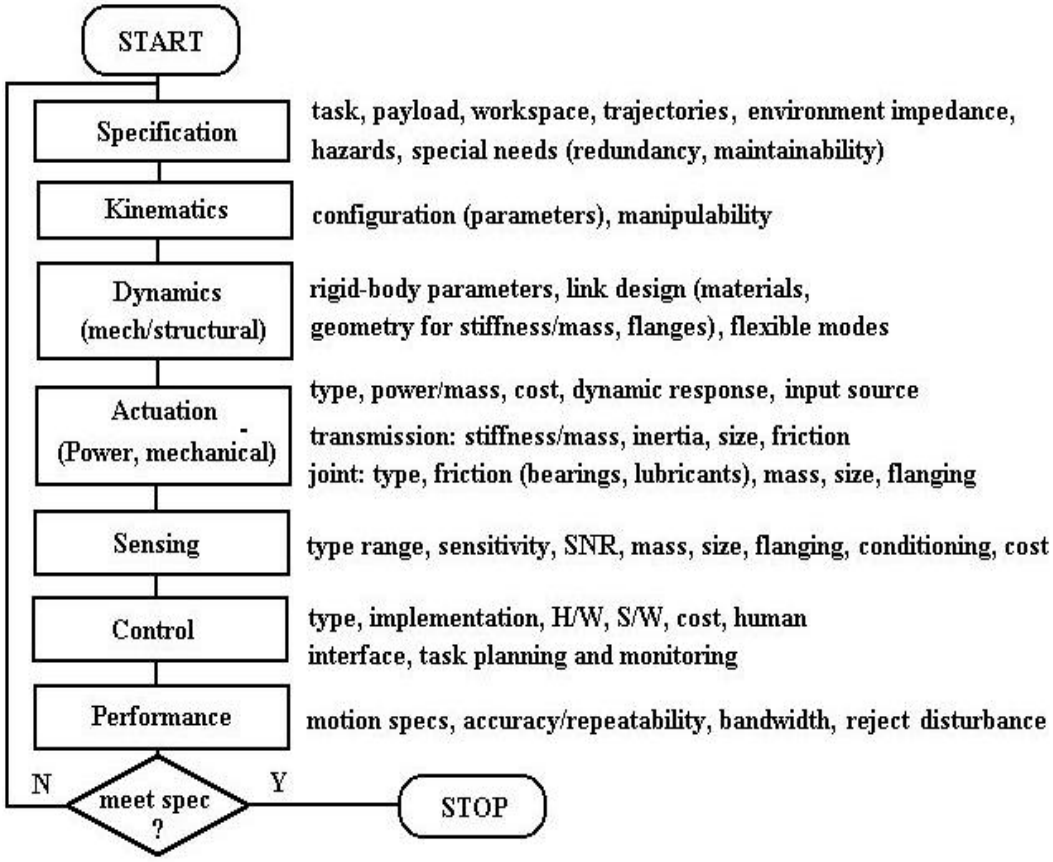

Figure 6.1: Design steps

dynamics and actuation steps were themselves iterative.

Specifications

The robot had a circular workspace in the horizontal plane with an outer diameter of 0.81 m. The manipulator was not designed to operate in harsh environments, nor

was it intended to perform contact tasks, as it had no gripper. The robot had a two degree-of-freedom articulated configuration. Figure 6.2 shows an isometric assembly

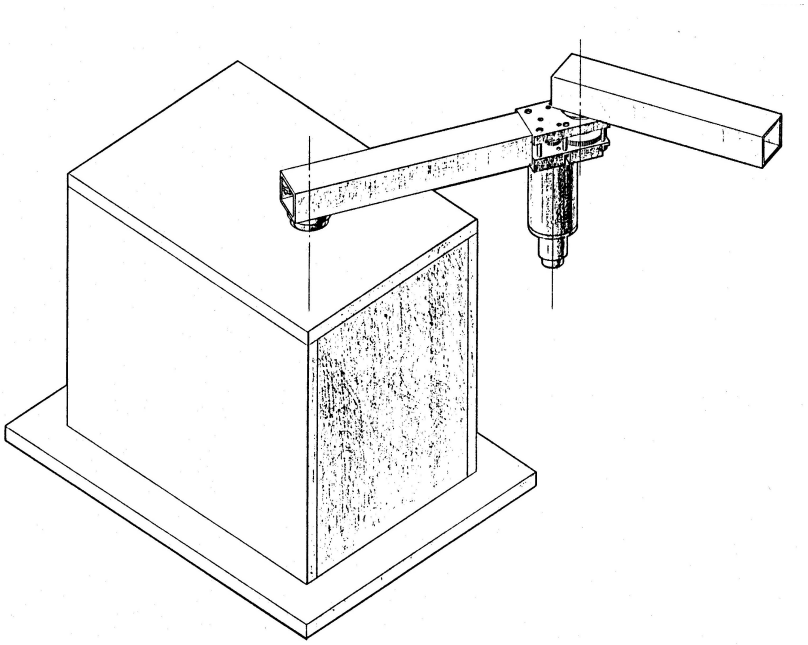

Figure 6.2: VERA assembly

of the VERA manipulator.

Neither joint 1 nor joint 2 had mechanical stops, and so their range of motion was not restricted[1], and both links were of the same length to maximise kinematic manipulability [133].

Kinematics

Kinematic parameters for VERA are shown in Figure 6.3. The position $\mathbf{p}$ of the end effector with respect to the world coordinate frame was

$$\mathbf{p} = \left\{ \begin{array}{c} l_1 C_1 + l_2 C_{12} \\ l_1 S_1 + l_2 S_{12} \end{array} \right\}. \tag{6.1}$$

[1] A tapered pin was, however, installed in joint 2 to block its motion in some tests.

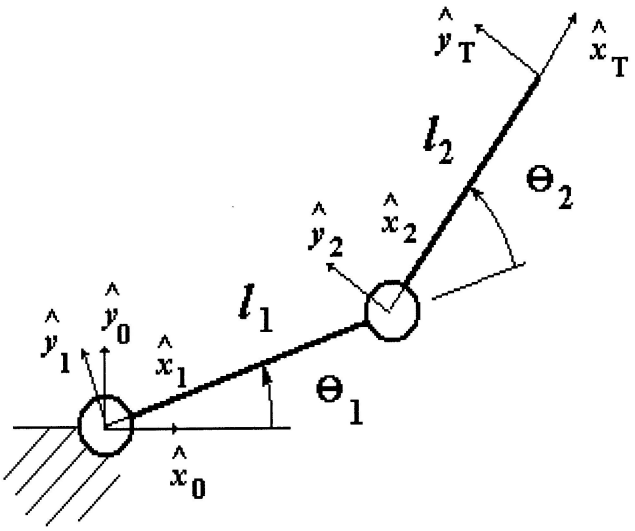

Figure 6.3: VERA kinematic parameters

Dynamics

The generalized coordinates for the equations of motion for the rigid-body dynamics of this manipulator were joint angles θ_1 and θ_2, and generalized forces were joint torques τ_1 and τ_2. State variables were $\theta_1,\ \theta_2,\ \dot{\theta}_1$, and $\dot{\theta}_2$.

The joint forces and torques for the planar manipulator were found using the Newton-Euler recursive formulation [36]:

$$
{}^1\tau_1 = \left\{ \begin{array}{c} S_2 m_2 l_{c2} g \\ -(m_1 l_{c1} + m_2 l_1 + C_2 m_2 l_{c2}) g \\ (I_1 + m_2 l_{c1}^2)\ddot{\theta}_1 + l_1(S_2 f_{x2} + C_2 f_{y2}) + n_{z2} \end{array} \right\}, \tag{6.2}
$$

$$
{}^2\tau_2 = \left\{ \begin{array}{c} 0 \\ -l_{c2} m_2 g \\ l_{c2} m_2 [l_{c2}\ddot{\theta}_{12} + l_1(S_2\dot{\theta}_1^2 + C_2\ddot{\theta}_1)] + I_2\ddot{\theta}_{12} \end{array} \right\}, \tag{6.3}
$$

$$
{}^1 f_1 = \left\{ \begin{array}{c} -m_1 l_{c1}\dot{\theta}_1^2 - m_2[l_{c2}(C_2\dot{\theta}_{12}^2 + S_2\ddot{\theta}_{12}) + l_1\dot{\theta}_1^2] \\ m_1 l_{c1}\ddot{\theta}_1 + m_2[l_{c2}(-S_2\dot{\theta}_{12}^2 + C_2\ddot{\theta}_{12}) + l_1\ddot{\theta}_1] \\ (m_1 + m_2) g \end{array} \right\}, \tag{6.4}
$$

$$
{}^2f_2 \;=\; \left\{ \begin{array}{c} m_2(-l_{c2}\dot{\theta}_{12}^2 - C_2 l_1 \dot{\theta}_1^2 + S_2 l_1 \ddot{\theta}_1) \\ m_2(l_{c2}\ddot{\theta}_{12} + S_2 l_1 \dot{\theta}_1^2 + C_2 l_1 \ddot{\theta}_1) \\ m_2 g \end{array} \right\}, \tag{6.5}
$$

where f_{x2} was the first term of Equation (6.5), f_{y2} was the second term of Equation (6.5), and n_{z2} was the third term of Equation (6.3). The leading superscript referred to the basis with respect to which the vector was expressed.

The nominal equations of motion for this manipulator were the equations of ${}^1\tau_{z1}$ and ${}^2\tau_{z2}$; these equations were useful for sizing actuators. The other equations modeled the load on the manipulator during specified motions, which facilitated the design of joint bearings.

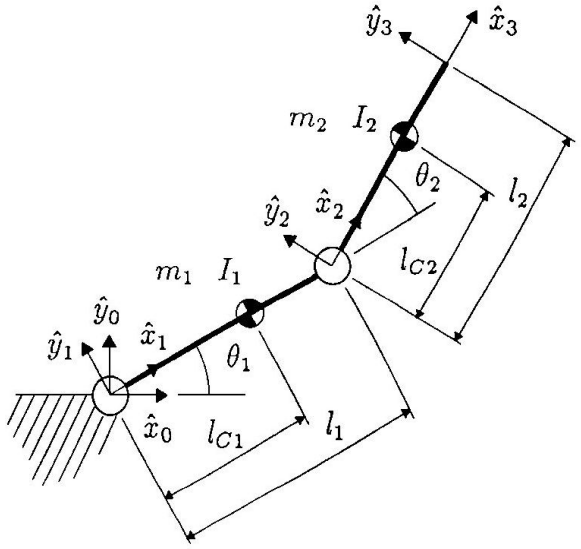

Figure 6.4: VERA dynamic parameters

With estimates of the dynamics parameters, the equations of motion were used to check actuator torque demand and rigid-body dynamic loading on the joints. But estimation of dynamics parameters could only follow preliminary mechanical design.

The robot mechanical design included joints, links, transmissions, and mounts for actuators and sensors.

The revolute joints of VERA each used a pair of tapered roller anti-friction bearings for low friction with high stiffness. A section view of joint 1 is shown in Fig-

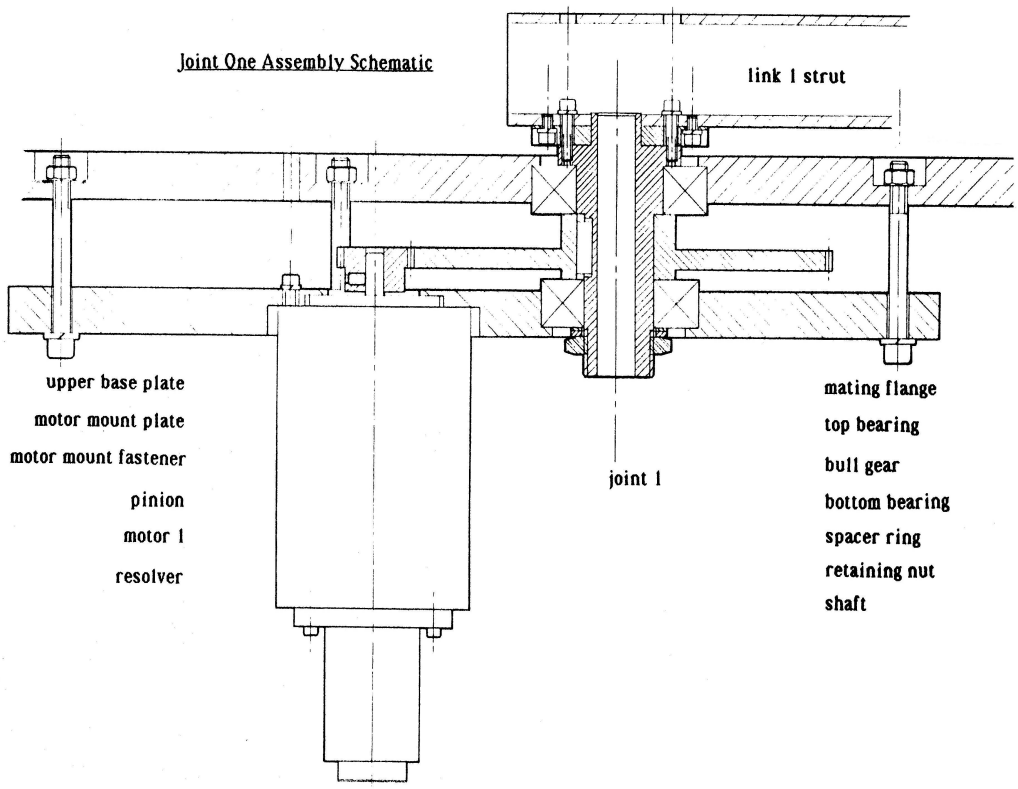

Figure 6.5: Joint 1 design

ure 6.5, and joint 2 is shown in Figure 6.6.

Gearing was a single spur-gear reduction with the motor mass proximal to the distal joint base, and thus reducing the moment of inertia of the proximal link. The single reduction allowed backlash adjustment between the motor pinion and the bull gear on the joint-axis shaft.

Each link of the manipulator was designed to be symmetrical about a line through the joint axes. This design feature eliminated products of inertia in the rigid-body equations of motion.

In the structural design of links, aluminum and steel were the materials of choice, for price and availability. Steel was used for components in contact. Aluminum formed the links and base. Since the operating temperature of the robot was room temperature, differences in coefficients of thermal expansion between aluminum and steel had little effect, and fracture toughness was not a concern [18].

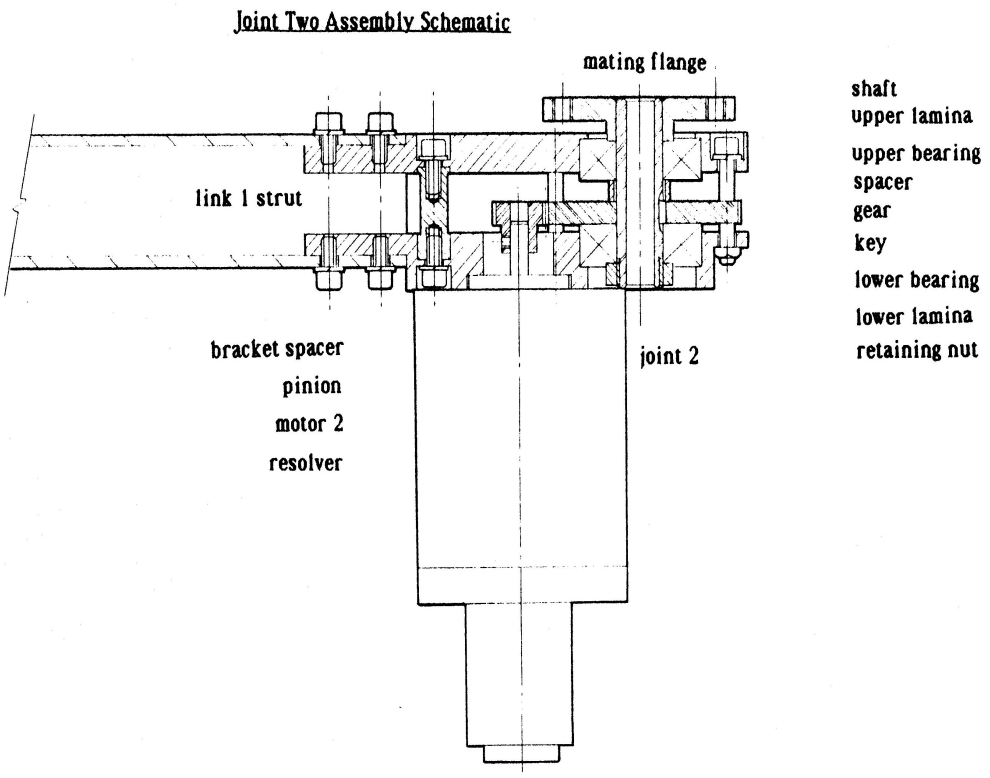

Figure 6.6: Joint 2 design

Preliminary sizes for the link cross-sections were selected without considering structural dynamics. After preliminary motor selection, link flexibility was calculated to ensure that the first structural resonance frequency of each link was high enough not to interfere with the controller.

Actuation

The Yaskawa Minertia DC servomotor was used to actuate VERA, with a peak torque to mass ratio of 0.606 Nm/kg. The motor had a peak torque τ_m of 120 oz-in (0.848 Nm); the gear reduction in joint 1 was $n_g = 6$ to deliver 5.08 Nm. Joint 2 had gear reduction $n_{g2} = 4$.

The DC servomotors were powered by EG& G Torque Systems Model C0501-002 linear amplifiers [13].

Having a preliminary motor and gear-set choice, most of the link mass was de-

fined. The next step was to choose a link structure that had a reasonably high natural frequency without being massive.

The lowest natural frequency of a prismatic beam of mass M_b with a mass M at its free end was approximately

$$\omega_n = \sqrt{\frac{3EI}{L^3(M + 0.23M_b)}}, \tag{6.6}$$

where E was the Young's modulus, and I was the area moment of inertia [19]. For length $L = 0.40$ m, and end mass $M = 3.2$ kg, the vibration parameters of the first link were

$$\begin{aligned} M_b &= 1.34 \text{ kg} \\ I &= 2.8 \times 10^{-7} \text{m}^4 \\ \omega &= 519 \text{ rad/s (83 Hz)}. \end{aligned}$$

The lowest vibration frequency of the second link was over 200 Hz.

Detailed Torque Calculations

The rigid-body equations of motion were used to calculate the joint torques required to achieve a desired end-effector motion for a set of joint poses and velocities.

A program was developed using the recursive Newton-Euler formulation. The program generated link velocities and accelerations from base to end effector. Then, D'Alembert equations were used recursively from the free end of the manipulator back to the base, from which came the joint forces and torques [36].

This program was used in designing VERA to verify gearing ratios for the transmissions. The program was also used to verify the bearing loads, by examining the joint forces for a representative set of poses spanning the workspace at maximum specified end effector motions. The program required the kinematic and dynamics parameters for VERA, which were estimated from the current version of the design.

Four cases were chosen for rigid-body simulation, varying the joint velocities and accelerations over a range of poses.

The velocity of joint 1 was $\dot{\theta}_1 = 0.5$ rad/s in two cases and $\dot{\theta}_1 = 5$ rad/s in the other two cases. The other variable was $\ddot{\theta}_2$, which was 1 rad/s^2 or 10 rad/s^2. This tangential acceleration would result in end-effector linear acceleration of almost 9 m/s^2. The acceleration of $\ddot{\theta}_2$ was fixed at 1 rad/s^2.

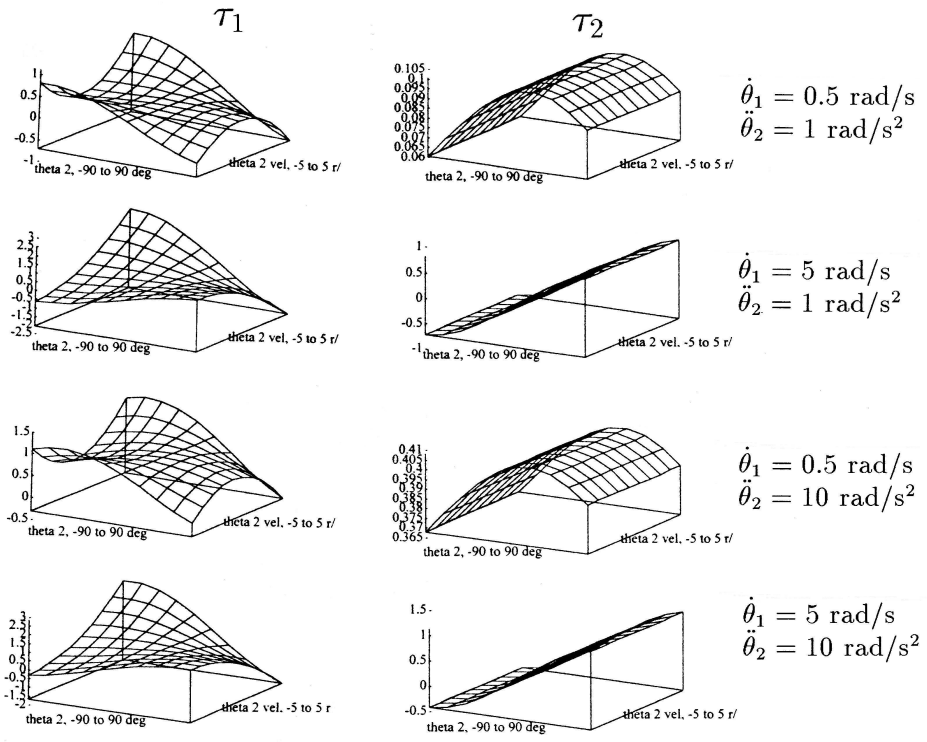

Figure 6.7: Preliminary rigid-body torque requirements

Case results are shown in Figure 6.7 between $\dot{\theta}_2 = -5$ rad/s and $\dot{\theta}_2 = 5$ rad/s in the range of θ_2 between $-90°$ and $90°$. This range of poses formed the outer ring of the workspace where experiments were to be performed. Because the workspace lay in the plane perpendicular to gravity, results were the same for any value of θ_1. For simplicity, $\theta_1 = 0$. The acceleration of $\ddot{\theta}_2$ was fixed at 0 rad/s^2.

After design was complete, the torque requirements for actual rigid-body dynamics parameters were recalculated; plots are shown in Figure 6.8. For this manipulator the highest torques occurred when the arm was bent and moving at high speed.

The calculated joint-torque neglected friction and shock loading, and the calculations of minimum torques for arm motions included no factor of safety for unmodeled

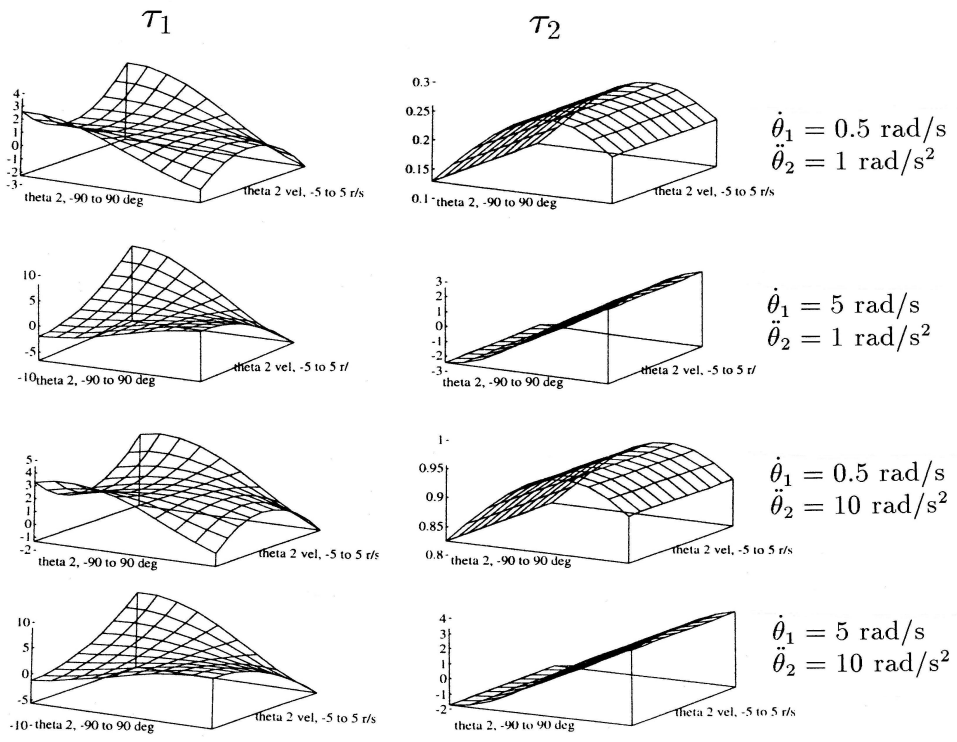

Figure 6.8: Final rigid-body torque requirements

dynamics.

The peak loading for bearing loads occurred on link 1 and on link 2 in the $\hat{x}$ direction when $\theta_2 = 0$. Unless there was pathological shock loading in other poses or very heavy operation in a narrow range of motion, the peak-load pose became the most likely candidate for looseness development.

6.1.3 Sensors

Resolvers were used to measure joint displacements on the double shaft of the Yaskawa motor at a given joint. Optical encoders and potentiometers were used in other manipulator development projects [71], but resolvers were chosen as robust, absolute-angle encoders with good frequency response [81, 108].

Figure 6.9 illustrates the interface required to bring resolver data into the controlling computer. Resolvers returned a set of analogue inputs to conditioning electronics, which delivered digital outputs to the bus when prompted by a handshaking

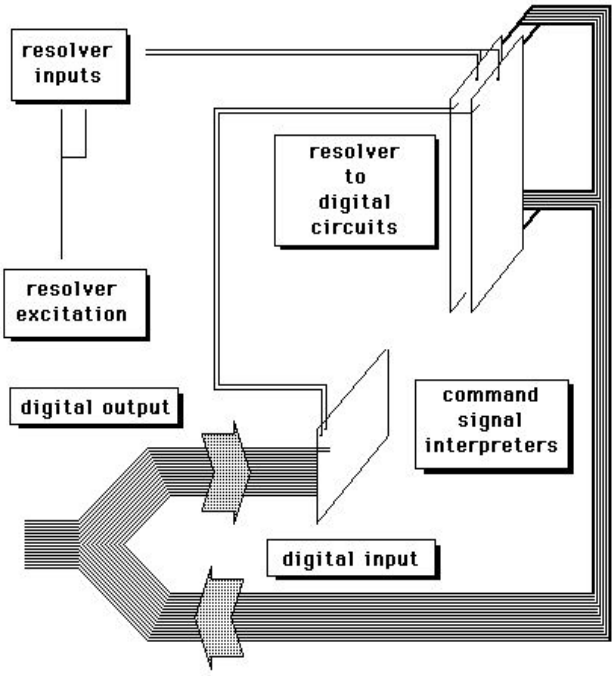

Figure 6.9: Resolver interface hardware overview

signal.

The CSI 168H299 resolver-to-digital converter (RDC) turned voltage signals from the rotor and stator into a sixteen-bit output (3.5 arc-minute resolution). The Harowe 11BRCX-300-J-10D resolver was selected for its small size, low inertia and friction, and its compatibility with the RDC [10]. Each resolver was driven by a 400 Hz, 7 V_{AC} signal from a Thandor TG503 function generator.

A special-purpose Handshaking Circuit (HC) was designed and built to connect the DIO bus between the DT2801A data acquisition board for the PC and the RDC circuits [3]. The digital output from each RDC went to tri-state buffers buffers tied into the DIO bus. Output was enabled when the handshake line to the buffer was low, allowing the data to appear on the bus at the buffer outputs[72].

6.1.4 Control

Controller software was written in C on an IBM-compatible PC. Two trajectory generation schemes were produced: point-to-point continuous control or Cartesian

straight-line continuous control.

The software was debugged using graphical simulations and a parallel-linkage 2-DOF planar robot with DC motors and potentiometer joint sensors[2], illustrated in Figure 6.9. The advantage of running software on another manipulator was the ability to debug during fabrication of VERA. The only software changes required were new kinematic parameters, new routines for reading joint encoders, and selection of new gains.

Robot Design Summary

VERA was a bench-sized planar revolute manipulator, electrically actuated through gear trains. Shielded cable carried power and transducer signals through hollow link members and hollow shafts. Joint encoders were collocated on DC servomotor shafts, and end-effector motion transducers were mounted to a cube at the end of link 2.

The robot controller was an IBM-compatible PC with 40486 CPU operating at 33 MHz. A real-time operating system was used to ensure reliable sensor readings.

6.1.5 Prismatic Looseness-Joint Development

There was one design feature unique to this rig: a looseness joint. Since looseness could occur in different links of a manipulator, VERA had to be capable of operating with looseness in different parts. Loosening existing bolted connections would have been difficult to do repeatably. It was reasonable, therefore, to design a machine element with controllable looseness that could be mounted in different locations on the robot.

Such a looseness link is shown in Figure 6.10. It ran on linear bushings with low friction, preloaded by set screws. The looseness travel d was limited by axial preload screws on each end, secured by lock nuts. The mating flanges allowed the looseness link to be introduced at the proximal end of either link 1 or link 2, at an angle β that was adjustable in 30° increments. Figure 6.11 shows the looseness link mounted

[2]The parallel-linkage robot was designed by the author and Lindsey Hutton.

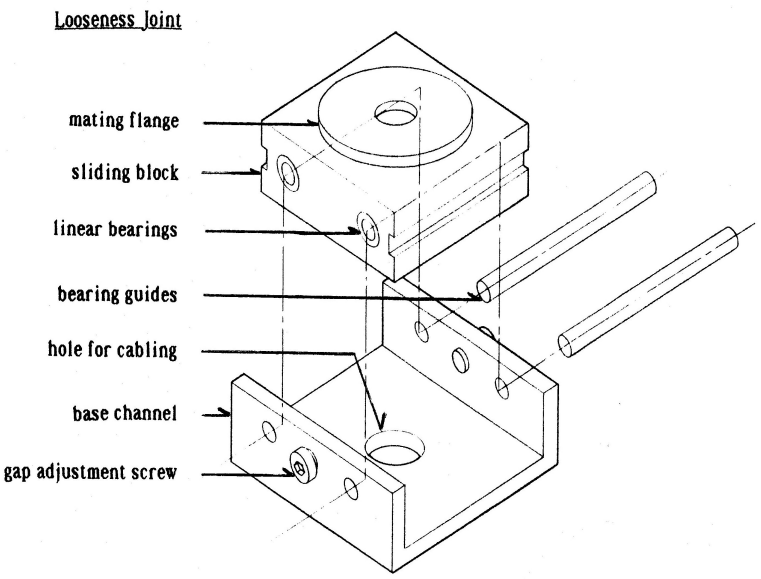

Figure 6.10: Looseness link, exploded view

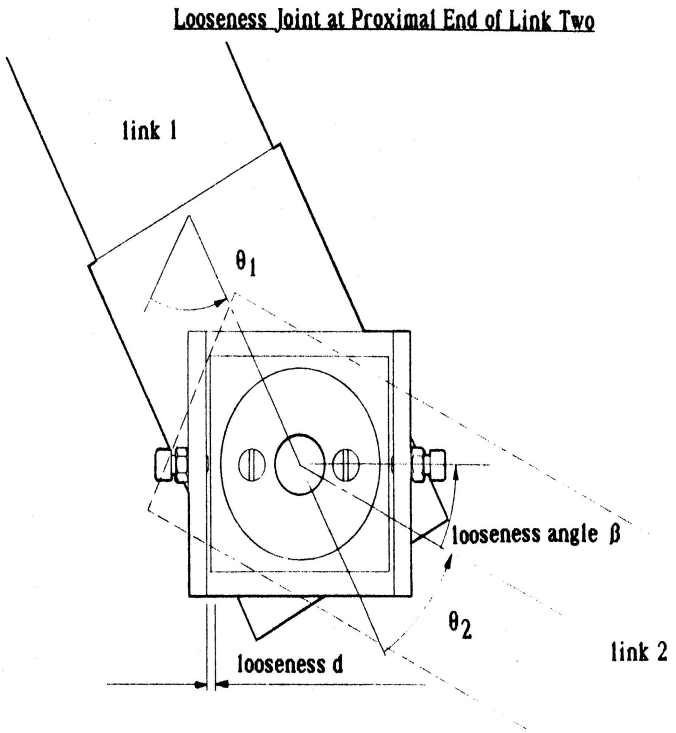

Figure 6.11: Looseness link on link 2, plan view

on the proximal end of link 2.

6.1.6 Slide Rig Design

A shaker table supplied external mechanical excitation of the manipulator. The shaker voice coil connected to a linear slide running on linear bearings through a pair of 0.5 inch diameter guide rails. A hitch assembly acted as a passive rotary degree of freedom connecting the slider to a link of the robot, as shown in Figure 6.12. This

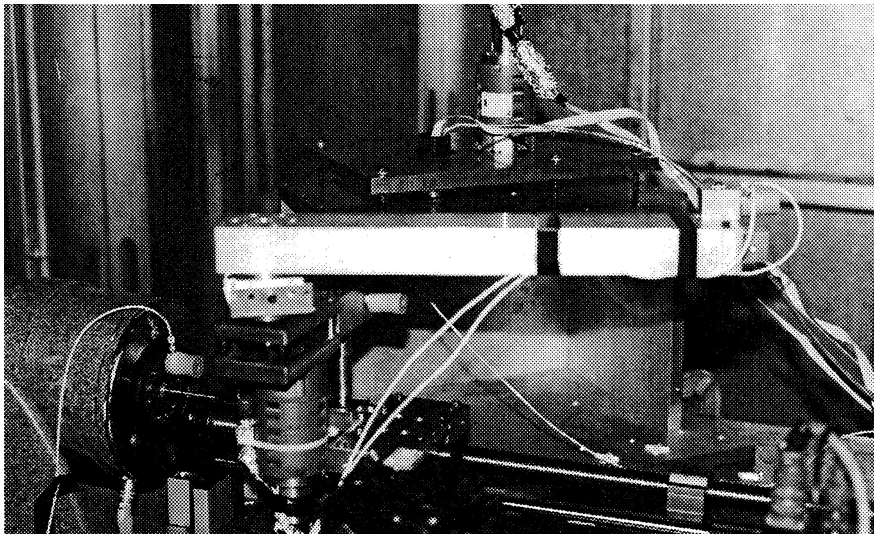

Figure 6.12: Photograph of VERA manipulator and slide rig

degree of freedom allowed linear actuation of the mechanism in varying orientations as the robot assumed different poses.

Excitation Sources

Excitation of the mechanisms came from the actuators of the mechanism or from an external source.

The hydraulic actuators of the industrial manipulator produced its motions. No random motion component was introduced.

The second rig had no internal actuators, and so it was driven by a shaker table with input from a white-noise generator with flat response from 0 to 350 Hz with

less than -3 dB rolloff per octave. The articulated robot arm was also actuated by the shaker table, and, in one test set, by open-loop DC motor excitation of its most proximal joint.

There was no attempt to compensate for system dynamics to achieve normal-random end-effector motions. It was assumed that the shaker acted as a force source, although in reality the actuator became coupled with the passive system of concern.

Instrumentation and Data Acquisition System

End-effector accelerations were sensed by seismic accelerometers. In the test on the industrial manipulator, a single-axis Bruel & Kjær accelerometer measured the repeatability of motions. The lower frequency limit was 2 Hz. The mount was electrically isolated. The B & K 2635 charge amplifier was mounted on the robot wrist, and the cable was also strapped to the wrist to prevent whip. The potentiometer signals were also recorded. The signals were displayed on a two-channel Nicolet 3091 digital storage oscilloscope, archived in the 0 to 600 Hz range on a two-channel TEAC FM tape recorder. Data were then plotted, or input to a PC for spectral analysis.

The accelerometers used in subsequent tests were PCB model 8612B5 accelerometers, with ±5% linearity from 0.5 to 5000 Hz, at an output of 1 V/g. Two accelerometers were mounted perpendicularly to an aluminum cube to measure planar accelerations. The cube was in turn bolted to the body of interest at a prescribed orientation. A transverse sensitivity test verified how the accelerometer response changed with orientation.

To correlate end-effector motions against joint motions, simultaneous recording of sensor outputs was necessary. Robot joint-sensor data from resolver-to-digital converters was accessible only through the robot controller. Enabling signals for encoder bus handshaking were used as timing pulses. While the controlling computer recorded resolver outputs to a file, a multi-channel recorder taped the 1 kHz resolver pulse train and the accelerometer signals. Actuator outputs were also recorded, to ensure that the output motion was of the appropriate distribution[3].

[3]In an industrial implementation, actuator output measurements would provide feedback for

A TEAC RD130T digital audio tape (DAT) recorder archived all analogue data in experiments two through six. This eight-channel DAT recorder accepted 20 V peak inputs with a minimum bandwidth of 5 kHz and 72 dB SNR. The maximum phase difference between channels was 3°. The low phase difference was an advantage for timing coordination when estimating planar acceleration from accelerometers and in cross-correlations [11]. Through a TEAC IF-RD101T GPIB interface board, digitised archived data entered the personal computer for further analysis [12]. The only disadvantage of the DAT recording and archiving system was that it was not possible to trigger data acquisition automatically.

A CSI 2100-3D machinery analyser displayed real-time power-spectrum estimates. Windowing options (Hanning or rectangular), number of averages, and frequency range could be user defined [2]. For archived data, CSI Wavepak was used to do spectral analysis in Experiment One, and LabVIEW to do the analysis in subsequent experiments [7].

All instrumentation, including the data acquisition system for the computer, was calibrated before use.

6.2 Validating Hypothesis One: Faults Are Observable and Repeatable

6.2.1 Experiment One: Repeatability of End-Effector Motions

Objective

To investigate whether fault effects caused repeatable end-effector motions.

modifying the actuator force distribution to achieve the desired actuator motion distribution.

Method

The Rig was a Prab Versatran FA600 robot, a six degree-of-freedom, cylindrical-coordinate manipulator that moved under point-to-point control. Each hydraulic actuator was servoed independently using analogue PID controllers, with no timing coordination between axes [8]. For test purposes, only major axis poses and motions

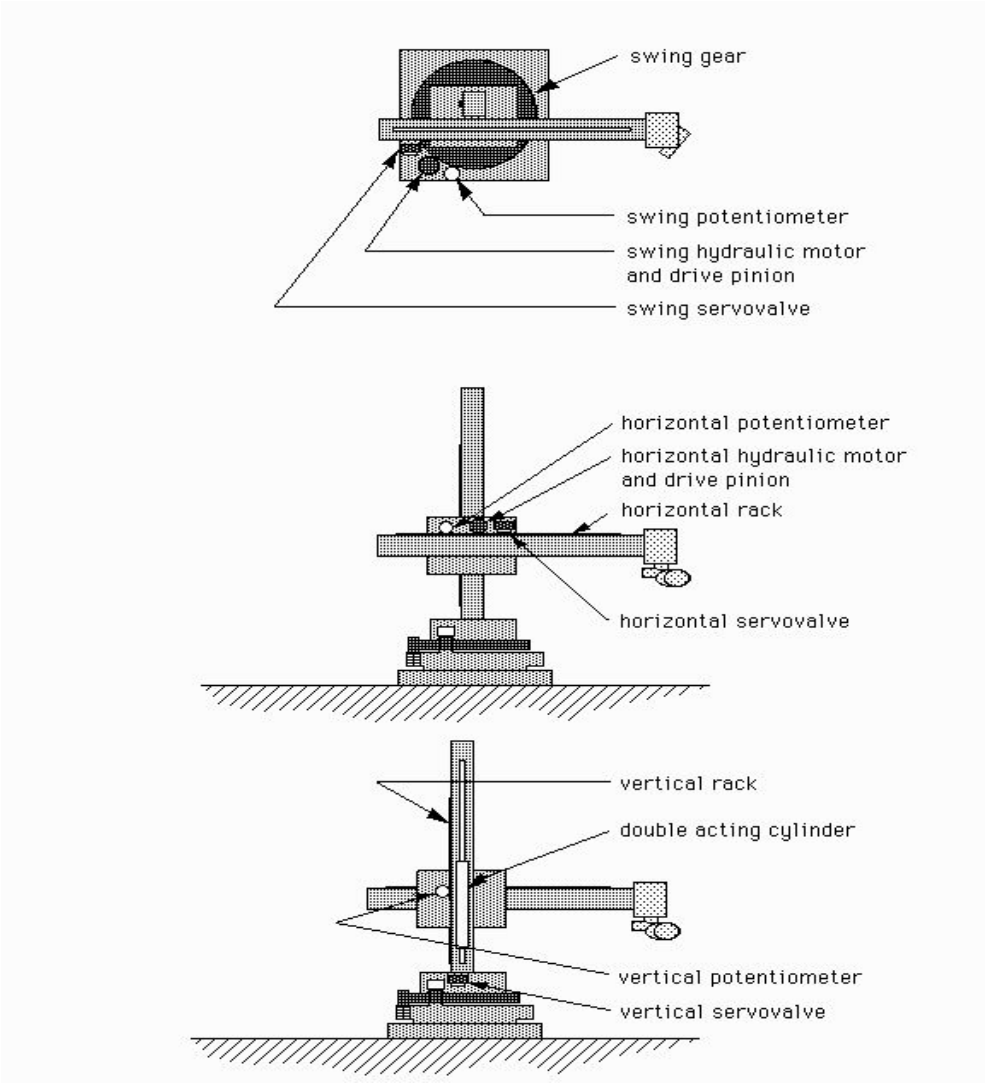

Figure 6.13: Prab robot major axis drive components

were considered. Potentiometers alone measured joint motions, so the derivative signal was found by differentiation. The layout of sensors and actuators for the

major axes is shown in Figure 6.13.

The Input to the system was a standard single-axis repeated motion program. During each cycle, in the same pose, the joint motion was nominally the same. There was no random input signal superimposed on the command signal to the servovalves.

The Outputs measured were the voltage signal from the potentiometer of the joint being moved, and the acceleration in the direction of joint motion at the end effector. A normally-open relay output from the controller triggered data collection at an intermediate through-point in the middle of a motion cycle.

A single-axis accelerometer was magnetically mounted horizontally to the base of the robot wrist with its charge amplifier. Coaxial cables ran to an FM tape recorder and to a digital storage oscilloscope, both triggered by an output relay signal from the robot controller.

The Procedure of this experiment was to stroke the horizontal axis through nominally identical repeated motions in five different poses, with data collection triggered by the robot controller at a set time into the motion. Three of the poses are shown

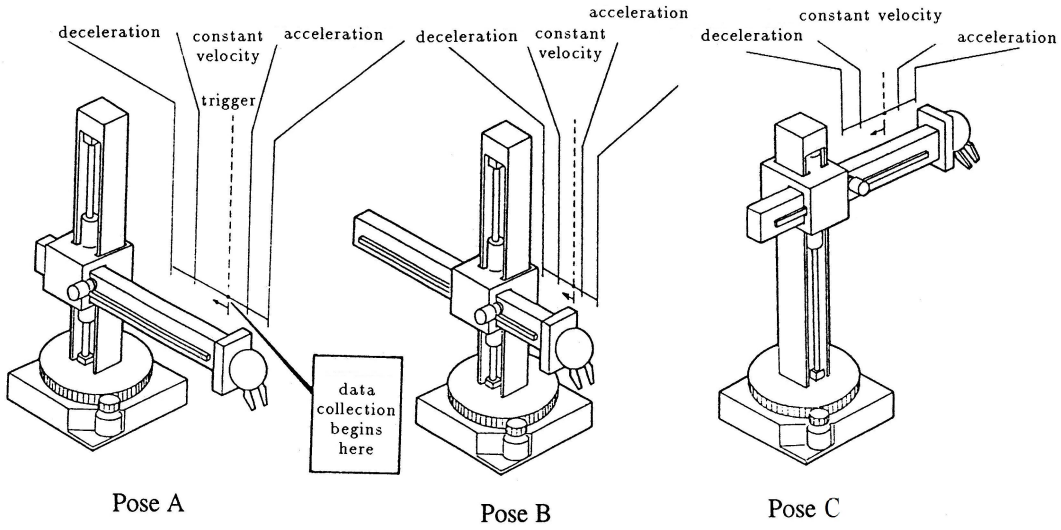

Figure 6.14: Repeatability test poses

in Figure 6.14. Pose A had the arm out and low; Pose B had the arm in and low. Pose C (not shown) had the arm out and high; Pose D (not shown) was in and high. Swing orientation was the same in Pose A, B, C, and D. Pose E was similar to Pose C, but swung 90°.

The manipulator stroked for fifty cycles. To simulate poor repeatability, the robot then repeated the stroking motion for an additional fifty cycles for an end position that was +2 mm from the original recording position. For the third set of fifty cycles, the end position was +4 mm from the original position; and in the fourth and fifth sets of trials, the end position was -2 mm and -4 mm respectively from the original end position.

Observations

The guideway that supported the horizontal boom was supported by four bearings. The roller bearing blocks had some play, which introduced a minor looseness fault: the arm shuddered whenever it stroked horizontally through the point where the preload transferred from one diagonal pair to the other. There was an 8 Hz vibration mode when the arm was fully raised and extended. Noise on the potentiometer signal was 25 mV peak-to-peak.

Results

Figure 6.15 shows time-domain signals of horizontal stroke motions in three different poses, A, B, and C. Each pair of signals was for the same nominal pose.

Figure 6.16 shows spectra for Pose A and Pose B, with the arm lowered. The upper plot is of Pose A motion with arm extension. The middle plot shows the spectrum for Pose B, and the lower plot shows the difference between spectral magnitudes for motions of Pose A and Pose B. Each spectrum was averaged ten times.

Because the tape recorder could accept only two inputs at a time, separate trials recorded triggered accelerometer signals, shown schematically in Figure 6.16, and triggered joint signals.

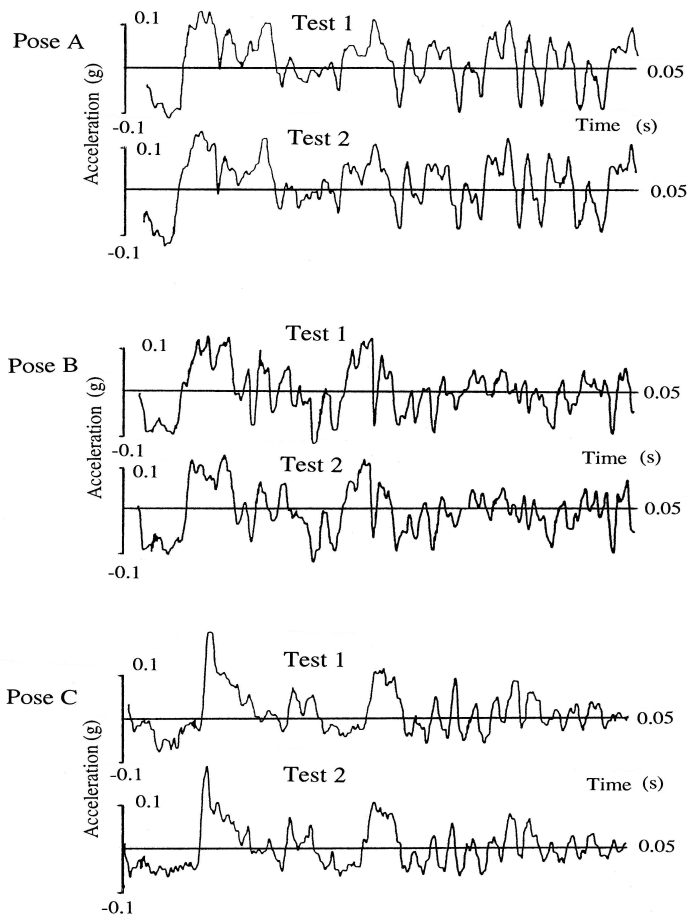

Figure 6.15: Time domain signals of Prab horizontal motion

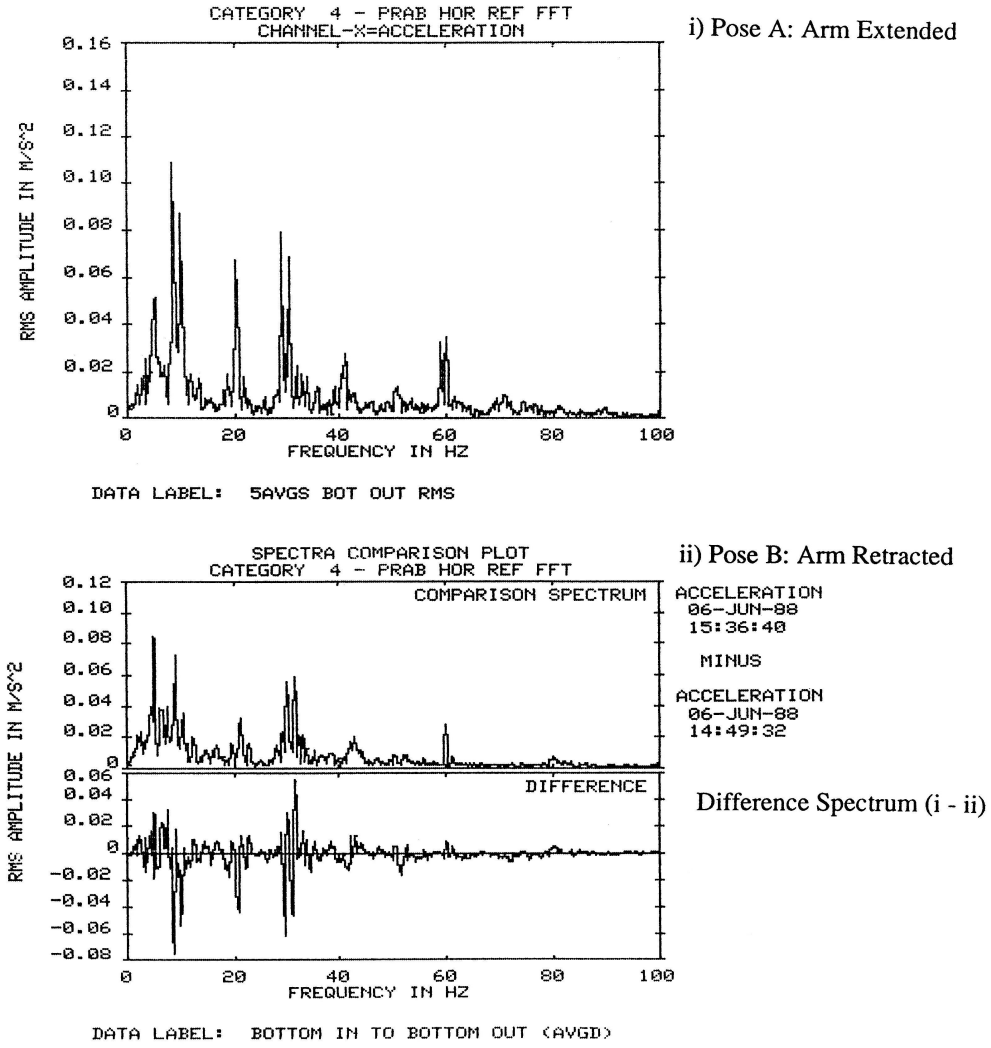

Figure 6.16: Spectral plots of Prab horizontal motions, arm low (Poses A and B)

The time-domain plots were compared qualitatively for variations in shape and time delays. The time-domain signals showed that there was apparently good repeatability between strokes in a given arm pose. Different poses, however, produced different signals; the spectral plots supported this interpretation.

There were a number of difficulties with the controller of the Prab robot. Drift in certain axes persisted even after switching controller cards with other axes. After shutdowns, some axes began oscillatory motions and the control cards had to be tuned again. The Prab controller differentiated the potentiometer signals. These signals were sometimes noisy, contributing to controller problems.

The electrohydraulic servovalves tended to stick because there was no dither circuit on the controller boards[4]. The controller gains were sensitive to the robot state. The swing axis was particularly sensitive to radial extension; the change in inertia about the swing axis from horizontal arm extension introduced a conspicuous underdamped motion at full extension. The interim solution was to make the arm critically damped at near full extension and overdamped at less than full extension. An axis that was critically damped could be made to drift merely by shutting down the hydraulic system and then repressurizing it: null adjustments were susceptible to drift.

There was a progressive loss of voltage in the vertical-axis potentiometer signal when hydraulics were locked and the controller was inactive, but not when the controller was active. This condition was probably caused by a leaky bypass valve, because the vertical axis drifted down to the lower mechanical stop when unpowered.

The shudder of the prismatic guideway was caused by the manipulator passing through the pose in which gravity pulls the load from one looseness stop to the other. This transient vibration was also repeatable. Because predicting the pose where such a transition would occur may be difficult in practice, on-line monitoring of end-effector motion would have to look continually for motion excursions from such a fault, unless there was a way to excite the looseness motion in a given pose.

[4]Dither is a small amplitude signal that continually excites the servovalve to allow it to break stiction; without dither, joint axes tend to drift.

Because motion data was archived only as paper plots, it was not possible to analyze the data further without digitising it. Also, the Prab robot was decommissioned soon after repeatability tests were done and it was unavailable for subsequent tests.

Qualitatively, however, time-domain plots and frequency spectra on a given pose set were very similar, leading to the conclusion that there was good repeatability between end-effector motions at a given time (and pose) during a repeated cycle.

Changing pose introduced a change in operating conditions that affected the outputs in a repeatable manner. The results thus supported the hypothesis that motions were repeatable for a given set of conditions that included the pose and fault effects.

6.3 Validating Hypothesis Two: Fault Effects Are Measurable

6.3.1 Experiment Two: Calibration of Perpendicular Accelerometers

Without accurate multi-dimensional motion measurements, fault effects at the end effector are not be measured with certainty [98]. The fidelity of multi-dimensional acceleration measurement using perpendicular components was investigated in this experiment, so that fault effects on motion were measured accurately.

Objective

To calibrate an perpendicular pair of accelerometers to measure acceleration in a measurement plane.

Method

The Rig was the linear slide shown in Figure 6.17, actuated by the shaker table, with an accelerometer mounting cube that could be set at a variable angle α to the

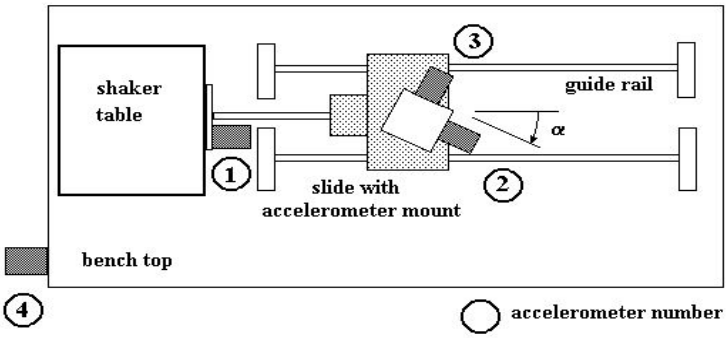

Figure 6.17: Linear motion rig schematic

direction of sliding motion.

The Input to the system was a white noise analogue voltage from an Elgenco model 632A Gaussian noise generator to an MBIS model SS500 power amplifier and shaker table.

The Outputs measured were four accelerometer signals (shaker acceleration, bench base acceleration, and acceleration on two faces of the variable-angle slide-mounted cube), and the voltage from the noise generator.

The Procedure of this experiment was to fix the mounting cube to the slide with a bolt and nut, well torqued, and then to apply the white-noise signal to the power amplifier of the shaker table. The shaker table drove the slide through a size 10-32 threaded rod, 12 cm in length. The same setting for the amplifier was used for most trials, and a floating ground on the noise generator prevented signal drift from driving the shaker table to the end of its travel.

A protractor measured the angle of the accelerometer mount with respect to the side of the slide, which was perpendicular to the slide guide rails to within 0.5°.

Data Reduction was done in two ways. The RMS signal between 2 Hz and 200 Hz for each accelerometer reading was used to estimate the mean acceleration magnitude

$\bar{A}^*$ and direction $\bar{\alpha}^*$ with respect to frame (t), from

$$\overline{A}^* = \sqrt{{}^t\bar{a}_x^2 + {}^t\,\bar{a}_y^2}, \tag{6.7}$$

$$\overline{\alpha}^* = \arctan(\frac{{}^t\bar{a}_x^2}{{}^t\bar{a}_y^2}), \tag{6.8}$$

where ${}^t\bar{a}_x$ was the estimate of the mean acceleration in the x-direction of the cube, and ${}^t\bar{a}_y$ was the estimated mean acceleration in the y-direction. The angle estimates

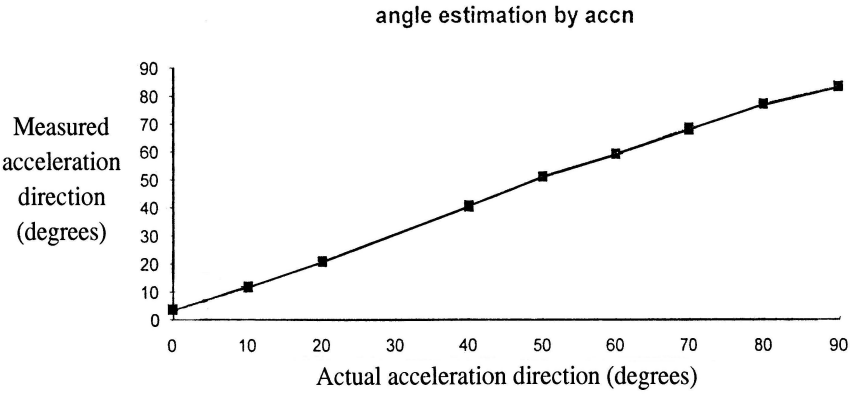

Figure 6.18: Angle estimation using RMS acceleration values

using RMS accelerations are plotted in Figure 6.18. Signals were also matched in

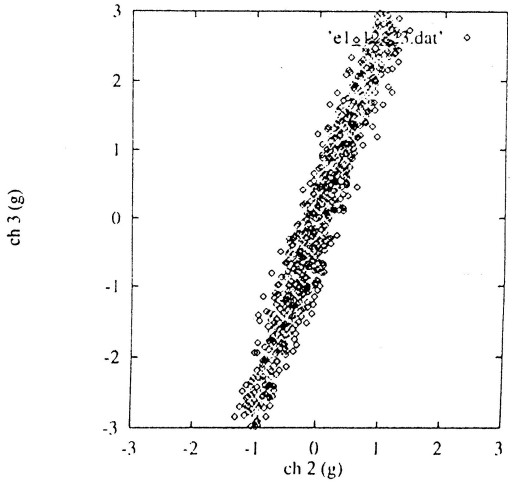

Figure 6.19: Instantaneous perpendicular accelerations

time to calculate instantaneous magnitude $A(t)$ and direction $\alpha(t)$, as illustrated in Figure 6.19.

Observations

The shaker table amplifier saturated easily, and tripped if the gain was too high. The acceleration spectrum of the shaker driving the slide was attenuated below 40 Hz, and uniform beyond 400 Hz. The base acceleration was uniform, even at low frequencies.

Acceleration spectra were similarly uniform above 40 Hz for the accelerometers on the slide, except when an accelerometer had its axis nearly perpendicular to the axis of the slide. In those cases, the spectra showed peaks at 50.5 Hz and 101 Hz, although the RMS value of the signal was low.

Results

Angle estimation based on rms acceleration values was within 2% of actual values in 90% of cases where the $10° < \alpha < 80°$.

Agreement of measured angle to actual angle became poorer the closer the accelerometer set came to being at right angles to the motion. The 50.5 Hz structural resonance peak contributed to signal power disproportionately to the actual motion, and so increased the average power.

For that reason, the angle calculation from the arctangent function was inaccurate, although agreement was still within 5% in one perpendicular orientation and within 8% in the other orientation.

Instantaneous estimation of acceleration parameters A and α showed similar variance to the rms calculations, with direction estimates being most steady and accurate when α was near 45°, with correlation $r > 0.98$ for linear regression of one signal with respect to the other.

This experiment demonstrated that the accelerometers could estimate the direction of motion with good engineering accuracy, especially when neither transducer was perpendicular to the direction of motion, and that measurements were sufficiently close to simultaneous to produce accurate estimates of planar motion.

6.3.2 Experiment Three: Integration and Differentiation of Motion

Joint velocities, or accelerations with small velocities, are related to end-effector motions through the Jacobian. Since end-effector accelerations and joint displacements were measured, accelerations had to be integrated and displacements differentiated to yield velocities.

Reliable methods were necessary to convert VERA resolver motions to joint velocities, and to convert end-effector acceleration signals to velocities.

Objective

To demonstrate whether measured random motions could be numerically integrated and differentiated.

Method

The Rig for integration tests was the slide rig. The rig for differentiation was the first joint of VERA, backdriven by the shaker table.

The Input to the system was the shaker table force as in Experiment Two.

The Outputs were the same as for Experiment Two—shaker acceleration, bench base acceleration, acceleration on two faces of the variable-angle slide-mounted cube, and the noise-generator voltage—plus an additional recorded output: the timing pulse train for VERA joint 1 resolver. The resolver outputs were recorded in the controller PC to ensure that they were synchronised with the other recorded signals.

The Procedure for converting acceleration motions to velocities was numerical integration of digitised signals from Experiment Two. Displacements for differentiation came from the resolver data file in the PC.

Data Reduction for numerical integration compared two quadrature techniques.

Data reduction for differentiation compared the two lowest-order difference equations.

Observations

The sampling period of resolver data by computer through DIO was longer than the resolution of data recording on tape. Clear handshaking signals were recorded through DIO to a PC file, from which it was possible to match resolver readings to accelerations recorded on tape.

There was little resolver motion of VERA joint 1 during the test, typically less than 8 resolver units. Only with high gear preload was it possible to make the resolver track the random link motion through the gearing system, but the joint was difficult to move by hand when highly preloaded.

Results

Integration

The first quadrature formula evaluated was:

$$\int_{t_1}^{t_2} g(t)dt = \frac{\Delta t}{2}(3g_1 - g_2) \quad + O(\Delta t^2, g^{(1)}), \tag{6.9}$$

where Δt was the time step, and g_i was the value of the function at time $(t + t_i)$, where $t_{i+1} > t_i$. The error $O(\bullet)$ was on the order of Δt^2 after the first derivative of the function $g^{(1)}$. The data being integrated were sampled values of the function g.

The other quadrature formula evaluated was the Newton-Cotes method [99]:

$$\int_{t_1}^{t_2} g(t)dt = \frac{\Delta t}{24}(55g_1 - 59g_2 + 37g_3 - 9g_4) \quad + O(\Delta t^5, g^{(4)}). \tag{6.10}$$

The first tests attempted integration of accelerometer signals to estimate velocity $\tilde{\dot{p}}$. Figure 6.20 shows a typical pair of end effector (slide) perpendicular accelerations.

Figure 6.21 shows the shaker velocity and the velocities for accelerometers on the slide calculated by Equation (6.9). Correlation between the accelerometer velocities was $r = 0.99$ in the case of $\alpha = 50°$.

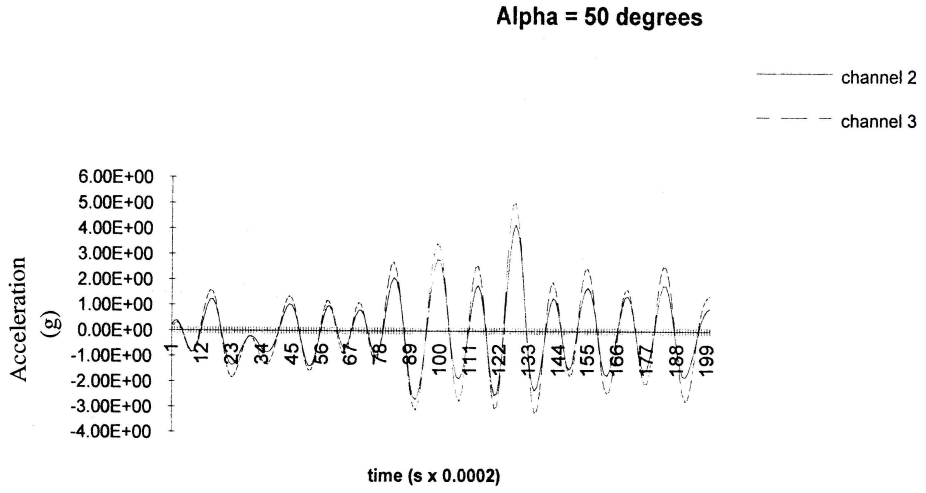

Figure 6.20: Slide acceleration

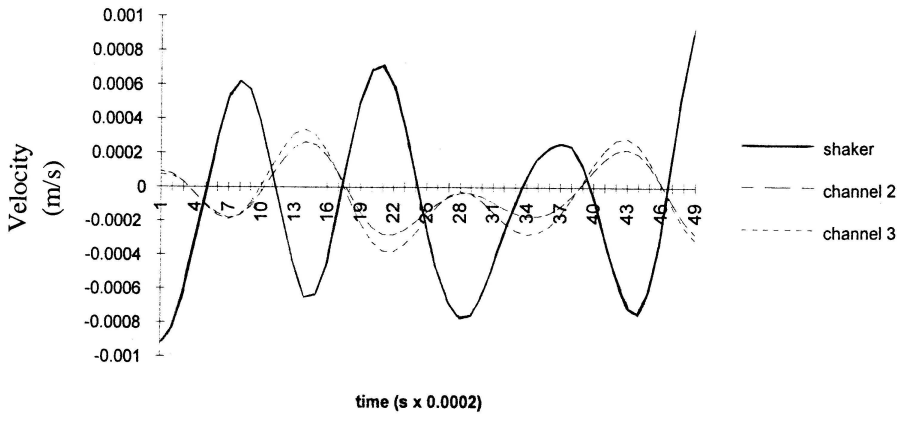

Figure 6.21: Slide velocity approximation: $\tilde{\dot{p}} = \Delta t(1.5g_1 - 0.5g_2)$

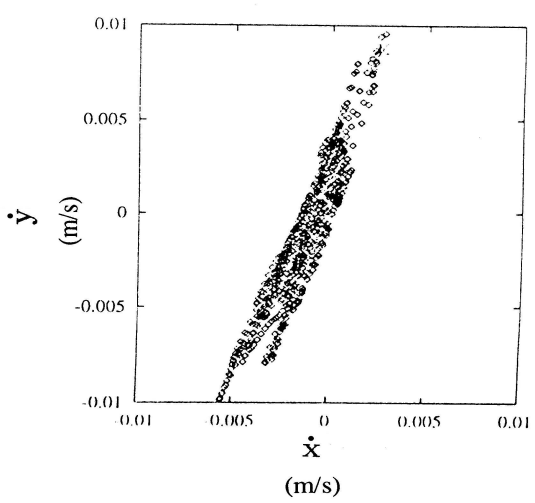

Figure 6.22: Slide velocity approximation, ${}^2\hat{\mathbf{y}}$ versus ${}^2\hat{\mathbf{x}}$

Figure 6.22 shows the first quadrature-calculated velocity, a zero-mean, almost normal-random variable process; it is shown again over a longer time period in Figure 6.23.

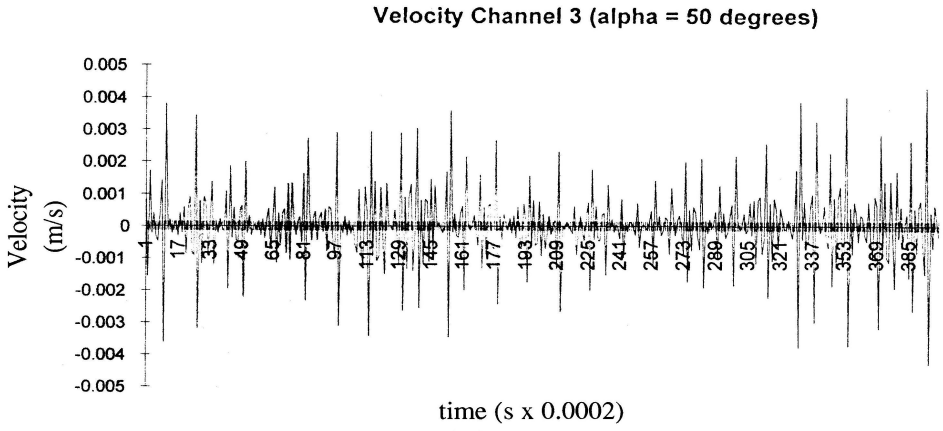

Figure 6.23: Slide velocity approximation over 0.08 s

The Newton-Cotes method produced velocity signals that were not zero-mean in a 0.04 s interval, as Figure 6.24 shows. The two signals generally followed the same velocity trend, but the correlation between velocity approximations was poor.

The Newton-Cotes method was a less successful quadrature procedure than the first quadrature method. The random nature of the signal made the assumption of

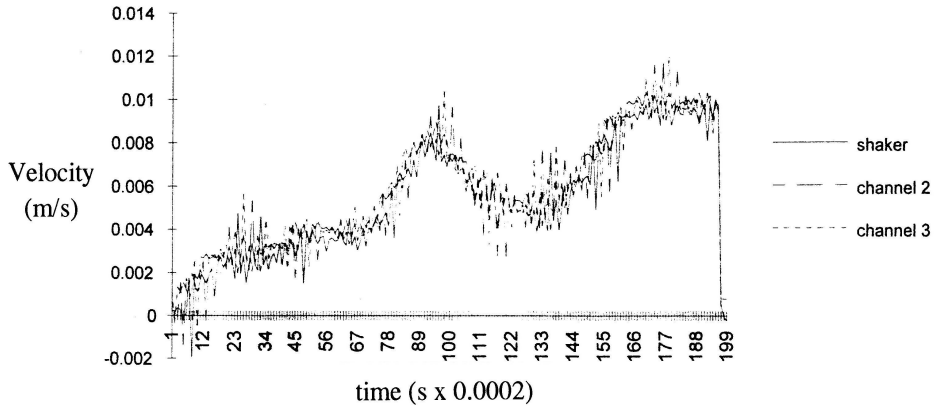

Figure 6.24: Newton-Cotes velocity approximation over 0.04 s

small errors above the fourth derivative invalid, and so the quadrature wandered. While it was possible that the velocities had low-frequency components calculated by the Newton-Cotes method, the correlation between signals was 0.09—the same signals that had correlations between accelerations of 0.98. Also, the response of the shaker table in the 0-40 Hz range was very poor, making it unlikely that signals in the 10 Hz range could persist.

There was an apparent lack of correlation between velocities, although the process actually was well correlated. The slide moved in a single direction, and the motions were measured components of that linear motion. This lack of correlation between signals showed that it was inappropriate to use quadrature with more than a small number of data samples for each calculation. The first quadrature method was chosen for use in subsequent experiments.

There was a pronounced 710 Hz dominant frequency. The dominant frequency and the phase shift between the shaker-table velocity and the perpendicular velocities of the slide were dynamic effects of the stinger stiffness. The first resonance frequency of the stinger was

$$\omega = \sqrt{\frac{k}{M + \frac{1}{3}m_s}}, \tag{6.11}$$

where

$$k = \frac{AE}{L}, \tag{6.12}$$

and k was the spring constant for a longitudinal rod of length L, cross-sectional area A, Young's modulus E, and mass m_s. The mass M of the slide and accompanying attachments was 0.50 kg. For $L = 0.17$ m, the minimum area of a 10-32 threaded rod $A = 0.0199$ m^2, and $E = 2.07 \times 10^5$ MPa, the calculated natural frequency was 720 Hz. Uncertainty in the effective area of the rod explained the discrepancy with the measured natural frequency.

Since the mass of the slide could not be reduced significantly, a stiffer stinger replaced the full-length threaded rod to raise the natural frequency in subsequent tests.

Differentiation

Numerical integration smoothes data and so errors in data tend to cancel out, provided that the errors are zero-mean, as is usually the case for measurement errors [25, 99]. Numerical differentiation, however, accumulates errors, because of two main factors: the time step interval enters as Δt^{-n}, where n is the order of differentiation; and each formula uses an nth order difference. The differentiation has less accuracy than the accuracy to which the functions were evaluated [25].

It was desirable to use a forward-difference scheme with nearby points only, to avoid conspicuous discontinuities from the random excitation. Two low-order difference equations were used:

$$g_0^{(1)} = \frac{g_1 - g_0}{\Delta t} + O(\Delta t^2), \tag{6.13}$$

and

$$g_0^{(1)} = \frac{-g_2 + 4g_1 - 3g_0}{2\Delta t} + O(\Delta t^3). \tag{6.14}$$

The resolver signals were very clean, and so it was thought that the errors would be low enough to allow numerical differentiation. But differentiation of resolver signals was unsuccessful, because the resolver motions were jerky and small. This was caused by backlash in the existing gear train for joint 1. Tightening the gear train to reduce play introduced excessive interference.

Because it was not reasonable to drive the system with very high friction, and

an alternative gear train with higher precision was unavailable, further numerical differentiation of joint displacements was abandoned.

As a result, it was not possible to relate joint velocities to end-effector velocities in this study, and so the acceleration relationship for small velocities was used in subsequent experiments. Revolute joint 1 acceleration $\ddot{q}_1$ of VERA was measured indirectly from tangential accelerations of link 1.

6.3.3 Experiment Four: Looseness Motions

The distribution of looseness motions was not known, and so it was important to determine experimentally the distribution of actual motions.

Objective

To determine whether the two-dimensional acceleration distribution changed in a consistent manner when looseness appeared.

Method

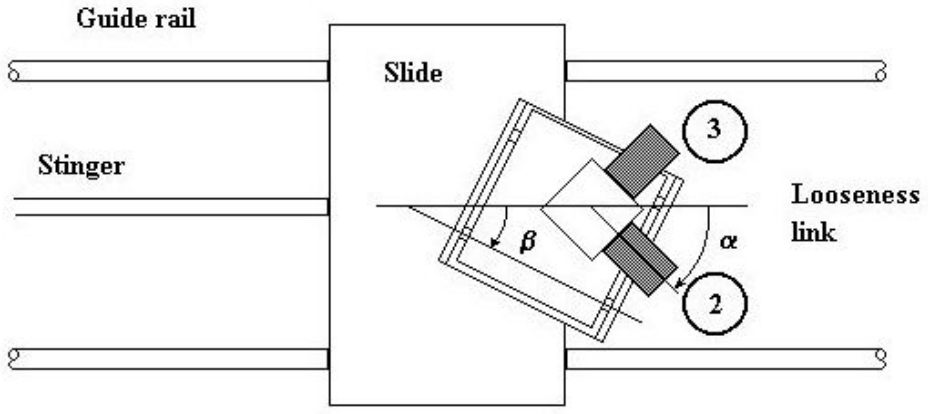

Figure 6.25: Schematic of slide with looseness joint and distal link

The Rig comprised the prismatic looseness joint assembly installed on the slide (Body 1), with the accelerometer mount distal to the joint, as shown in Figure 6.25.

The angle of the accelerometer mount with respect to the looseness joint was α. (In all cases described, $\alpha = 0$.) The looseness joint angle was β with respect to the motion of Body 1.

The Input was white noise to the shaker table driving the slide.

The Outputs measured were signals from accelerometers mounted perpendicularly on the distal link, on the shaker table, and on the bench in the direction of slide motion.

The Procedure was to introduce looseness in four poses, at angle β of 309°, 339°, 351°, and 230°. In each case, the mechanical stops were adjusted to high preload (tight, meaning greater than 4 Nm of torque), low preload (finger tight, meaning one-quarter turn of preload after contact, 0.2 mm of lead engaged), and no preload (loose one-quarter turn: 0.2 mm of looseness). These cases are shown in the figures as t, f, and l respectively.

Data Reduction included descriptive statistics and correlation against proximal link accelerations, both with respect to angle. Relative acceleration between the distal link and the slide was also found, and correlations were generated between the relative acceleration and the acceleration of the slide.

Observations

There was an audible growl from the rig when the amplifier for the shaker table was engaged. At high preload, the sound was of a lower pitch than for the case of looseness. It was not the sound of pure tones, but rather a random hiss. There was little difference in the sound of high and low preload.

Results

Two sets of trials were done. After the first trials were completed, the rig was disassembled in preparation for a later test. The single mounting screw between the mounting plate and the slide had lost its preload. Analysis of the data from those

trials showed no relationship between angle β and the direction of lowest correlation.

The original design of the looseness link included no lateral support of the guide rails on the looseness link, only a single vertical set screw at each end. Lateral set screws were added, and the trials were repeated with a new mounting scheme using two screws.

In the correlation polar plots, the horizontal line was the direction of looseness. The correlation vectors for the four cases all showed the minimum correlation occurring near the horizontal when absolute accelerations were correlated against the slide acceleration. The looseness direction was 270° in each case.

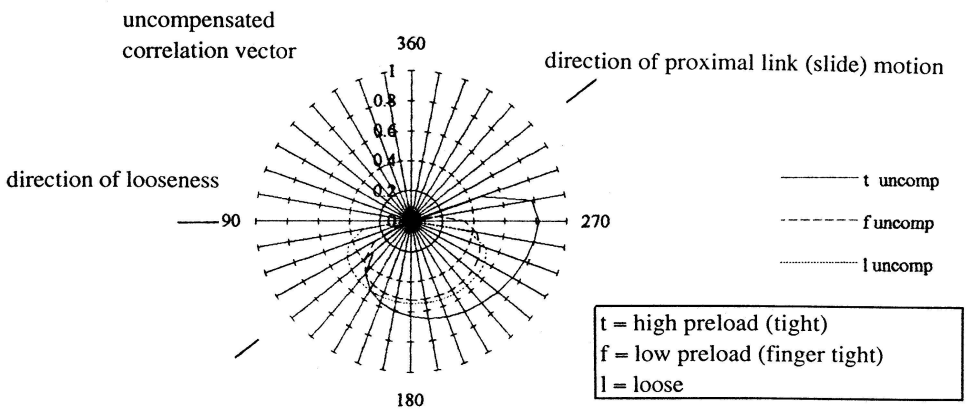

Figure 6.26: Correlation vector, $\beta = 309°$

Figure 6.26 shows the correlation vector plots when $\beta = 309°$. The magnitude of the looseness vector approached zero as the direction approached 270°. When there was preload, the direction of the minimum magnitude was nearly perpendicular to the direction of slide motion.

In figure 6.27, the left-hand plot shows the correlation vector plot for the case of $\beta = 339°$. Again, the direction of minimum correlation was perpendicular to the slide motion when there was preload, but when looseness appeared, the direction of minimum correlation moved to the direction of looseness, at 270°.

The right-hand plot shows the correlation between relative acceleration and slide acceleration. There was no clear change in minimum correlation direction for this or the other compensated cases. Relative accelerations of the distal link with respect

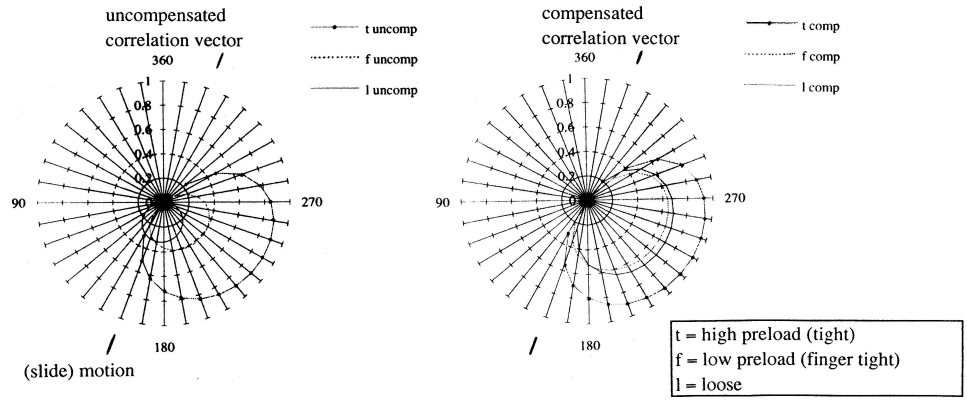

Figure 6.27: Correlation vector, $\beta = 339°$

to the proximal were not correlated against acceleration of the proximal link.

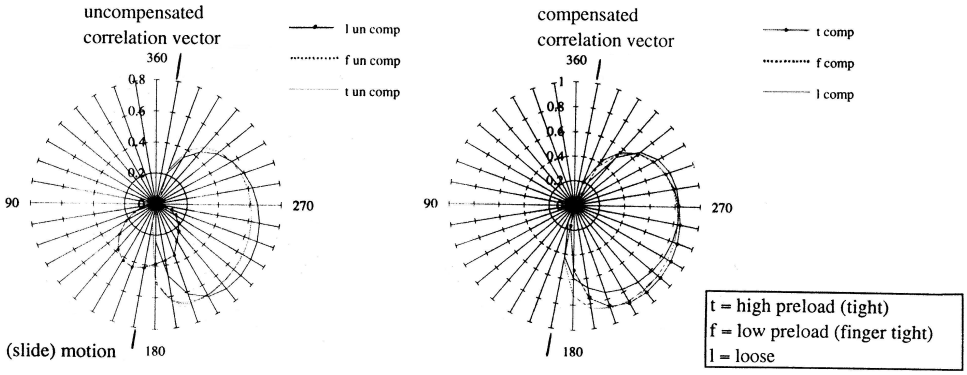

Figure 6.28: Correlation vector, $\beta = 351°$

Figure 6.28 shows the uncompensated correlation vector in the left-hand plot and the compensated correlation in the right-hand plot for the case of $\beta = 351°$. In Figure 6.29, uncompensated and compensated plots are shown when $\beta = 230°$.

In the four cases, with a different slide orientation in each case, the uncompensated correlation vector had minimum magnitude at or near the direction of looseness motion.

The maximum magnitude of the correlation dropped markedly as looseness developed. This drop indicated that the motion distribution of the distal body was different than that of the proximal body. The descriptive statistics supported that interpretation.

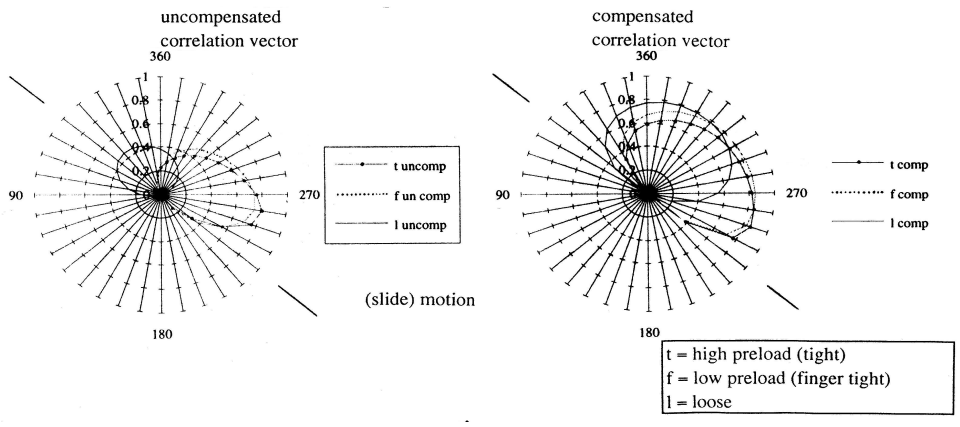

Figure 6.29: Correlation vector, $\beta = 230°$

Skewness and kurtosis in the direction of slide motion with looseness were on the order of those of the nominal case when the joint was tight. Figure 6.30 shows the

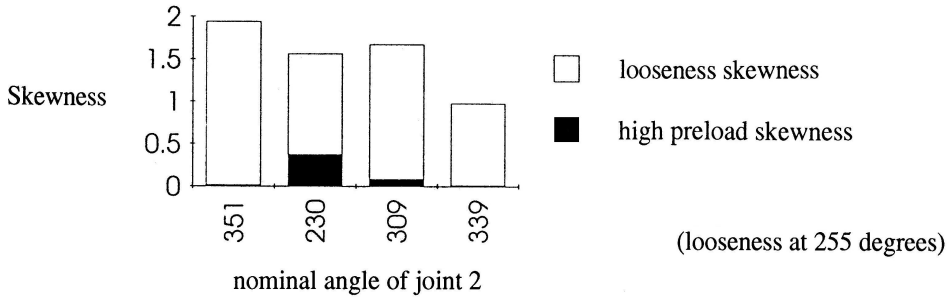

Figure 6.30: Effect of looseness on skewness

effect of looseness on the skewness of the acceleration distribution for the component in the direction of looseness. In the case of nominal joint angle 230°, the skewness was nonzero even when tight. It was possible that the preload was not very high, and non-normal random motions were already developing.

Since skewness was a measure of asymmetry in the data, acceleration data with high skewness indicated an asymmetric distribution of accelerations. There was no evidence that the shaker table force was asymmetric; the acceleration distribution for the voice coil alone had skewness of almost zero[5].

[5]Installing a load cell in the stinger would have supported or disproved this assumption of a

Assuming that the distribution of the input force vector **F** was symmetric, the asymmetric acceleration **a** resulted from anisotropic dynamic behaviour. Each mechanical stop may have had different stiffness and damping coefficients. If the dynamic stiffness parameters were different at each stop, higher accelerations would have occurred at one end than at the other, producing a skewed acceleration distribution. Other possible causes of dynamic anisotropy were different friction coefficients in each direction of motion and varying lateral preload on the rails along the travel of the joint.

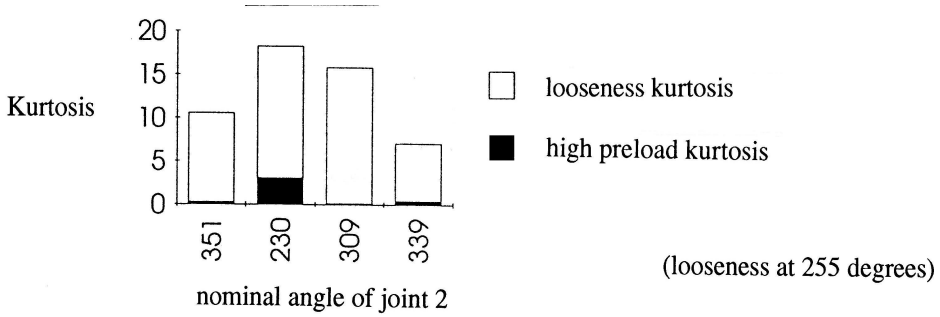

Figure 6.31: Effect of looseness on kurtosis

The effect of looseness on kurtosis of the acceleration component in the direction of looseness is illustrated in Figure 6.31. In three of the four cases shown, kurtosis was an order of magnitude lower when there was no looseness present. In the case of nominal joint angle 230°, the kurtosis was nonzero even when tight. The skewness was also high in this case, which supported the conjecture that the preload was not very high and non-normal random motions were already developing.

From these four tests, it was reasonable to conclude that increasing looseness led to increased kurtosis in the acceleration distribution. A likely physical reason was that there were higher acceleration peaks due to impacts at the stops, with intermediate periods with low acceleration when the distal body was moving freely. Since there were only short periods when the two bodies were in contact at the stops

symmetric force distribution directly. As is, it was assumed that shaker force was proportional to acceleration with no dissipative forces of friction or back EMF.

and moving together, there was a lower correlation coefficient during motions with looseness.

The first set of trials showed that it was important that looseness be diagnosed before the fault progressed to general looseness in more than one direction.

The sounds from the rig were of a low pitch with no pure tones, which indicated that the sound emissions were from random vibrations of the rig. The change in overall pitch with looseness was due to ringing following impacts. While some preload persisted, impacts did not occur, and so the sounds did not change noticeably.

6.4 Validating Hypothesis Three: Diagnosing Faults from Model-Based Analysis

Having shown that looseness and backlash motions were observable, the investigation turned to validating the third hypothesis: that actual fault effects could be related to their respective origins using model-based analysis.

6.4.1 Experiment Five: Looseness in a Planar Robot

Experiment Four showed that the correlation vector between accelerations across a looseness joint indicated the direction of looseness. The fifth experiment looked at the effect of manipulator pose on locating looseness faults.

Objective

To demonstrate how end-effector motions from random joint excitations changed when looseness occurred.

Method

The Rig comprised the shaker table actuating VERA link 1, with the looseness link attached at the proximal end of link 2, shown in Figure 6.32 and in Figure 6.33. In looseness tests, joint 2 was blocked with a tapered pin holding the gear to the distal

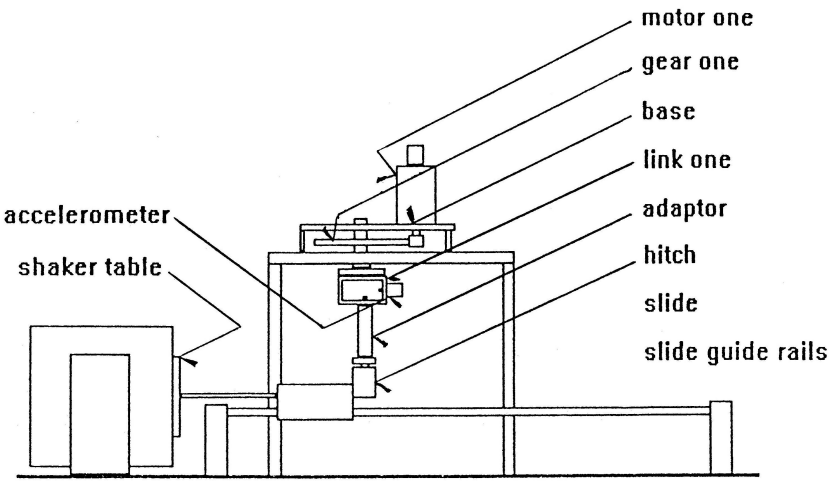

Figure 6.32: VERA external excitation rig, elevation view

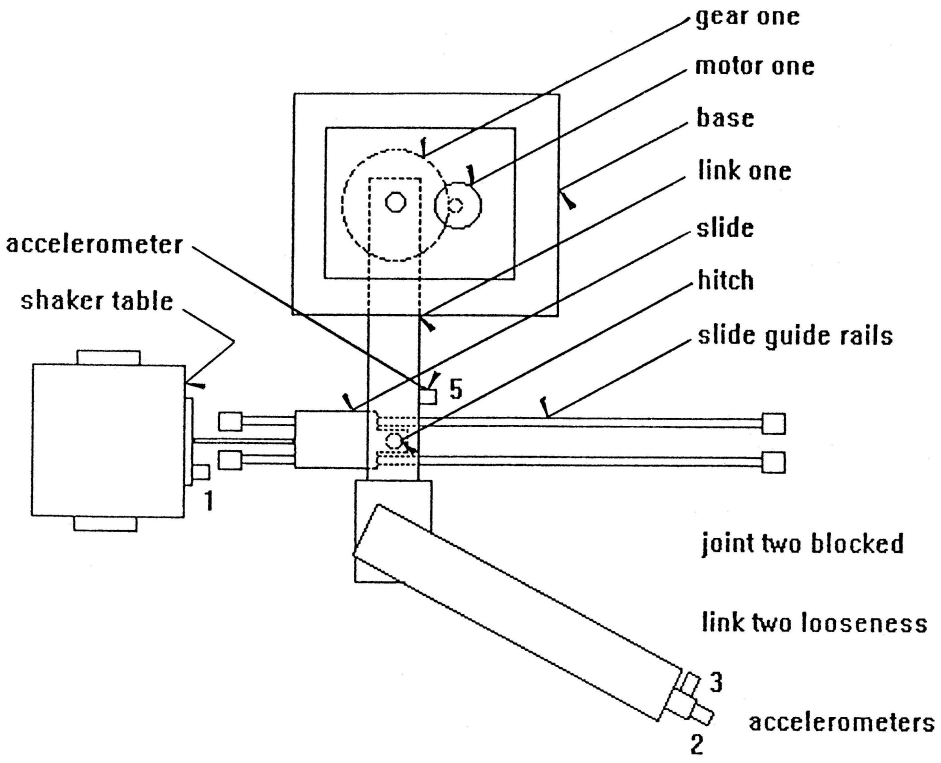

Figure 6.33: VERA external excitation rig, plan view

end of link 1. The rig was adapted to connect the shaker table directly to link 1 with the threaded rod, secured by two lock nuts.

The Input to the shaker table amplifier was random voltage from the white-noise generator.

The Outputs were accelerations of the shaker table, VERA link 1 tangentially, and link 2 tangentially and radially.

The Procedure included five sets of cases, varying the nominal joint angle of joint 2 through a broad portion of its range: 122°, 98°, 56°, 28°, and 302°, where 0° was the pose with joint 2 extended straight. Cases comprised high preload, low preload, and looseness at 15° CCW from the long axis on link 2.

Observations

Once preload was lost, the sound emissions from the apparatus took on higher pitch ringing tones, similar to the sounds observed in Experiment Four.

Results

Histograms of accelerations at the end effector are shown in Table 6.1 for 1.2 s of motion. Each histogram was scaled equally in both directions: the horizontal direction ${}^2\hat{\mathbf{x}}$ (collinear with the long axis of link 2), and the perpendicular direction ${}^2\hat{\mathbf{y}}$. No outliers were discarded. For each manipulator pose, correlation-vector polar plots were generated, histograms of distal link acceleration were produced, and the kinematic manipulability ellipsoid was calculated.

Looseness Case 1

The excitation direction in Looseness Case 1 (Figure 6.34) was 238° with respect to ${}^2\hat{\mathbf{y}}$. In the tight and low preload cases, correlations were poorest in the direction perpendicular to this direction, 328°, estimated here at 320° and 330°, respectively. In contrast, the looseness case exhibited lowest correlation at 240°, a −15° error with respect to the actual direction of looseness, 255°.

experiment		range (g)
122°	H preload	-3.2, 3.2
122°	L preload	-4.4, 5.2
122°	loose	-1.7, 1.7
98°	H preload	-3.6, 4.2
98°	L preload	-3.1, 4.3
98°	loose	-2.2, 1.7
56°	H preload	-3.1, 3.1
56°	L preload	-2.8, 3.1
56°	loose	-1.7, 1.7
28°	H preload	-2.3, 2.3
28°	L preload	-2.8, 3.1
28°	loose	-2.1, 2.0
302°	H preload	-3.0, 2.9
302°	L preload	-1.9, 2.2
302°	loose	-1.7, 1.9

Table 6.1: Histogram ranges

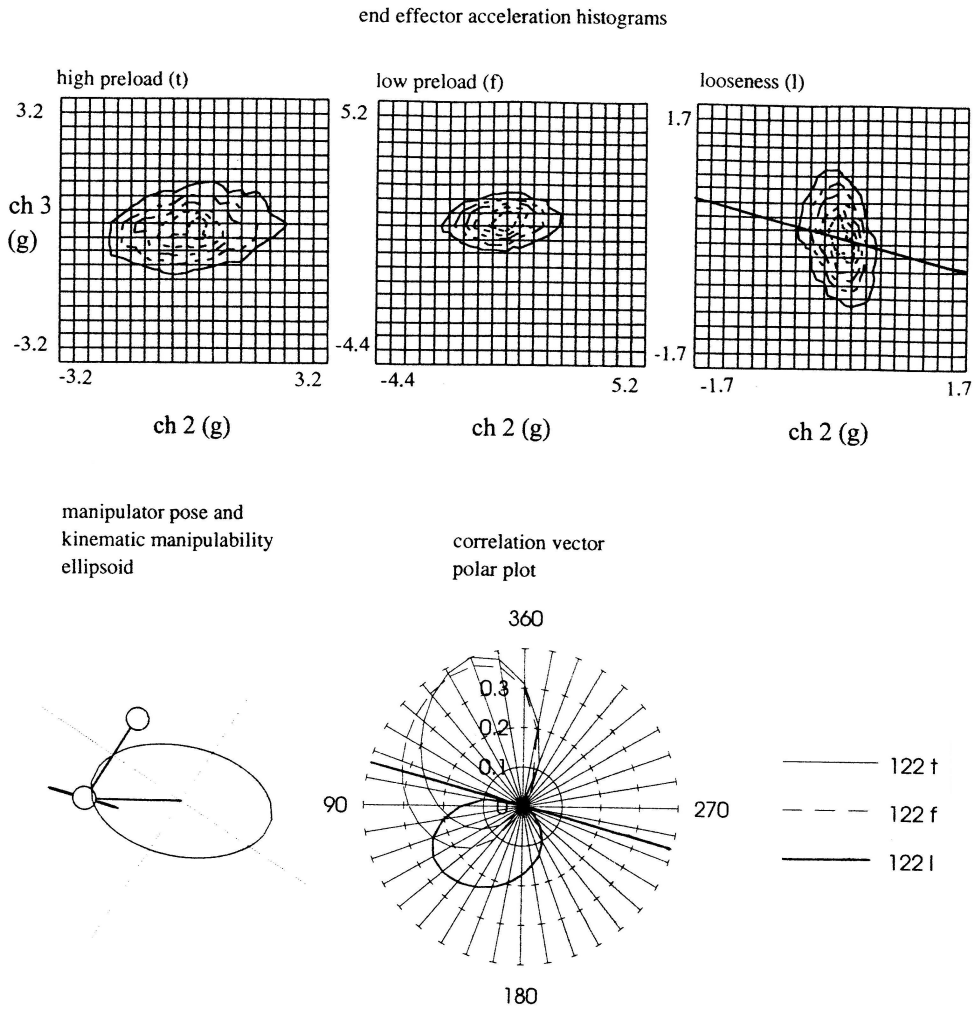

Figure 6.34: $\theta_2 = 122°$ nominal pose, $\beta = -15°$

The three motion histograms were roughly ellipsoidal, each with an aspect ratio of approximately 2:1, matching the aspect ratio of the kinematic manipulability ellipsoid. Ellipsoid directions did not, however, match. The manipulability ellipsoid major axis lay at 260°. The direction tangential to the excitation motion of joint 1, $\dot{\mathbf{p}}_1 = (\dot{\theta}_1 \times \vec{R}_1)$, was 299°. The direction of the principal axis in the tight and preload cases was about 285°, which was consistent with a dominant single DOF motion of joint 1. In the looseness case, however, the principal axis was at 195°.

Looseness Case 2

In Looseness Case 2, the direction perpendicular to excitation was at 352°; minimum correlation was at 325° for high and low preload. Looseness was again at 255°. The direction of lowest correlation was at 240°, an error of −15° to the direction of looseness.

In Figure 6.35, the histograms for high and low preload looked similar, with aspect ratio of 3:1 at an orientation of 280°. The orientation of the major axis of the ellipsoid in the looseness case was 200°, with aspect ratio of 2:1. The kinematic ellipsoid major axis was at 328°; the $\dot{\mathbf{p}}_1$ line lay at 311°.

Looseness Case 3

In Looseness Case 3, the looseness direction was 255°, with excitation at 304°. The direction perpendicular to excitation was 214°. The minimum magnitude of the correlation vector in the high preload case occurred at 210°; in low preload the direction of the minimum was 220°. With looseness, the minimum correlation was at 280°, an error of 25°.

The histograms for high and low preload in Figure 6.36 were similar, with the ellipsoid major axis at approximately 280° and aspect ratio 1.5:1 in each case. With looseness, the acceleration ellipsoid turned to long-axis orientation near 195°. The kinematic manipulability ellipsoid major axis was at 338°; the direction of $\dot{\mathbf{p}}_1$ line was at 332°.

Looseness Case 4

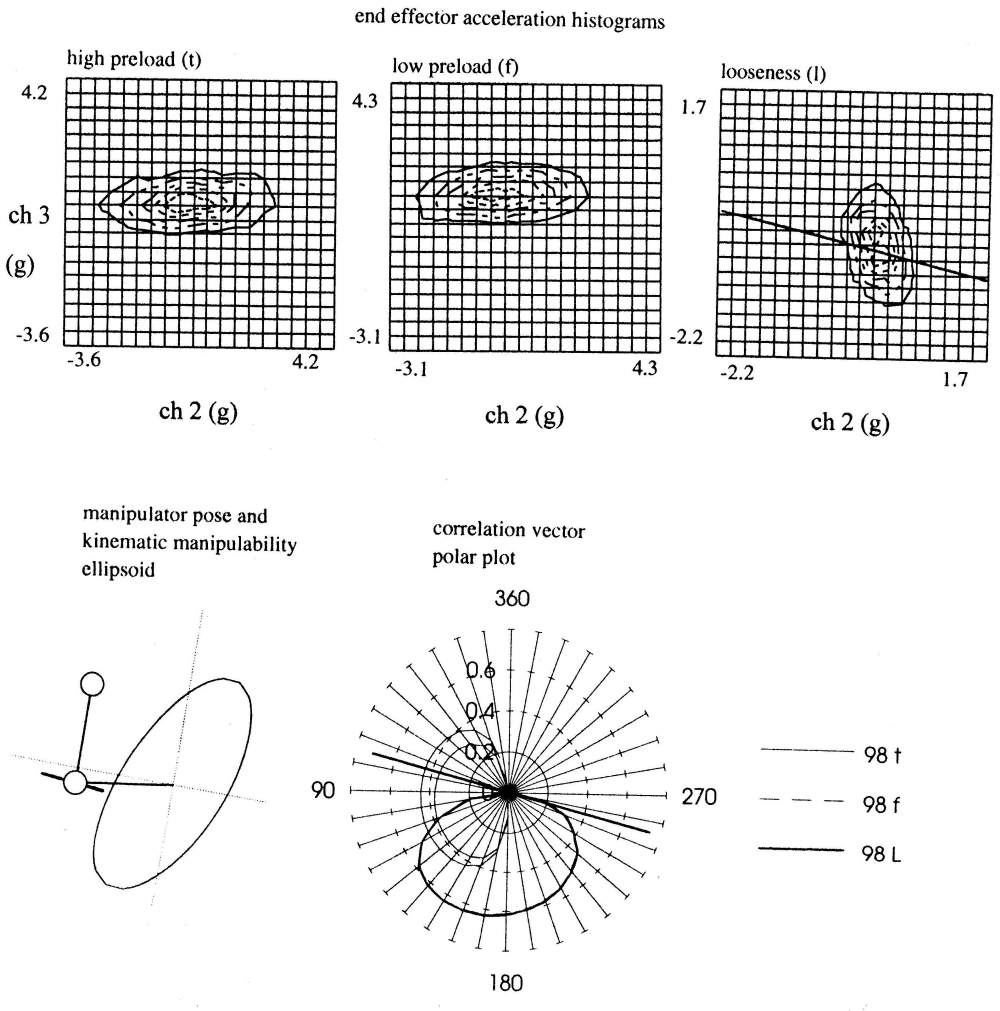

Figure 6.35: $\theta_2 = 98°$ nominal pose, $\beta = -15°$

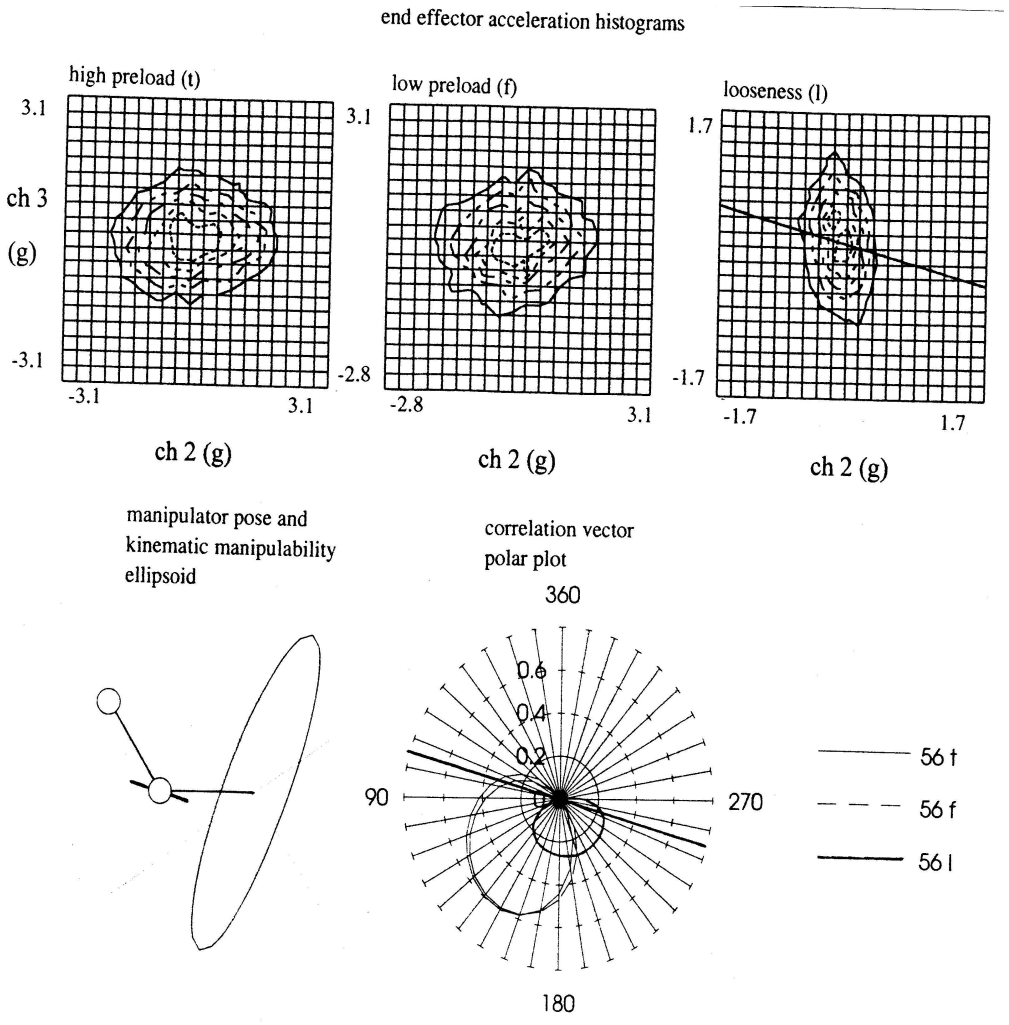

Figure 6.36: $\theta_2 = 56°$ nominal pose, $\beta = -15°$

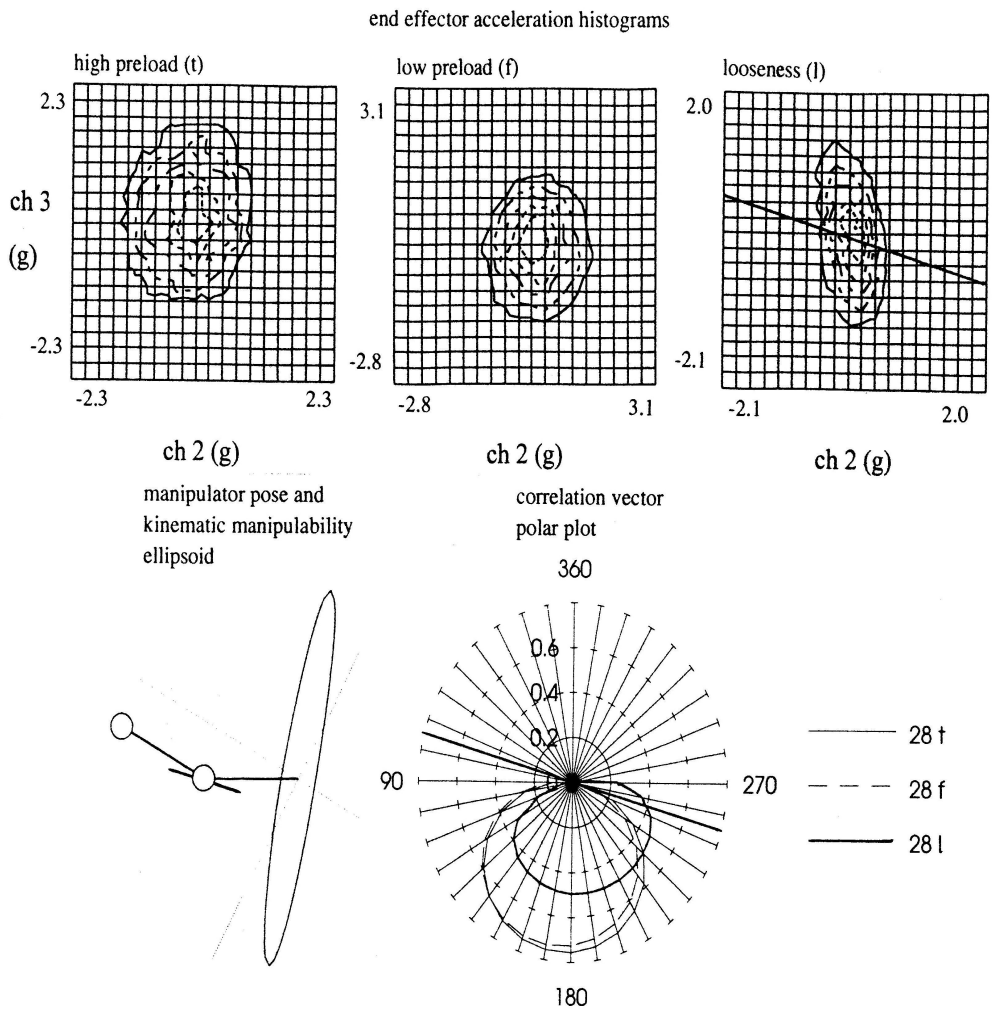

Figure 6.37: $\theta_2 = 28°$ nominal pose, $\beta = -15°$

In Looseness Case 4, the excitation direction was 242°; the direction perpendicular to excitation was 332°. The kinematic manipulability ellipsoid long axis direction was 349°, and the line of $\dot{\mathbf{p}}_1$ was at 346°. This case is illustrated in Figure 6.37.

The direction of minimum correlation for high and low preload was 265°. Minimum correlation for looseness occurred at 280°, an error of 25°.

Looseness Case 5

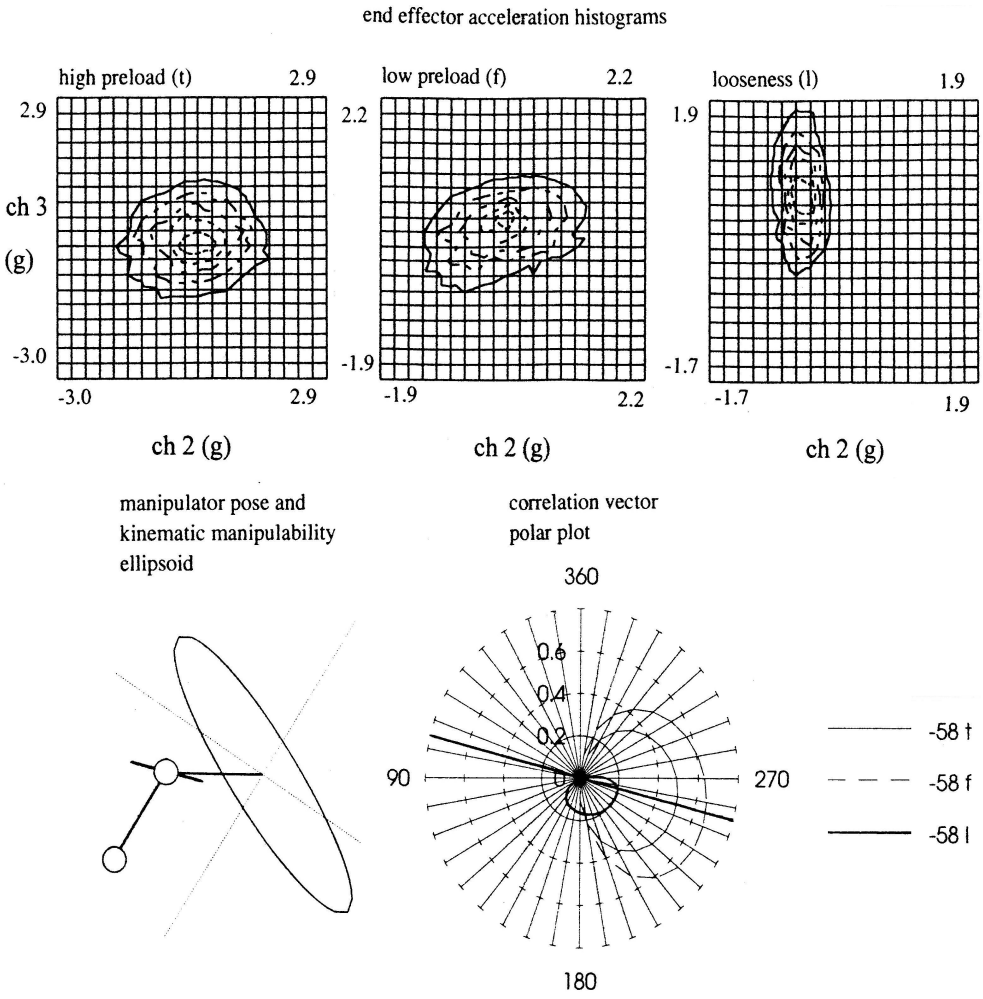

Figure 6.38: $\theta_2 = 302°$ nominal pose, $\beta = -15°$

In the fifth looseness case, with θ_2 nominally at 302°, the excitation direction was 328°, with the perpendicular at 238°. The line of $\dot{\mathbf{p}}_1$ was at 29°, and the kinematic manipulability ellipsoid long axis line was at 215°. The minimum correlation direc-

tions were: 355° for high preload; 355° for low preload; and 290° for looseness, an error of 20°. This case is shown in Figure 6.38.

The dominant effect was that the acceleration in the direction of looseness dropped when preload was lost. But there was also an effect on skewness and kurtosis. Figure 6.39 shows the change in skewness in the direction of looseness

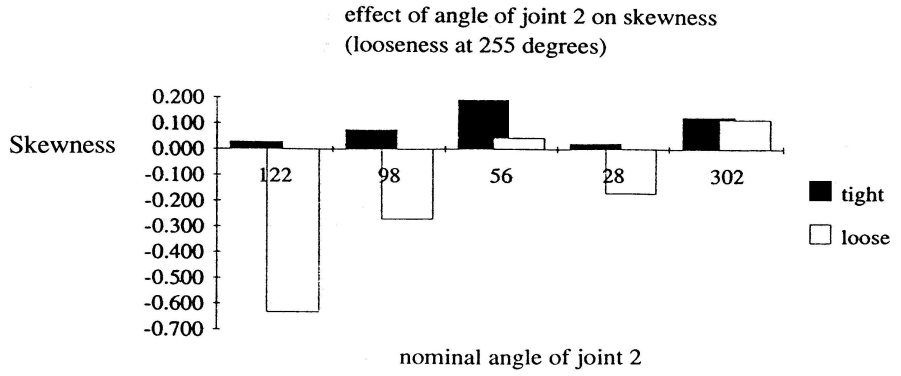

Figure 6.39: Effect of looseness on acceleration skewness in looseness direction

(255°). With high preload, skewness was close to zero (a Gaussian distribution has zero skewness). With looseness, the skewness became nonzero, but the amount of skewness depended on the pose. When the direction of looseness motion was almost perpendicular to the direction of joint actuation tangential motion (the direction of $\dot{\mathbf{p}}_1$), the skewness was low.

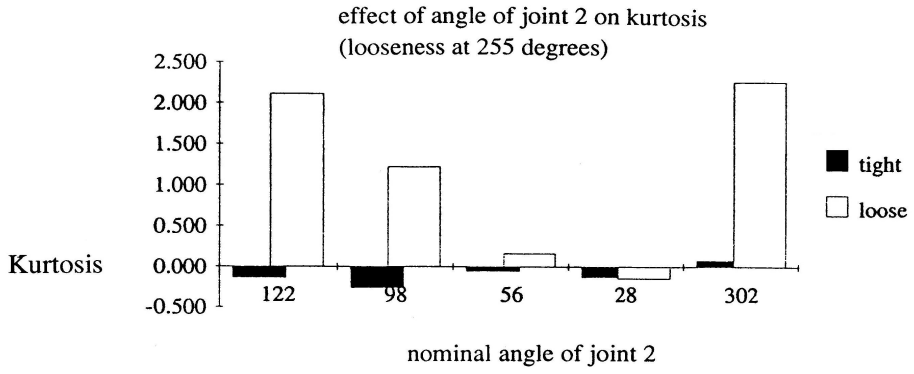

Figure 6.40: Effect of looseness on acceleration kurtosis in looseness direction

Figure 6.40 shows the effect on kurtosis. As with skewness, kurtosis was depen-

dent on pose. When the direction of looseness motion was almost perpendicular to the direction of $\dot{\mathbf{p}}_1$, the kurtosis became lower, approaching that of a Gaussian distribution.

6.4.2 Experiment Six: Backlash in a Planar Robot

The final experiment examined the effect of manipulator pose on locating backlash faults.

Objective

To demonstrate how end-effector motions from random joint excitations change when looseness occurred.

Method

The Rig comprised the shaker table actuating VERA link 1, with joint 2 blocked with a tapered pin for high preload cases. In backlash tests, the preload on this pin was relaxed, and then released, so backlash was actually between the gear and the pin, not between the gear and the motor pinion.

The Input to the shaker table amplifier was voltage from the white-noise generator.

The Outputs were end-effector tangential and radial accelerations, and the acceleration of VERA joint 1.

The Procedure included five sets of cases, varying the nominal joint angle of joint 2 through a broad portion of its range: 122°, 98°, 56°, 28°, and 302°, where 0° was the pose with joint 2 extended straight. Backlash cases comprised high preload, low preload, and backlash between the spur gear attached to link 2 and the locking pin on the proximal link.

Observations

Sound emissions from the rig changed in pitch when preload was lost.

Results

The change in sound emissions indicated that the vibrations in the rig changed with the loss of preload. This effect was also observed in the looseness motion experiment.

experiment		range (g)
122°	H preload	-3.2, 3.2
122°	backlash	-4.7, 4.3
98°	H preload	-3.6, 4.2
98°	backlash	-2.7, 3.3
56°	H preload	-3.1, 3.1
56°	backlash	-3.1, 2.6
28°	H preload	-2.3, 2.3
28°	backlash	-1.9, 2.1
302°	H preload	-3.0, 2.9
302°	backlash	-1.7, 2.1

Table 6.2: Histogram ranges

Histograms of accelerations at the end effector are shown for 1.2 s of motion. Figures 6.41 to 6.45 are scaled as in Table 6.2.

In the backlash case with nominal $\theta_2 = 122°$, the histogram in Figure 6.41 shows that there was an excursion from the usual ellipsoidal behaviour. With acceleration steady in the radial direction at 4.2 g, the radial acceleration ranged from -4.7 g to 4.3 g, well above the 1.5 g of most of the rest of the motion distribution.

With backlash, the lowest correlation was at 20°, an error of 20° from the direction of backlash motion. This contrasted with the 325° direction of low correlation for the high preload case.

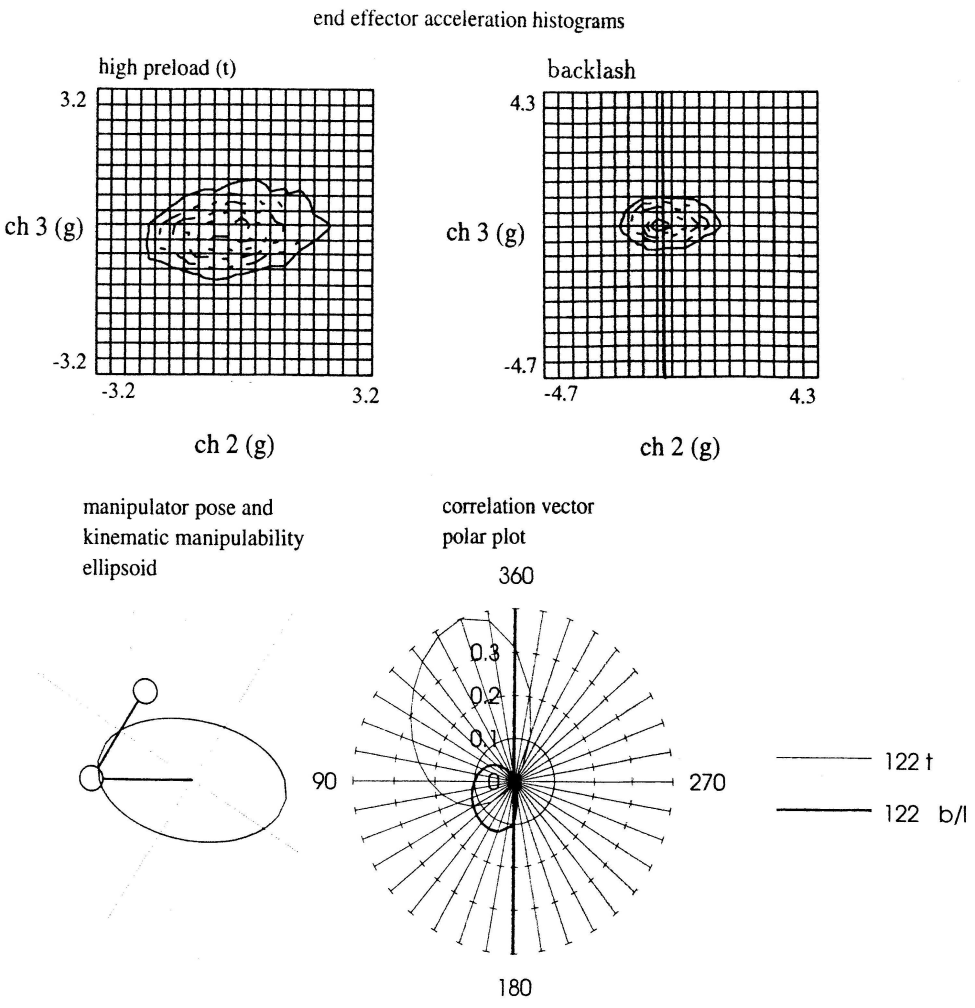

Figure 6.41: $\theta_2 = 122^\circ$ nominal pose, backlash

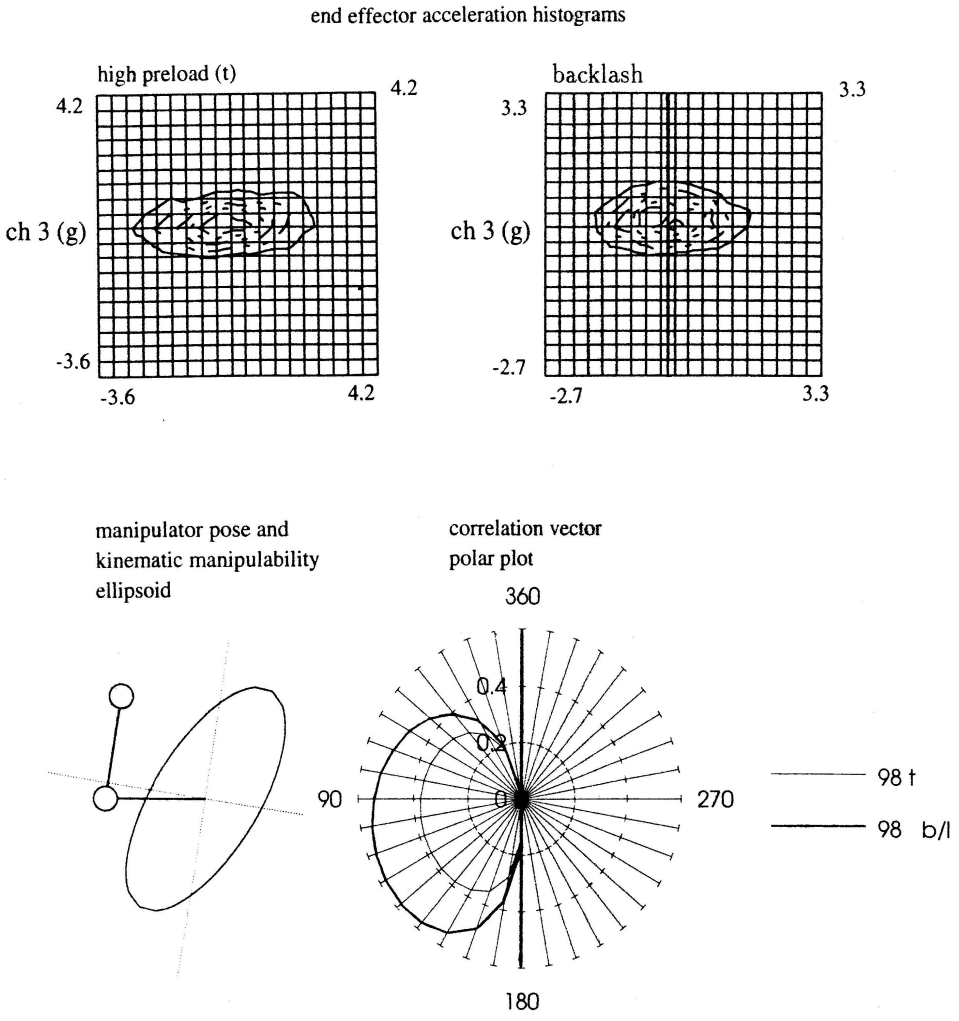

Figure 6.42: $\theta_2 = 98°$ nominal pose, backlash

In the second backlash case, at a nominal pose of $\theta_2 = 98°$, the minimum correlation value appeared at 185°, with the actual backlash motion direction at 180°, an error of 5°. The correlation plot is shown in Figure 6.42. The backlash histogram orientation in the figure was similar to that of the no looseness case, with a smaller aspect ratio.

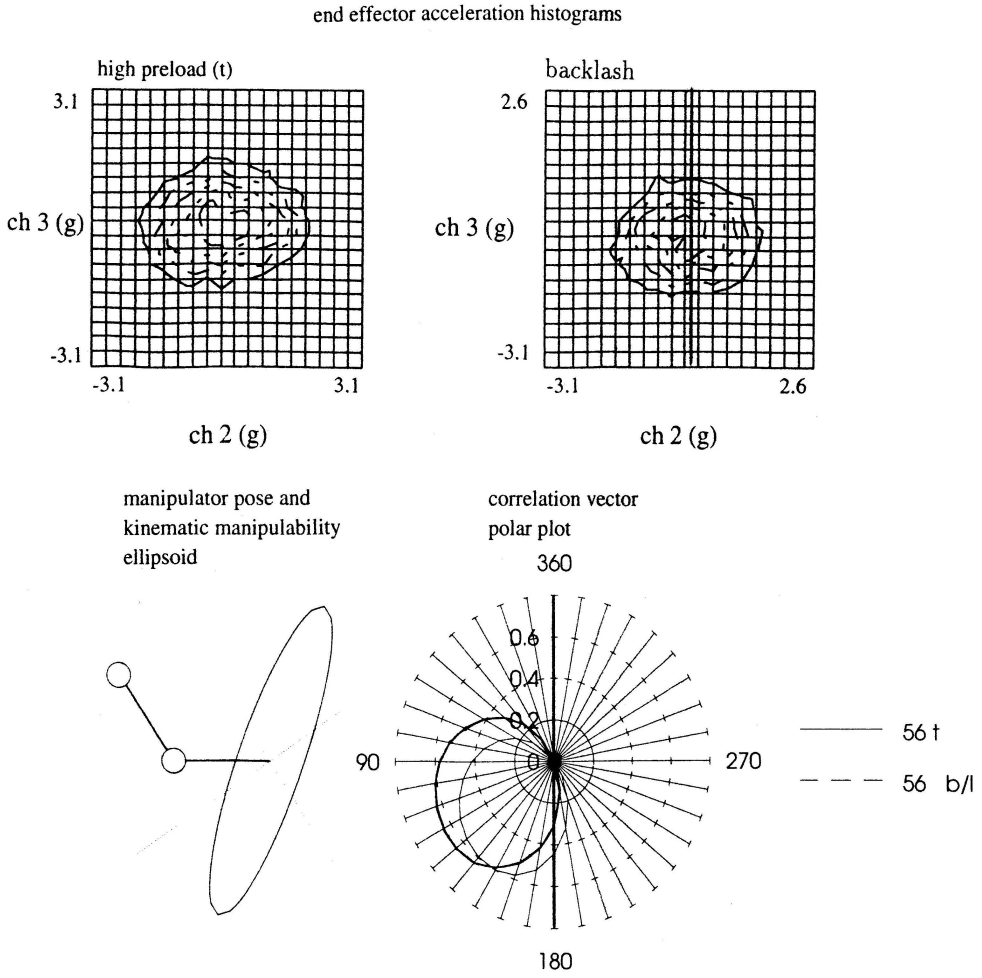

Figure 6.43: $\theta_2 = 56°$ nominal pose, backlash

In the backlash case at the nominal pose of $\theta_2 = 56°$, the minimum value of the correlation vector was at 20°, as shown in Figure 6.43. The error was 20°.

In the backlash case for nominal $\theta_2 = 28°$, the minimum correlation was at 195°, an error of 15°. The results of this case are shown in Figure 6.44.

Figure 6.45 shows the backlash case for θ_2 nominally at 302°. The direction of

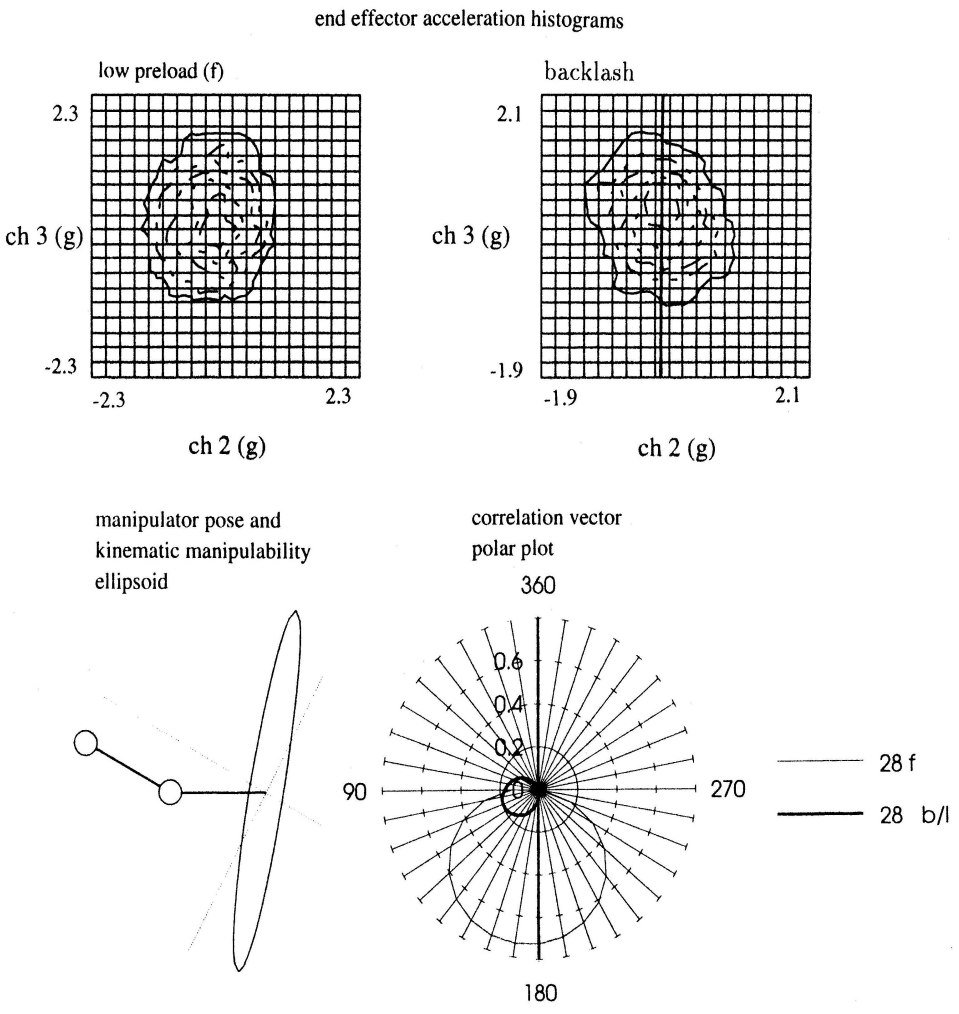

Figure 6.44: $\theta_2 = 28°$ nominal pose, backlash

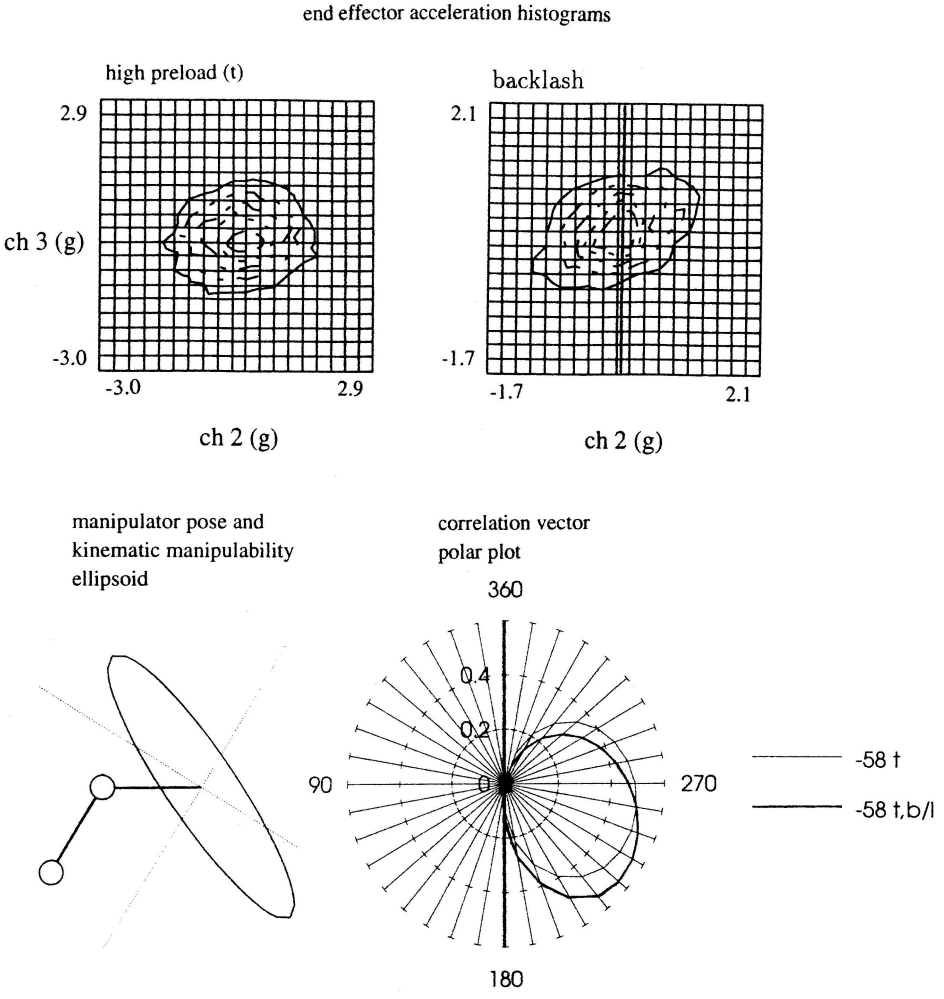

Figure 6.45: $\theta_2 = 302^\circ$ nominal pose, backlash

the minimum value of the correlation vector was 345°, an angular error of −15°.

The five cases of backlash affected skewness and kurtosis in the direction tangential to backlash motion (at 360° with respect to the end-effector coordinate frame vector ${}^2\hat{\mathbf{y}}$), as shown in Figure 6.46 and Figure 6.47, but the results did not show a

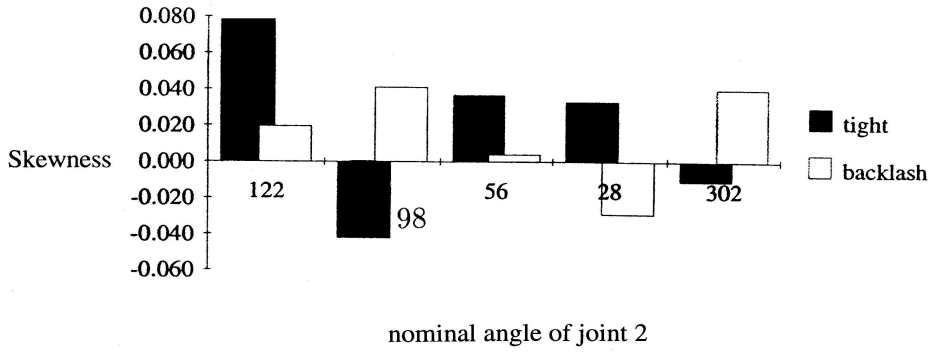

Figure 6.46: Effect of backlash on tangential acceleration skewness at 0°

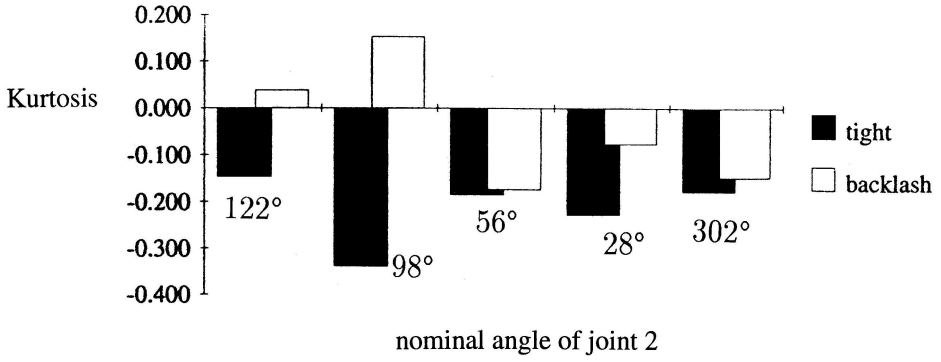

Figure 6.47: Effect of backlash on tangential acceleration kurtosis at 0°

conclusive trend. Skewness and kurtosis were low for both high-preload cases and looseness cases. The probable reason for the small change in descriptive statistics in this direction was that vibrations were almost normal-random in both preload and looseness. The correlation vector results showed the direction of looseness because the correlation improved in other directions, but the results show that the change in motion was otherwise small. The manipulator revolute joint was probably angularly stiff, exhibiting only a small amount of motion for a given the excitation force, but

still enough to reveal backlash looseness with the Correlation Vector Method. There may have been some compliance in the rest of the joint, which affected both motion distributions the same way.

6.5 Discussion of Experimental Results

6.5.1 Direction of Looseness and Backlash Motion at End-Effector

The difference in kurtosis when looseness appeared on the planar robot was not as pronounced as the difference for the looseness tests on the slide rig. The probable reason was that the distal link of VERA was more massive than the distal link on the slide rig: for equal input force and equal end conditions in the mechanical stops, accelerations were lower. There may also have been joint compliance.

The results did show that acceleration correlations between neighbouring links effectively identified local looseness and backlash across a robot revolute joint to within 20°. Averaging the error for cases of multiple poses spanning the range of

case	loose	b/l
122	-15	20
98	-15	5
56	25	20
28	25	15
302	20	-15
avg	8	9

Table 6.3: Averaging to reduce measurement error

motion of a joint improved that estimate, as given in Table 6.3. Averaging was only valid for cases with the same number of independently measured points.

The maximum correlation values also contributed to the diagnosis, as shown in

case	C_n	C_f	C_b
122	0.4	0.25	0.13
98	0.4	0.6	0.55
56	0.6	0.3	0.65
28	0.75	0.5	0.2
302	0.5	0.2	0.55

Table 6.4: Maximum correlation values

Table 6.4. The magnitude of the correlation vectors for nominal high preload C_n, looseness fault C_f, and backlash C_b changed in almost every case, but in no consistent way, until the direction was also considered.

Both direction and magnitude of correlation vectors changed as faults developed. An effective fault index therefore included both the maximum magnitude of the correlation vector and the direction where the minimum occurred. $\vec{E}$ was the cross product between the nominal correlation vector $\vec{C}_n(C_n^*, \phi_n)$ and the fault correlation vector $\vec{C}_f(C_f^*, \phi_f)$. These were functions of the directions of minimum correlation ϕ and the maximum correlation values C^*, normalized with respect to the magnitude of $\vec{C}_n$, $C_n = \text{mag}(\vec{C}_n)$, from which came the vector $\vec{E}$:

$$\vec{E} = \vec{C}_f^* \times \vec{C}_n^* \tag{6.15}$$

$$= (C_f^* \cos\phi_f C_n^* \sin\phi_n - C_f^* \sin\phi_f C_n^* \cos\phi_n)\hat{\mathbf{z}}, \tag{6.16}$$

where $\hat{\mathbf{z}}$ was the unit vector perpendicular to the plane spanned by the correlation vectors. Since $C_n^* = 1$ always, the magnitude of the cross product was

$$\text{mag}(\vec{E}) = C_f^* \sin(\phi_n - \phi_f). \tag{6.17}$$

and the cross product for the difference between vectors with normalised magnitudes $\vec{D}$ yielded the magnitude

$$\text{mag}(\vec{D}) = (1 - C_f^*) \sin(\phi_n - \phi_f). \tag{6.18}$$

The magnitudes of the cross products for the difference between normalised magnitudes are given in Table 6.4. This was the comparative index used for assessing whether looseness was present.

case	$(1 - C_f^*)$	$(\phi_n - \phi_f)$	mag$(\vec{D})$
122	0.38	100	0.37
98	0.50	80	0.49
56	0.80	70	0.75
28	0.33	20	0.11
302	0.60	120	0.52

Table 6.5: Comparative index for looseness cases

Table 6.5 has three columns. The leftmost column shows the relative change in magnitude $(1 - C_f^*)$ of the maximum value of the correlation vector as preload was lost and looseness appeared. The middle column gives the difference in angle between the direction of lowest correlation for the nominal case ϕ_n and looseness case ϕ_f. The rightmost column shows the value of the cross product of a unit vector in the direction of nominal minimum correlation ϕ_n with a vector of magnitude $(1-C_f^*)$ at an angle ϕ_f.

This cross product was the comparative index used for assessing whether looseness was present. It included both changes in the direction of the minimum correlation and in the magnitude of the maximum correlation. A high value of the index indicated a fault.

These results contrasted with the comparative case of high preload (the nominal case) and low preload (C_p), which is not a fault. There was little change, as preload decreased, between maximum correlation magnitudes and the difference in minimum correlation directions for vectors of high preload $\vec{C}_n$ (the nominal case) and low preload $\vec{C}_p$ (which was not a fault case).

The comparative index for the low preload case is given in Table 6.6, using the normalized magnitude error $(1-C_p^*)$, where C_p^* was C_p normalized with respect to the

case	$(1 - C_p^*)$	$(\phi_n - \phi_p)$	$\text{mag}(\vec{D})$
122	0.08	10	0.014
98	0.13	10	0.022
56	0	-5	0
28	0.27	0	0
302	0.32	10	0.055

Table 6.6: Comparative index with low preload case

case	$(1 - C_b^*)$	$(\phi_n - \phi_b)$	$\text{mag}(\vec{D})$
122	0.68	50	0.52
98	0.38	5	0.03
56	0.08	20	0.03
28	0.73	-60	0.63
302	0.18	0	0

Table 6.7: Comparative index for backlash cases

nominal maximum correlation magnitude. This index remained close to zero while some preload persisted. The comparative index was thus well suited to looseness fault diagnosis.

There was a limitation to this index. In cases where the direction of the lowest correlation did not change, the index did not reveal that there was a fault. For a single check, the index falsely supported the null hypothesis that no fault existed.

For backlash cases, comparative index of the magnitudes of the cross products are given in Table 6.7. The backlash cases showed the limitations of the index. If there was little change in the maximum correlation value, or if there was little change in the direction of the minimum correlation, then the index was low.

This situation occurred when the direction of lowest correlation in the nominal case coincided with the direction of lowest correlation with a fault. This situation was dependent on pose, and so multiple poses with changes in joint angle prevented the

false negative results from being accepted as correct. The backlash cases illustrated, however, the sensitivity of the method to the nominal pose, and the need for multiple poses to reduce the effect of fault sensitivity on pose.

The correlations related the end-effector motion to the motion of the proximal link. The histograms of absolute end-effector accelerations in the plane also yielded useful qualitative diagnostic information. The histograms did not show conspicuous directions of normal-random motion, but the shapes did change when preload was lost.

The descriptive statistics gave an indication of how normal- random motion proximal to the joint propagated through a geared revolute joint. The descriptive statistics parallel and perpendicular to the direction of looseness and backlash motion for the cases above were not calculated. Those statistics would have given an indication of whether the search method using a fit to a marginal Gaussian distribution might have worked. Since, however, the nonlinear searches did not converge well even for simulated data with very different marginal distributions, that diagnostic method was not pursued further.

Summary Discussion of the Looseness Location Method

The normalized correlation-vector cross product was a useful fault diagnosis index. This index depended on having motion sensors both proximal and distal to the link of concern.

The descriptive statistics of end-effector motions were key in determining whether an end-effector sensor can be used to identify looseness in the chain manipulator. If normal-random motion—excited in an actuator joint—propagated well through the links to the end effector, then non-normal random motion became an indicator of a change in motion. Thus, the method of searching for the most non-normal direction of motion at the end effector was valuable for identifying the location of structural faults in a manipulator.

The descriptive statistics showed the value of trying to match the experimen-

tal end-effector motion data to a Gaussian distribution. The descriptive statistics revealed approximately normal distributions perpendicular to the direction of fault motion, with an expected value and variance but little or no skewness or kurtosis. In the direction of fault motion, the distribution was not normal random, and in some cases there were conspicuous changes in skewness and kurtosis. It was important that the normal random motions were not corrupted while being transmitted through the structure, except when looseness motion appeared.

6.5.2 Limitations of the Present Method

The present implementation of the method is not ready for industrial application. The limitations are described below.

Three-Dimensional Search

The present implementation of the method was two-dimensional for a planar manipulator. But the method can be extended to three dimensions to suit spatial manipulators.

Automatic Search for Looseness Direction

The study did not include a method for locating the looseness direction automatically from the end-effector motion data. But the nature of the correlation vector was such that the direction of minimum correlation corresponded to the direction of looseness, at the point that the magnitude of the correlation vector crossed through zero.

Two-dimensional zero-finding methods can be applied to locate the direction of looseness in spherical coordinates. There are two zero-crossing regions, one at the antipole of the other, and so the search space can be restricted to one hemisphere. Candidate angles for correlation calculations should initially be uniformly spaced in the hemisphere. Refinement of the search can proceed by bisection.

6.5.3 Restrictions in the Present Study

There are questions raised by the present study on the influence of structural compliance and controller dynamics on the method.

Influence of Compliance

Results pointed to a need for further experimentation on industrial manipulators, with joint excitation more proximal than a single joint.

Compliance in the robot joints was recognized as a contributor to experimental error, because the method assumed that motions were faithfully transmitted through the linkage to the transducers. All nonlinear response of the mechanism was assumed to be caused by a single looseness fault.

To model joint compliance, the locking pin for joint 2 was partially disengaged from the bull gear mesh to release some preload stiffness on joint 2. There was some drop in the maximum amplitude of the correlation vector, but the direction did not change. It would have been possible to have estimated the preload stiffness by observing the change in resonance frequency for different preload torques on the holding pin. An empirical estimate of joint compliance would be preferred over a theoretical model. The relationship between preload torque and joint stiffness would be difficult to calculate, because the preload stiffness would depend on the torque on the pin, the axial load in the presence of lubrication uncertainty, with some assumed contact geometry, and torsional stiffness of the joint in the presence of bending of the gear under axial pin load. Such an analysis was beyond the scope of the present work.

Influence of Controller

The influence of the controller on looseness motion transmission through the mechanism was not studied. The looseness joint could not be mounted on the first link of VERA, for two reasons. The shaker table was used to actuate the first link, and the looseness link would have to be redesigned to mount at the distal end of link 1.

The present study examined looseness in the link upon which the sensors were mounted. Backlash tests did transmit joint motions through the joint proximal to the looseness joint, which was preloaded so as not to be loose. But the question remained open as to whether joints under closed-loop control would have had sufficient compliance to affect the transmission of motions through the structure to the end effector.

6.6 Summary of Results

The Marginal Distribution Matching Method was not successful in identifying the direction of looseness. The nonlinear two-dimensional estimator did not converge well for the model used: a bivariate distribution with normal and uniform marginal distributions. This poor fit was possibly a consequence of using a modest number of bins in the histogram. A binomial distribution of data (such as was generated in the histograms from a pseudo-normal random process) only approaches a Poisson distribution when there are a large number of data [113].

Spectral representations of motions were not used for diagnostics because they contained too much information: there was a need for a single parameter for assessment of direction.

Kurtosis and skewness were good measures of the appearance of looseness. The descriptive statistics of end-effector motion changed significantly when looseness or backlash appeared. The descriptive statistics were somewhat sensitive to preload and the nominal pose, which would present problems in applying descriptive statistics for diagnostics on industrial manipulators with compliance.

The search for looseness direction succeeded when using the minimum correlation of motion across a joint. The Correlation Vector Method, relating motions proximal to the looseness joint to the end-effector motions, showed itself to be reliable in the tests conducted in this study for identifying the direction of looseness and backlash motions in a planar revolute manipulator in different poses.

The Correlation Vector Method (coupled with the Looseness Link Finding

Method developed in Chapter Four) therefore validated the third hypothesis that fault effects could be related to their respective origins using model-based analysis.

Chapter 7

Conclusions

Happy is the man who has learned the causes of things... *Virgil*

This chapter reviews the steps that were followed in validating the hypotheses for a method of diagnosing robot looseness faults.

There was a comprehensive examination of robot modeling, from which came the choice of model for an analysis-based diagnostic method. Two methods were implemented for identifying looseness in robots; these methods were reviewed in light of simulation and experimental results on a planar manipulator with a single looseness fault. The work also included development of experimental rigs, from which came a methodology for designing robotic manipulators.

7.1 Development of Looseness Identification Methods

A looseness identification method required diagnostic parameters that were appropriate for describing looseness. Since the effect on manipulator performance at the end effector was of concern, modeling alternatives were assessed in the context of the effect of looseness (an additional degree of freedom) on end-effector motion and/or end-effector forces. Desired features of a model were: a minimum number of addi-

tional parameters required to add a looseness fault; a linear relationship between the looseness joint variable and the end-effector variable; and simplicity of measurement.

Looseness was included in a rigid-body kinematic manipulator model by recognising that looseness was an extra, unactuated degree of freedom in the mechanism. A kinematic technique was developed to locate a looseness fault given the direction of looseness motion at the end effector in a set of poses. Two methods were developed to find the direction of looseness motion at the end effector. Both these methods assumed that any change in bandwidth-limited normal-random motion through the mechanism was caused by a single looseness fault.

7.1.1 Review of Modeling Alternatives

Alternatives considered for modeling robot looseness were: displacement; velocity; acceleration; static force; unconstrained dynamics; lumped-parameter, flexible-body dynamics; and constrained dynamics. Linear kinematic relationships between joint motion and end-effector motion were: velocity, and acceleration with negligible velocity.

Choice of Diagnostic Parameter

Velocity and acceleration with low velocity were chosen as diagnostic parameters. These alternatives were preferred because linear relationships existed between joint motions (including that of the looseness joint) and end-effector motions. The static-force parameter also had a linear relationship, but this alternative was not pursued because of the practical implementation challenges of force measurement in a number of poses in the workspace of an industrial manipulator.

Including Looseness in a Manipulator Model

Looseness was modeled as an additional, unactuated degree of freedom to the manipulator mechanism. For the purpose of this study, it was assumed that looseness added only one additional degree of freedom to the manipulator. This assumption,

and the assumption that only looseness would corrupt the propagation of random motions through the mechanism, may limit its industrial application.

A strategy was described for including a looseness joint in a rigid-body kinematic model using the Denavit-Hartenberg convention, without affecting the parameters in neighbouring links.

7.1.2 Locating Looseness on the Manipulator Mechanism

Limitation of Recursive Parameter Estimation

Although kinematic parameters in revolute-joint, serial-link manipulators can be estimated recursively using the Jacobian, the present work showed the limitation of recursive parameter estimation for manipulators with prismatic links: revolute motion is described by a line vector, whereas prismatic motion is described by a free vector. The kinematic parameters of a manipulator with prismatic looseness can not be found by recursion in a single pose.

Looseness Link Finding Method

A strategy was developed to find the location of a prismatic joint in a revolute-joint, serial-link mechanism. If there is a revolute joint between the end effector and the prismatic joint, then a change in that revolute joint angle changes the direction of the end-effector motion due to the prismatic joint in the end-effector frame. Conversely, a change in angle of a revolute joint that is proximal to the prismatic joint does not affect the end-effector motion from the prismatic joint. By changing the joint angles starting from the most distal revolute joint, the link of concern is found.

There is a limitation when there are prismatic joints, in that their displacement does not change the end-effector orientation. But as motions are made across the range of a prismatic joint, the looseness may leave the load-bearing part of the link, which would aid in identification; however, this conjecture has not been validated.

7.1.3 Finding Looseness Direction

The Looseness Link Finding Method depends on knowing the contribution of the looseness motion to the end-effector motion. Two methods were developed to find the direction of looseness motion: the Marginal Distribution Matching Method, and the Correlation Vector Method.

Both methods rely on random excitation of the manipulator, with the assumption that it is possible to drive a manipulator with Gaussian motion in its joints, and that any motion in the unactuated looseness joint is not independent and Gaussian. If compliance is low (and there is no looseness), then there is end-effector motion in only one direction when a single joint is actuated. When looseness appears, spurious end-effector motion appears.

Marginal Distribution Matching Method

In this method, a parametric model of a normal distribution is fitted to the distribution of random end-effector motion. The distribution of motion data in the direction of looseness is assumed to have the poorest fit to a normal distribution.

Correlation Vector Method

This method considers the fidelity of the transmission of motion across the joint of concern. The method is used in one of two ways, generally or locally.

In the general method, the end-effector motion is compared to the joint excitation motion. The direction of lowest correlation between signals is the direction of looseness motion. The Looseness Link Finding Method is then applied to identify the link on which the looseness occurs.

In the local method, the link motion at the distal end is compared to the motion at the proximal end; as this is a direct looseness-motion measuring method, there is no need to apply the Looseness Link Finding Method.

7.2 Simulations

7.2.1 Looseness Motions

Stochastic and deterministic looseness simulations were performed. The two looseness-direction identification methods were evaluated using the simulated data.

Monte Carlo kinematic simulations were done to generate looseness distributions. The requirements were examined for stochastic looseness distributions in displacement, velocity, and accelerations, including conditional probabilities in going from free motion to contact. In the direction of looseness, the displacement distribution was modeled as a uniform distribution in the region of free looseness motion, with point probabilities at the ends where there contact occurred. Perpendicular to the looseness direction was a Gaussian distribution.

The Marginal Distribution Matching Method converged on the correct solution if the trial values of the direction and variance parameters were within 10 % of the correct value. While it was possible to make an estimate of the variance, there was no *a priori* information of the direction of looseness, and so it was necessary to do multiple trials to cover the range of the direction parameter.

The Correlation Vector Method successfully found the direction of looseness in each case with an error on the order of the step size. This method also lent itself to automatic processing by searching for zero-crossing of the correlation coefficient as a function of angle, so the Correlation Vector Method was pursued as a looseness-direction finding method.

7.2.2 Probable Looseness Locations and Directions

The equations of motion were used to examine the joint loading on a planar manipulator for a range of motions. The joint displacements where maximum loads occurred indicated probable directions where looseness would develop. This information can be applied to manipulator diagnostics to identify pose sets to check for looseness first at those locations.

7.3 Experimental Rig Development

Simulation results relied on assumptions about looseness-motion distributions. Experiments were done to generate actual looseness motion in two rigs developed for this study, and in an industrial manipulator.

A linear slide rig was driven at the proximal end by a shaker table; accelerometers were mounted distally to a custom looseness joint. Preload and looseness trials were done with the looseness joint at several different angles to the direction of excitation. The looseness joint was then mounted on a planar revolute manipulator, and looseness and backlash trials were done in different poses.

7.3.1 Design Methodology

A methodology was developed for designing the manipulator: specification choices, kinematic design, dynamic design, actuation selection, sensor selection, control implementation, and performance checking to ensure that the specifications were met. The iterative nature of manipulator design was considered, particularly in dynamic analysis and actuator selection.

7.3.2 Implementation

The planar manipulator was designed according to this methodology. The rigid-body equations of motion were used to size the actuators of the manipulator. A sensor interface was designed for an IBM-compatible PC that was used for control; trajectory-generation software and joint-control software was implemented separately on a manipulator that did not require the interface. A strategy was developed for generating normal-random joint motion, although in the looseness experiments the shaker table was used for excitation.

7.4 Validation of Hypotheses

This section assesses whether the hypotheses for robot looseness diagnostics have been validated.

7.4.1 Hypothesis One

The first hypothesis to be validated was that repeatable faults existed in manipulators that could be measured. A proof-of-concept test showed that fault motions were indeed repeatable on an industrial manipulator. The experiment also showed that the manipulator pose affected the end-effector motion, which confirmed that the looseness-identification method had to accommodate changes in pose.

7.4.2 Hypothesis Two

The second hypothesis was that there was a relationship between faults and their manifestation. The counter hypothesis was there was no relationship between faults and measurable machine variables. The counter hypothesis was refuted by seeding different faults into a slide rig and a planar articulated manipulator rig. Consistent effects appeared for different fault conditions.

7.4.3 Hypothesis Three

The third hypothesis to validate was that there was a diagnostic relationship between faults and their manifestation, using a model relating measured data to root causes.

There was an unsuccessful attempt to fit a parametric model to the data using the Marginal Distribution Matching Method. The model was nonlinear, a two-dimensional motion distribution. In one direction the motion had a Gaussian marginal distribution; the perpendicular direction had a uniform marginal distribution. The goodness-of-fit to the model was the criterion by which the degree of looseness and its severity were judged. Solutions for model parameters converged only if the trial parameters were well chosen, and it was not possible in practice to

ensure good selection of trial parameters.

Nonparametric models looked for the poorest correlation between proximal and distal motions across a loose connection—be it from structural looseness or joint motion backlash—and examined the descriptive statistics to see in which direction the motion was non-normal random.

The poorer the correlation, the less coherence between motions on either side of the looseness joint, indicating looseness motion. For the two planar test rigs used, the Correlation Vector Method successfully identified the direction of looseness and backlash in different kinematic poses.

Descriptive statistics examined the third and fourth moments of end-effector motion data. This method also showed a change in the direction of looseness motion. The greater the third and fourth moments of the data in the distribution, the more non-normal random it became. For a nominally normal-random input, such moments indicated a change in motion across the joint, that is, looseness. This was an indicating factor of looseness when the nominal motion was normal-random, but this method was not used to find the direction of looseness.

The Correlation Vector Method was therefore concluded to be a useful method for identifying looseness faults in serial-link robotic manipulators.

Since the Looseness Link Finding Method could locate the link on which the looseness was present once the looseness direction is known, a model-based analysis was therefore able to identify looseness and backlash faults on a serial-link manipulator with predominantly revolute joints. A diagnostic relationship using model-based analysis was therefore available, validating the third hypothesis.

7.5 Contributions of the Present Work

This work presents several original contributions to robot diagnostics. Methods for modeling looseness in robotic manipulators were critically evaluated. For diagnostic purposes, it was appropriate to assess whether a simple approach would be adequate, and so a kinematic model was used.

Two kinematic techniques were developed for identifying the presence of looseness in end effector motions, and a method was found for finding looseness in serial-link manipulators with revolute joints. Looseness faults were simulated kinematically. Limitations were found in the simulation results, and so the diagnostic methods were experimentally verified on a planar manipulator with a custom looseness link. The Correlation Vector Method was found to be a useful looseness diagnostic method.

A methodology for manipulator design was also developed that included applying the Newton-Euler recursive equations of motion to sizing actuators and bearings for serial-link manipulators [72].

The present work thus contributes to both robot design and maintenance.

Chapter 8

Recommendations

Today is yesterday's pupil. *Thomas Fuller*

Recommendations for future work include augmented analysis methods for more general applicability, additional experiments to ensure that the results described above are not limited to the experimental rigs used, and implementation on an industrial spatial manipulator.

The culmination of future efforts is a diagnostic method applicable to industrial manipulators.

8.1 Analysis Methods

8.1.1 Development of Three-Dimensional Search Method

A spatial-manipulator implementation requires a three-dimensional looseness direction finding method. There should be a confidence interval test so that the number of points required for a correlation can be optimised.

8.1.2 Static-Force Method

The static-force method would obviate the need for stochastic excitation of the mechanism to find the direction of looseness. Further work should consider the design of

stiff, movable jigs that allow a manipulator to dock for static-force measurements across the workspace.

8.2 Additional Experiments

8.2.1 Study of Effect of Compliance

The change in motion during transmission through the mechanism should be examined. This can be done by transfer function estimates with a manipulator under closed-loop control.

8.2.2 Compensation of Excitation

It is likely that some manipulators have uncompensated dynamics effects (such as compliance) that affect the transmission of normal-random noise through the mechanism to the end effector.

Provided that the excitation bandwidth is below resonance frequencies, and that actuators have good performance throughout that band, it should be possible to compensate for the dynamics to ensure normal-random end-effector motions when operating normally.

There was no attempt to compensate for system dynamics to achieve normal-random motions. Compensation involves estimating the transfer function in the pose of concern, and then generating a random signal that is the inverse of that transfer function. The bias effect of gravity load must be considered as well. Implementing such a technique remains future work.

8.2.3 Excitation Source on Manipulator

The effect of an alternative excitation source on the end-effector motions should be studied. The present study used excitation of the proximal joint only. Other joints may be more effective at producing looseness motions, especially if the looseness is

in the link immediately distal. Alternatively, poses should be chosen that have good sub-manipulator dynamic manipulability, that is, a distal segment of the manipulator that is in a set pose is driven by the joints of the proximal segment, which changes pose. The distal segment is effectively the end effector of the proximal segment. The energy manipulability measure would be appropriate for weighting the excitation [40]. More development is required in choosing pose sets.

8.2.4 Looseness Motion Distributions

There should be further experimental study of the nature of looseness motions, to produce better models of looseness. Computer simulations that truly mimic the effect of the fault of concern would be valuable for developing new diagnostic methods.

Spectral information is less helpful for diagnostics, because it is difficult to reduce spectral data to a single quantitative parameter. It may be possible to do a parametric model fit in the frequency domain—equivalent to using a time-domain model with sinusoidal functions—to produce a diagnostic relationship through goodness-of-fit. Spectral representations of looseness motion, and effective indices of their appearance, remain topics of further work.

8.3 Industrial Implementation

8.3.1 Implementation on Spatial Manipulator

The present investigation considered only planar mechanisms. The method should be implemented on a spatial manipulator to make it useful for general robot diagnostic applications.

8.3.2 Improvements to the Experimental Rig

VERA was intended to be useful beyond the scope of this work. But if VERA is to be used for further studies, it requires modification. The controller requires a

real-time operating system or an embedded controller for communicating with the resolvers. The gear trains should be replaced with higher-precision sets. The existing motors can be kept if the links are shortened. Provision for an end effector should be included so that the machine can manipulate objects. A number of looseness cases should be examined beyond the one looseness joint style of this study.

8.3.3 Multiple Sensor Locations

The assumption of this work was that the measurements were to be made at the end effector: since the end effector is where a manipulator usually interacts with its environment, it was reasonable to look for changes in performance there. The experimental results have forced a rethinking of this position.

There may well be merit in considering multiple sensor locations. It is important not to neglect transmission effects in vibration measurement through the structure. It is those very changes that reveal deficiencies in the mechanism as looseness develops—or, more properly, as compliance increases on the way to looseness. The farther the transducer from the location of interest, the greater the influence of structural dynamics on the signal. The greater the structural influence, the greater the uncertainty that the observed effect comes from the area of interest.

The search procedure of pose sets serves to identify the location of looseness that is already sensible to the robot end effector. This is an unappealing maintenance tactic, because the effect has already progressed to the point where there has been a degradation of machine performance at the end effector. The technique has to be sensitive enough that faults are detected before the degradation in performance affects product quality.

It would be far better to attempt to sense and identify growing faults before the fault manifests itself at the end effector. To this end, joint sensing would be analogous to monitoring vibration on process equipment as close to the component of concern as possible.

It was observed that the sound emissions from the manipulator under random

excitation changed when looseness developed. Acoustic monitoring under random excitation would be a coarse indicator of whether looseness were developing. The acoustic signature and the direction would be indicators of the looseness location. Diagnosing robotic manipulator faults using sounds remains the subject of future work.

8.3.4 Minimising the Number of Transducers

Sensors must be robust—and inexpensive—so that a sufficient amount of data can be collected on a continuing basis. A number of sensors allows redundancy, and ensures that all parameters necessary for diagnostics can be measured.

It has been said that the future of robotics depends on cheap sensors [63]. The present work indicates that looseness effects are more visible locally than globally. It would be of greater advantage to instrument a manipulator to do comparative analyses of motions across joints than to rely on the late appearance of spurious end-effector motions after the damage has been done.

The highest forces in VERA acted in the tangential direction of the proximal link. The mechanical design of VERA was similar to the two proximal degrees of freedom of SCARA robots, and similar to the second and third links of articulated robots. It is reasonable to expect that those types of robots would also encounter high forces in the tangential direction of the proximal member of that pair of links. (That conjecture should, however, be confirmed by analysis on a given manipulator.) Assuming that wear acts in the direction of highest load, wear is thus expected to appear first in the tangential direction at the distal end of the proximal link at the joint of concern.

Installation of joint-vibration sensors on lower-pair joints may initially be limited to the tangential direction of the joint motion, where wear would be expected to be highest. For a manipulator with n joints and m DOFs, $n + m$ motion sensors would be required, one on each link and m on the end effector.

If compliance is a problem, then the correlation index should be used with ac-

celerometer installations on each link. If revolute joint design is adequate, then looseness and backlash motion should be restricted to the plane normal to the axis of joint rotation. In that case, two accelerometers on the link measuring motion in that plane would be sufficient to monitor robot looseness and backlash. A third accelerometer would be necessary for a spatial manipulator with non-parallel joints. Generally, n triaxial accelerometers are required on a manipulator with n rigid bodies. The capital cost of installing accelerometers on the links of a manipulator has dropped now that miniaturised accelerometers with integral conditioning electronics have become available.

8.3.5 Data Collection

Since the key to diagnostics is to gather information about a system of concern, there exists a need for more avenues of data collection from machines, and more involved means of processing.

It would not be onerous to include extra signal-carrying conductors in robot cabling. Some vendors already offer specialty cables that include power conductors and small-gauge, shielded conductors; signal conductors can even be included on hydraulic lines [5].

An alternative communication medium for electrically-driven robots is the power conductors for the motors. A high-frequency, low-power AC signal can be added to the electrical load with minimal effect on the performance. The sensor uses the conductors as a serial data bus, and the diagnostic system reads the data from the conductors outside the workspace. Such a scheme is already used for remote diagnostics on motor-operated process valves [4]. Radio or infrared communication links may also be used. The merits of different data communication methods should be investigated.

A design issue that should be examined is a bus architecture for robotic manipulators. Robots should have a bus that propagates along the mechanism for internal sensing. Each link should contain a chip that contains information about

link kinematic and dynamics parameters, and perhaps what components might interface with it. Maintenance, calibration, and operating information then becomes an artifact within the machine rather than separate from it. The requirements of such a system, and its design, remain future work.

As machinery diagnosticians find more analytical and empirical relationships between monitored processes and machine faults, telecommunications and computer networks become more valuable in timely diagnosis of faults. At present, inspection and fault diagnosis are done on location or nearby. Centralized monitoring used to rely on hard-wiring sensors to readouts or recorders, but now portable dataloggers are capable of recording many spectra as well as doing local analysis. Serial communication by modem is also available, which allows datalogging by station personnel with analysis at a distance.

In the long term, telepresence for inspection would add qualitative inspection information. Future work in this field is the choice of diagnostic parameters, the design of a human-machine interface that displays diagnostic information to the remote inspector, and the implementation of such a system. The near-term solution remains for the diagnostician to inspect in person when unusual machine conditions arise. The advantage of recent databases is that more complete machine condition records can be kept—with the associated fault diagnoses. Such records require the diagnostician to do physical inspections for new fault situations only, aided by techniques for automatic diagnostics that supplement empirical diagnostic relationships. Developing appropriate maintenance procedures for integrating robot fault diagnostics with maintenance planning remains the subject of future work.

The ultimate solution is to have a set of self-contained diagnostic and repair routines in a robot's control software. This goal of future work in robot diagnostics and maintenance is illustrated in Figure 8.1.

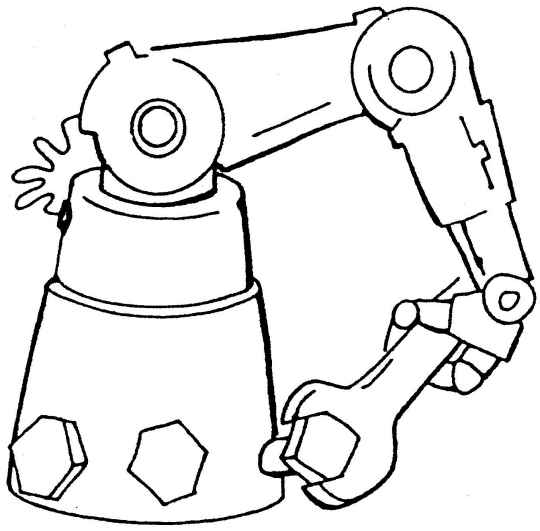

Figure 8.1: Function `robot_heal_thyself()`

8.4 One Step Toward Improved Robot Reliability

Improved robot reliability through predictive maintenance demands diagnostic procedures. The procedures offered in this work allow diagnosis of a structural looseness fault in a serial-link robotic manipulator, one step toward that goal.

Bibliography

[1] Anonymous. *Standard Guide for Classifying Industrial Robots.* ASTM Standard F 1034–86, reapproved 1991.

[2] Anonymous. Computational Systems Incorporated User's manual for the CSI 2110 Machinery Analyzer, 1991.

[3] Anonymous. *User's Manual for the DT2801 Series.* Marlboro, MA: Data Translation, 1988.

[4] Anonymous. *FIELDVUE Digital Valve Controller.* Fisher Controls Bulletin 62.1:DVC5000, 1994.

[5] Anonymous. Gore Technologies Product Catalogue.

[6] Anonymous. *IRD Mechanalysis Advanced Training Manual.* Columbus, OH: IRD Mechanalysis, 1985.

[7] Anonymous. *LabVIEW User's Manual.* Austin, TX: National Instruments, 1994.

[8] Anonymous. *PRAB Versatran FA600 Operating Manual.* Kalamazoo, MI, 1981.

[9] Anonymous. *QNX v.4.2 User's Manual.* Ottawa, ON: QNX, 1994.

[10] Anonymous. *Servo Systems Catalogue.* Montville, NJ: Servo Systems, Inc., 1990.

[11] Anonymous. Teac RD130T Operating Manual, 1992.

[12] Anonymous. Teac IF–RD101T Interface Board Operating Manual, 1992.

[13] Anonymous. CO501 and PA501 Set-Up Procedure. Bulletin 18856-003-Rev. A, EG& G Torque Systems, Inc.

[14] Atkeson, C.G.; An, C.H.; Hollerbach, J.M. "Estimation of Inertial Parameters of Manipulator Loads and Links." *The International Journal of Robotics Research,* Vol. 5, Fall 1986, pp. 101–119.

[15] Arai, H.; Tachi, S. "Position Control of a Manipulator with Passive Joints Using Dynamic Coupling." Proceedings 20 ISIR, pp. 617–624.

[16] Asada, H.; Slotine, J-J.E. *Robot Analysis and Control.* Toronto: John Wiley and Sons, 1986.

[17] Bendat, J.S.; Piersol, A.G. *Measurement and Analysis of Random Data.* New York: John Wiley and Sons, 1966.

[18] Barsom, J.M.; Rolfe, S.T. *Fracture and Fatigue Control in Structures.* Toronto: Prentice–Hall Canada, 1987.

[19] Baumeister, T.; Vallone, E.A.; Baumeister, T. (III). *Marks' Standard Handbook for Mechanical Engineers.* Toronto:McGraw–Hill, 1978.

[20] Benfasi, Y.; Penny, J.E.T.; Friswell, M.I. "A Method of System Identification for Nonlinear Vibrating Structures." *Proceedings of 8th International Modal Analysis Conference*, Kissimmee, FL, 1990, pp. 1284–1290.

[21] Bennekers, B.; Teal, H. "Robot Runaway Protection System." *Proceedings of 1988 IEEE International Conference on Robotics and Automation*, pp. 1474–1476.

[22] Bennett, D.J.; Hollerbach, J.M. "Autonomous Calibration of Single-Loop Closed Kinematic Chains Formed by Manipulators with Passive Endpoint Constraints." *IEEE Transactions on Robotics and Automation*, 10/1991, pp. 597–606.

[23] Bennett, D.J.; Hollerbach, J.M.; Henri, P.D. "Kinematic Calibration by Direct Estimation of the Jacobian Matrix." *Proceedings of 1992 IEEE International Conference on Robotics and Automation*, pp. 351–357.

[24] Bernhardt, R.; Albright, S.L. (Ed.) *Robot Calibration.* New York: Chapman & Hill, 1993.

[25] Beyer, W.H. *CRC Standard Mathematical Tables.* Boca Raton: CRC Press, 1981.

[26] Bicker, H.; Daadbin, A. "The Monitoring of Vibration in Industrial Robots." *1989 ASME Design Technical Conference.* Montreal, pp. 273–277.

[27] Boggs, P.T.; Byrd, R.H.; Rogers, J.E.; Schnabel, R.B. *User's Reference Guide for ODRPACK Version 2.01.* NISTIR 92-48343, Gaithersburg MD, June 1992.

[28] Borm, J.H.; Menq, C.H. "Determination of Optimal Measurement Configurations for Robot Calibration Based on Observability Measure." *International Journal of Robotics Research*, Vol. 10 No. 1, 1991, pp. 51–63.

[29] Braun, S. (Ed.) *Mechanical Signature Analysis: Theory and Applications.* Toronto: Academic Press, 1986.

[30] Bronwell, A. *Advanced Mathematics in Physics and Engineering.* Toronto: McGraw–Hill, 1953.

[31] Canepa, G.; Hollerbach, J.M.; Boelen, A.J.M.A. "Kinematic Calibration by Means of a Triaxial Accelerometer." *Proceedings of 1994 IEEE International Conference on Robotics and Automation*, pp. 2776–2782.

[32] Carlson, A.B.; Gisser, D.G. Electrical Engineering: Concepts and Applications. Don Mills: Addison–Wesley, 1981.

[33] Čačko, J.; Bílý, M.; Bukoveczky, J. *Random Processes: Measurement, Analysis and Simulation.* New York: Elsevier, 1986.

[34] Cempel, C. "Passive Diagnostics and Reliability Experiment: Application in Machine Condition Monitoring." *ASME Journal of Vibrations, Acoustics, Stress, and Reliability in Design,* Jan. 1989, pp. 82–87.

[35] Chen, J.; Chao, L-M. "Positioning Error Analysis for Robot Manipulators with All Rotary Joints." *IEEE Journal of Robotics and Automation,* Vol. RA-3, No. 6, Dec. 1987, pp. 539–545.

[36] Craig, J.J. *Introduction to Robotics: Mechanics and Control.* Don Mills: Addison-Wesley, 1986.

[37] Crandall, S.H. *Engineering Analysis: A Survey of Numerical Procedures.* Malabar, FL: Robert E. Krieger Publishing, 1986.

[38] Dakalakis, N.G. "Analysis of Robot Performance Operation." *Proceedings 13th ISIR,* 1983, Vol. 1 pp.7/73–7/95.

[39] Dhillon, B.S. *Robot Reliability and Safety.* New York: Springer-Verlag, 1991.

[40] Doty, K.L.; Melchiorri, C.; Schwartz, E.M.; Bonivento, C. "Robot Manipulability." *IEEE Transactions on Robotics and Automation,* Vol. 11, No. 3, 1995, pp. 462–468.

[41] Driels, M.R.; Pathre, U.S. "Generalized Joint Model for Robot Manipulator Kinematic Calibration and Compensation." *Journal of Robotics Systems*, Vol. 4 No. 1, 1987, pp. 77–114.

[42] Driels, M.R.; Pathre, U.S. "Robot Manipulator Kinematic Calibration and Compensation Using a Generalized Jacobian Formulation." *Journal of Robotics Systems*, Vol. 4 No. 2, 1987, pp. 259–280.

[43] El-Saeidy, F.M.A. "Effect of Backlash on Vibration Spectrum in Spur Gear Boxes Incorporating Ball Bearings with Radial Clearance." *Proceedings of 8th International Modal Analysis Conference*, Kissimmee, FL, 1990, pp. 1158–1164.

[44] Engelberger, J.F. *Robotics in Service.* Cambridge, Massachusetts: MIT Press, 1989.

[45] Everett, L.J.; Driels, M.R.; Mooring, B.W. "Kinematic Modeling for Robot Calibration," *1987 International Conference on Robotics and Automation,* pp. 183–189. Note that the minus sign in the equation for the necessary number of parameters is incorrect; it should be a positive sign.

[46] Everett, L.J. "Models for Diagnosing Robot Error Sources." *Proceedings of 1993 IEEE International Conference on Robotics and Automation*, pp. 155–159.

[47] Fu, K.S.; Gonzalez, R.C.; Lee, C.S.G. *Robotics: Control, Sensing, Vision, and Intelligence.* Singapore: McGraw–Hill, 1987.

[48] Graham, J.H (Ed.) *Safety, Reliability and Human Factors in Robotic Systems.* New York: Van Nostrand Reinhold, 1991.

[49] Graham, J.H.; Guan, J. "Intelligent Diagnostics in Robotics and Integrated Manufacturing Systems." *Proceedings of 1993 IEEE International Conference on Robotics and Automation*, pp. 174–179.

[50] Grosch, D.L. *A Primer of Reliability Theory.* Toronto: John Wiley and Sons, 1989.

[51] Hahn, G.J.; Shapiro, S.S. *Statistical Models in Engineering.* Toronto: John Wiley and Sons, 1967.

[52] Harris, C.M. *Shock and Vibration Handbook.* Toronto: McGraw–Hill, 1988.

[53] Hartenberg, R.S.; Denavit, J. *Kinematic Synthesis of Linkages.* Toronto: McGraw–Hill, 1964.

[54] Hayati, S.; Tso, K.; Roston, G. "Robot Geometry Calibration." *Proceedings of 1988 IEEE International Conference on Robotics and Automation*, pp. 947–951.

[55] Helferty, R.; Jeswiet, J. "Implementing ANSI/RIA R15.05 and ISO/DIS 9283 Standards for Testing Robot Repeatability," *Proceedings of CSME Forum,* Toronto, 1994, pp 562–570.

[56] Helstrom, C.W. *Probability and Stochastic Processes for Engineers.* New York: MacMillan, 1984.

[57] Hogan, N. "Impedance Control: An Approach to Manipulation, Part One." *ASME Journal of Dynamic Systems, Measurement, and Control*, Mar. 1985, pp. 1–8.

[58] Hollerbach, J.M. "A Survey of Kinematic Calibration." *The Robotics Review 1.* Cambridge MA: MIT Press, 1989, pp. 207–242.

[59] Hughes, K.; Ranganathan, N. "A Model for Determining Sensor Confidence." *Proceedings of 1993 IEEE International Conference on Robotics and Automation*, pp. 136–141.

[60] Hundal, M.S. "Mechanical Signature Analysis." *Shock and Vibration Digest.* Vol. 22, No. 10, Oct. 1990, pp.3–10.

[61] Hunt, K.H. "Robot Kinematics—A Compact Analytic Inverse Solution for Velocities." *ASME Journal of Mechanisms, Transmissions, and Automation in Design,* Mar. 1987, pp. 42–49.

[62] Ibarra, R.; Perreira, N.D. "Determination of Linkage Parameter and Pair Variable Errors in Open Chain Kinematic Linkages Using a Minimal Set of Pose Measurement Data." *ASME Journal of Mechanisms, Transmissions, and Automation in Design,* Vol. 108, June 1986, pp 159–165.

[63] Jacobsen, S. Keynote Address, *American Nuclear Society Fifth Topical Meeting on Robotics and Remote Systems,* Knoxville, TN, April 1993.

[64] Klafter, R.D.; Chmielewski, T.A.; Negin, M. *Robotic Engineering: An Integrated Approach.* Toronto: Prentice-Hall, 1989.

[65] Kolhatkar, S.; Budynas, R.G. "Modal Analysis of a Robot Arm Using Finite Element Analysis and Modal Testing." *Proceedings of 8th International Modal Analysis Conference*, Kissimmee, FL, 1990, pp. 67–70.

[66] Kryter, R.C.; Haynes, H.D. "Condition Monitoring of Machinery Using Motor Current Signature Analysis," *Sound and Vibration,* September 1989, pp. 14–21.

[67] Kumar, A.; Waldron, K.J. "Numerical Plotting of Surfaces of Positioning Accuracy of Manipulators." *Journal of Mechanism and Machine Theory,* Vol. 16(4), 1981, pp. 361–368.

[68] Lawrence, P.D.; Mauch, F. *Real-Time Microcomputer System Design.* Toronto: McGraw–Hill, 1988.

[69] Liégeois, A. *Robot Technology, Volume 7: Performance and Computer-Aided Design.* Englewood Cliffs NJ: Prentice-Hall, 1985.

[70] Lipsett, M.G.; Moore, T.N. "Using Robot End Effector Vibration Monitoring For Machinery Diagnostics and the Effect of Looseness in Joints," *Proceedings of CSME Forum,* Toronto, 1990.

[71] Lipsett, M.G.; Yoshikawa, T. "Design of an Experimental Robotic Manipulator for Fast Transition Between Proximity and Force Control," *Proceedings 32nd Joint Automatic Control Conference, Japan Controls Society.* Tokyo, Oct. 1989.

[72] Lipsett, M.G. *Development of a Slide Rig and Planar Manipulator for the Study of Mechanical Looseness Faults.* Kingston, ON: Queen's University Mechanical Engineering, 1995.

[73] Ljung, L. *System Identification Toolbox for MATLAB: User's Guide.* Natick, MA: MathWorks, Inc., 1986.

[74] Luh, J.Y.S.; Fisher, W.D.; Paul, R.P.C. "Joint Torque Control by a Direct Feedback for Industrial Robots." *IEEE Transactions on Automatic Control,* Vol. AC-28, Feb. 1983, pp. 153–161.

[75] Lynn, P.A.; Fuerst, W. *Introductory Digital Signal Processing.* Toronto: John Wiley and Sons, 1989.

[76] Lyon, R.H. *Machinery Noise and Diagnostics.* Toronto: Butterworth, 1987.

[77] Mannan, M.A.;, Richardson, M.H. "Detection and Identification of Structural Cracks Using FRF Measurements." *Proceedings of 8th International Modal Analysis Conference*, Kissimmee, FL, 1990, pp. 652—657.

[78] McCarthy, J.M. *An Introduction to Theoretical Mechanics.* Cambridge, MA: The MIT Press, 1990.

[79] McConnell, K.G. "Errors in Using Force Transducers." *Proceedings of 8th International Modal Analysis Conference*, Kissimmee, FL, 1990, pp. 884–890.

[80] McGarty, T.P. *Stochastic Systems and State Estimation.* Toronto: Wiley-Interscience, 1974.

[81] McKerrow, P.J. *Introduction to Robotics.* Don Mills: Addison-Wesley, 1991.

[82] Menq, C.; Borm, J. "Statistical Measure and Characterization of Robot Errors." *Proceedings of 1988 IEEE International Conference on Robotics and Automation*, pp. 926–931.

[83] Mitchell, J.S. *An Introduction to Machinery Analysis and Monitoring.* Tulsa, OK: PennWell Publishing, 1981.

[84] Monroe, J.E. *Industrial Robot Maintenance: The Design and Implementation of a Diagnostic Monitoring System for an Industrial Robot.* MSc Thesis, Queen's University, March 1987.

[85] Moore, T.N. "A Health Monitoring System for Robots." *Proceedings of IASTED International Symposium on Advances in Robotics.* Santa Barbara, CA, 1985, pp. 30–34.

[86] Moore, T.N.; Jeswiet, J.; Lipsett, M.G. "Machinery Fault Diagnosis for Automated Machining Systems," *Proceedings 7th International Conference on Computer–Aided Production Engineering.* Cookeville, TN, June 1992.

[87] Mooring, B.W.; Roth, Z.S.; Driels, M.R. *Fundamentals of Manipulator Calibration.* Toronto: Wiley-Interscience, 1991.

[88] Mooring, B.W.; Pack, T.J. "Determination and Specification of Robot Repeatability." *Proceedings of 1986 IEEE International Conference on Robotics and Automation*, pp. 1017–1023.

[89] Mooring, B.W.; Pack, T.J. "Calibration Procedure for an Industrial Robot." *Proceedings of 1988 IEEE International Conference on Robotics and Automation*, pp. 786–791.

[90] Nagler, B. "We Need Reliable, Ready-To-Use Robots, Not Fix-It Later Kits!" *Robotics Engineering.* April 1986, pp.7–10. An interview with Richard E. Dauch, Executive V.P. of Manufacturing, Chrysler Corp.

[91] Natsiavas, S. "Steady State Vibration of Oscillators with Motion Limiting Constraints." *Proceedings of 8th International Modal Analysis Conference*, Kissimmee, FL, 1990, pp. 509–514.

[92] Ohwovoriole, M.S.; Roth, B. "An Extension of Screw Theory." *ASME Journal of Mechanical Design*, Vol. 103, Oct. 1981, pp. 725–735.

[93] Orin, D.E.; Schrader, W.W. "Efficient Computation of the Jacobian for Robot Manipulators." *International Journal of Robotics Research.* Vol. 3, No. 4, Winter 1984, pp. 66–75.

[94] Osborn, J.F. "Applications of Robotics in Hazardous Waste Management." *Proc. World Conference on Robotic Research,* Gaithersburg MD, 1989.

[95] Papoulis, A. *Probability, Random Variables, and Stochastic Processes.* Toronto: McGraw-Hill, 1984.

[96] Patterson, T.; Lipkin, H. "Structure of Robot Compliance." Proceedings 1990 ASME Design Technical Conference on Cams, Gears, Robot and Mechanism Design, pp.315–322.

[97] Paul, R.P.; Shimano, B.; Mayer, G.E. "Differential Kinematic Control Equations for Simple Manipulators." *IEEE Transactions on Systems, Man, and Cybernetics,* Vol. 11, No. 6, June 1981, pp. 456–60.

[98] Peleg, K.; Shpigler, S. "Dynamic Matching of Acceleration Transducers." *ASME Journal of Dynamic Systems, Measurement, and Control*, Dec. 1986, pp. 306–312.

[99] Press, W.H.; Vetterling, W.T.; Teukolsky, S.A.; Flannery, B.P. *Numerical Recipes in C.* New York: Cambridge University Press, 1988.

[100] Proakis, J.G.; Manolakis, D.G. *Introduction to Digital Signal Processing.* New York: MacMillan, 1988.

[101] Ramsli, E. "Probability Distribution of Repeatability of Industrial Robots." *International Journal of Robotics Research.* Vol. 10, No. 3, June 1991, pp. 276–283.

[102] Randall, R.B. "A New Method of Modeling Gear Faults." *ASME Journal of Mechanical Design*, Vol. 104, April 1982, pp. 259–264.

[103] Readman, M.C. *Flexible Joint Robots.* Boca Raton: CRC Press, 1994.

[104] Rivin, E.I. *Mechanical Design of Robots.* New York: McGraw–Hill, 1988.

[105] Roth, B. "Screws, Motors, and Wrenches That Cannot Be Bought in a Hardware Store." *Robotics Research: The First International Symposium*, MIT Press, 1984, pp. 679–693.

[106] Roth, Z.; Mooring, B.W.; Ravani, B. "An Overview of Robot Calibration," *1987 IEEE Journal of Robotics and Automation,* Vol. RA-3, October 1987, pp. 377–385.

[107] Samuel, A.E.; McAree, P.R.; Hunt, K.H. "Unifying Screw Geometry and Matrix Transformations." *The International Journal of Robotics Research,* Vol. 10, Oct. 1991, pp. 454-472.

[108] Schuller, C.A.; McNamee, W.L. *Industrial Electronics and Robotics.* Toronto: McGraw–Hill, 1986.

[109] Shamma, J.S.; Whitney, D.E. "A Method for Inverse Robot Calibration." *Journal of Dynamic Systems, Measurement, and Control,* Vol. 109, 1987, pp. 36–43.

[110] Spiegel, M.R. *Probability and Statistics.* Toronto: McGraw-Hill, 1975.

[111] Stauffer, R.N. "Maintenance at a High-Tech Chrysler Plant." *Robotics Engineering.* Aug. 1986, pp.27– 28.

[112] Stepanenko, Y.; Sankar, T.S. "Vibro-Impact Analysis of Control Systems with Mechanical Clearance and Its Application to Robotic Manipulators." *ASME Journal of Dynamic Systems, Measurement, and Control*, Mar. 1986, pp. 9–16.

[113] Stewart, I. "Inside Science: Statistical Modeling." *New Scientist*, 17 Sept. 1994, pp. 1–4.

[114] Stone, H.W.; Sanderson, A.C. "A Prototype Arm Signature Identification System." *Proceedings of 1987 IEEE International Conference on Robotics and Automation*, pp. 175–182.

[115] Stone, H.W.; Sanderson, A.C. "Statistical Performance Evaluation of the S-Model Arm Signature Identification Technique." *Proceedings of 1988 IEEE International Conference on Robotics and Automation*, pp. 939–946.

[116] Tuttle, T.D.; Seering, W. "Modeling a Harmonic Drive Gear Transmission." *Proceedings of 1993 IEEE International Conference on Robotics and Automation*, pp. 624–629.

[117] Tzou, H.S.; Gruver, W.A.; Fang, M.; Rong, Y. "Diagnostic Monitoring of Industrial Robots." Computer-Aided Production Engineering, New York: Elsevier, 1991, pp. 353–362.

[118] Van Brussel, H. "Testing and Evaluation of Robots." *Proceedings CIRP 1990,* pp. 657–664.

[119] Varrasi, J. "Robots Can Play Vital Role in Environmental Restoration." *ASME News,* Feb. 1992, pp. 1–2.

[120] Veitschegger, W.K.; Wu, C. "Robot Calibration and Compensation." *IEEE Transactions on Robotics and Automation*, 12/1988, pp. 643–655.

[121] Visinsky, M.L.; Walker, I.D.; Cavallaro, J.R. "New Model-Based Fault Detection Thresholds for Robot Manipulators." *Proceedings of 1994 IEEE International Conference on Robotics and Automation*, pp. 1388–1395.

[122] Walker, M.W.; Orin, D.E. "Efficient Dynamic Computer Simulation of Robotic Mechanisms." *ASME Journal of Dynamic Systems, Measurement, and Control*, Sept. 1982, pp. 205–211.

[123] Wallrapp, O. "Geometric Stiffness Influence in Linearized Flexible Multibody Systems." *Proceedings of 8th International Modal Analysis Conference*, Kissimmee, FL, 1990, pp. 1093–1100.

[124] Wang, D. "Transfer Functions for a Single Flexible Link." *International Journal of Robotics Research.* Vol. 10, No. 5, Oct. 1991, pp. 540–549.

[125] Whitney, D.E.; Lozinski, C.A.; Rourke, J.M. "Industrial Robot Forward Calibration Method and Results." *Journal of Dynamic Systems, Measurement, and Control,* Vol. 108, 1986, pp. 1–8.

[126] Williams, T.; Kelley, C. *GNUPLOT: An Interactive Plotting Program.* Version 3.5, 1993.

[127] Wu, C. "A Kinematic CAD Tool for the Design and Control of a Robot Manipulator." *The International Journal of Robotics Research,* Vol. 3, Spring 1984, pp. 54–67.

[128] Wyckaert, K.; Vanherck, P.; Sas, P.; Van Brussel, H. "The Identification of the Nonlinear Behaviour of a Flexible Robot Link." *Proceedings of 8th International Modal Analysis Conference*, Kissimmee, FL, 1990, pp. 530–39.

[129] Xiaojiang, M.; Wenhu, H.; Zhenzhu, Z. "Coupling Effects of Rigidity and Flexibility in a Chain System." *Proceedings of 8th International Modal Analysis Conference*, Kissimmee, FL, 1990, pp. 1165–1168.

[130] Xiaojiang, M.; Jingxia, Y.; Peide, L. "Dynamical Tests of a Bearing Assembly and Nonlinear Analysis." *Proceedings of 8th International Modal Analysis Conference*, Kissimmee, FL, 1990, pp. 685–689.

[131] Xingui, M.; Chengshin, S.; Wenhu, H.; Zhenzhu, Z. "Coupling Effects of Rigidity and Flexibility in a Chain System." *Proceedings of 8th International Modal Analysis Conference*, Kissimmee, FL, 1990, pp. 1165–1167.

[132] Yoda, T.; Obokata, N.; Hioki, S. *Roller Bearings for Industrial Robots.* New York: Gordon and Breach Science Publishers, 1990.

[133] Yoshikawa, T. *Foundations of Robotics.* Cambridge, MA: The MIT Press, 1990.

[134] Youfang, L.; Bin W. "Modal Analysis Problems in the Nonuniform Inertial Field." *Proceedings of 8th International Modal Analysis Conference*, Kissimmee, FL, 1990, pp. 784–87.

[135] Zati, A.S.; ElMaraghy, W.H. "An Overview of the Experimental Facility for the Study of Flexible manipulators at UWO," *Proceedings of CSME Forum,* Toronto, 1994, pp. 641–652.

[136] Zhang, H.; Paul, R.P. "Non-Kinematic Errors in Robot Manipulators." *Proceedings of 1988 IEEE International Conference on Robotics and Automation*, pp. 1138–1139.

[137] Zhang, H.; Wang, L.; Roth, Z.V. "Simultaneous Calibration of a RObot and a Hand-Mounted Camera." *Proceedings of 1993 IEEE International Conference on Robotics and Automation*, pp. 149–154.

[138] Ziegert, J.; Datseris, P. "Basic Considerations for Robot Calibration." *Proceedings of 1988 IEEE International Conference on Robotics and Automation*, pp. 932–938.

Vita

Name: Michael George Lipsett

Place and Year of Birth: Deep River, Ontario, 1962

Certification: Registered Professional Engineer of Ontario

Education:
Mackenzie High School, 1975–80.
Queen's University, 1980–84,
B.Sc.Eng. (Honours) 1984.
School of Graduate Studies and Research,
Queens' University, 1987–88.
International Course in Mechanical Engineering,
Kyoto University, 1988–90.
School of Graduate Studies and Research,
Queens' University, 1990–95.

Experience:
Professional Engineer, mechanical equipment and robotics development, AECL Research, 1992–present.
Teaching and Research Assistant, Queen's University, 1987–88, 1990–92.
Professional Engineer, mine maintenance, Syncrude Canada Limited, 1984–86.
Stagiair (Student Trainee), Philips Electronics, Eindhoven, 1984.

Awards:
Ontario Graduate Scholarship, 1991–1992.
R.S. McLaughlin Teaching Fellowship, Queen's, 1990.
Japanese Government Monbusho Scholarship, 1988–90.
R.S. McLaughlin Teaching Fellowship, Queen's, 1987.
Peter White Memorial Award, Queen's, 1984.
James Hickey Memorial Prize, Queen's, 1982.
Dean's Scholar, Queen's, 1980–81.
Engineering Institute of Canada Centennial Postage Stamp Design Contest, 2nd Place, 1984.

Publications

Yoshikawa, T.; Lipsett, M.G. "Design of an Experimental Robotic Manipulator for Fast Transition between Proximity and Force Control." *Proceedings 32nd Joint Automatic Control Conference of the Japan Controls Society*, Tokyo, 1989.

Yoshikawa, T.; Lipsett, M.G. "Reducing End Effector Impacts Using Proximity Sensing." *Proceedings 7th Annual Conference of the Robotics Society of Japan*, Tokyo,

1989.

Lipsett, M.G.; Moore, T.N. "Using Robot End Effector Vibration Monitoring for Machinery Diagnostics and the Effect of Looseness in Joints." *Proceedings CSME Forum*, Toronto, 1990.

Lipsett, M.G. "Engineering Education in Japan." *Proceedings 8th Canadian Conference on Engineering Education,* Toronto, 1990.

Moore, T.N.; Jeswiet, J.; Lipsett, M.G. "Machinery Fault Diagnosis for Automated Machining Systems." *Proceedings 7th International Conference on Computer-Aided Production Engineering ICAPE,* Cookeville TN, 1991.

Brown, N.H.; Fraser, J.C.; Lipsett, M.G. *Motor Current Signature Analysis: Interim Report 1.* Report COG-92-08, AECL Research, Chalk River, 1992.

Schwarz, H.D.; Bell, R.A.; Hodgson, J.A.; Judkins, J.G.; Ko, K.; Kroll, N.; Ng, C.K.; Pendleton, R.P.; Skarpaas, K.; Lambertson, K.; Rimmer, R.; de Jong, M.S.; Tran-Ngoc, T.; Adams, F.P.; Lipsett, M.G.; Mellors, W. "Design of a High-Power Test Model of the PEP-II RF Cavity." *Proceedings of the 1993 Particle Accelerator Conference,* Volume 2, 1993.

Ellis, R.E.; Ismaeil, O.M.; Lipsett, M.G. *Design and Evaluation of a High-Performance Prototype Planar Haptic Interface.* Submitted to the ASME Journal of Machine Design. (Preliminary version presented at 1993 ASME Winter Annual Meeting.)

Lipsett, M.G., Brown, N.H., Fraser, T.L. *Motor Current Analysis: Interim Report 2.* Report COG-93-240, AECL Research, Chalk River, 1994.

Cheadle, R.J., Lipsett, M.G.; Martin, D.H. *Steam Generator Plug Leak Test Tool Proof-of-Concept.* Report COG-94-347, AECL Research, Chalk River, 1994.

Lipsett, M.G., Cheadle, R.J., Eyvindson, A. *Survey of Subatmospheric Air In-Leakage Detection and Sealing Methods.* Report COG-94-334, AECL Research, Chalk River, 1994.

Lipsett, M.G. *Development of a Slide Rig and Planar Robotic Manipulator for the Study of Mechanical Looseness Faults.* Technical Report, Department of Mechanical Engineering, Queen's University. Kingston, 1995.

Lipsett, M.G. *Motor Current Analysis: Interim Report 3.* Report COG-95-61, AECL Research, Chalk River, 1995.

Tallon, S.G.; Lipsett, M.G. *Falk 1040T Coupling Frequency Response Characteristics.* Report COG-95-75, AECL Research, Chalk River, 1995.

Lipsett, M.G., Eyvindson, A. *Subatmospheric In-Leak Detector Prototype.* Report COG-95-226, AECL Research, Chalk River, 1995.

Lipsett, M.G. *On-Line Monitoring of Electric Motor-Driven Equipment: Final Report.* Report COG-95-230, AECL Research, Chalk River, 1995.

Lipsett, M.G. *Mechanical Cleaning of Steam Generator Tube Inner Walls: System*

Design. Report COG-95-244, AECL Research, Chalk River, 1995.

Lipsett, M.G. *Mechanical Cleaning of Steam Generator Tube Inner Walls: Prototype Testing.* Report COG-95-243, AECL Research, Chalk River, 1995.

Lipsett, M.G. "Looseness Fault Diagnosis in Robotic Manipulators." *Proceedings Eighth International Congress on Condition Monitoring and Diagnostic Engineering Management,* Kingston, 1995.

Lipsett, M.G. "Machinery Diagnostics Using Motor Current Analysis." *Proceedings Eighth International Congress on Condition Monitoring and Diagnostic Engineering Management,* Kingston, 1995.

Lipsett, M.G.; Greenspan, M.; Ballantyne, W.J. "Using Range Vision for Telerobotic Control in Hazardous Environments." To be presented at the *SPIE Conference on Teleoperation and Telemanipulation,* Pittsburgh, October 1995.

Lipsett, M.G.; Rody, K.H. "Using Mobile Robots for Reactor Maintenance." To be presented at the *Third International Conference on CANDU Maintenance,* Toronto, November 1995.